

USING LAND-USE CHANGE TO MITIGATE IMPACTS OF FUTURE DROUGHTS ON WATER YIELD IN SOUTH AFRICA

Report to the
Water Research Commission

by

**Babatunde J. Abiodun¹, Myra Naik¹, Tlakale Mogebeisa¹,
Nokwethaba Makhanya¹, Mariam Nguvava^{1,2}, Rhoda Adaramola¹ &
Rosita Yocgo^{3,4}**

¹Department of Environmental and Geographical Science, University of Cape Town

²Sokoine University of Agriculture, Morogoro, Tanzania

³African Institute for Mathematical Sciences (AIMS), Kigali, Rwanda

⁴Institute for Plant Biotechnology, University of Stellenbosch, South Africa

WRC Project No. 2835/1/21

ISBN 978-0-6392-0324-9

February 2022

Obtainable from

Water Research Commission

Private Bag X03

Gezina

PRETORIA, 0031

orders@wrc.org.za or download from www.wrc.org.za

DISCLAIMER

This report has been reviewed by the Water Research Commission (WRC) and approved for publication. Approval does not signify that the contents necessarily reflect the views and policies of the WRC nor does mention of trade names or commercial products constitute endorsement or recommendation for use.

Executive Summary

Introduction

Water is a precious natural economic resource globally, and especially in South Africa, where it plays a central role in all of the country's socio-economic activities, like agriculture, mining, transport, tourism, industry, and communication. The importance of water is clearly articulated in various government policies in South Africa. For instance, the provision of adequate and suitable water for economic and social development is a cornerstone of the national water policy. However, South Africa is also a water-stressed country, because of its semi-arid to arid climate, which is characterised by low rainfall and high evaporation rates. The country's average annual rainfall (500 mm) is lower than the global average annual rainfall (860 mm). Less than 9% of the annual rainfall ends up in rivers, and only about 5% recharges groundwater in aquifers. Rainfall and river flow are unevenly distributed across the country, with only 12% of the land area generating 50% of the streamflow. In addition, South Africa's rainfall is highly variable in time and is unpredictable. For instance, decadal rainfall variability usually results in extended severe droughts across the country.

Such rainfall variability, coupled with the economic importance of water, has prompted the country to invest in large-scale water infrastructure development (such as dams, canals, pipelines, and reservoirs). However, population growth, increased urbanisation, and accelerated economic development are continuously increasing water demand and keeping the country water-stressed. This may worsen in the future because water demand is likely to increase in the future. Therefore, to ensure water security and sustainable water resource management in the future, there is a need to move beyond current infrastructure development solutions and towards research-driven environmental solutions, in which water availability can be increased by mitigating the impacts of environmental pressures (like climate change) on the water yields (like soil moisture and surface runoff) in the river basins.

Climate change is projected to have negative impacts on water storage in South Africa. For instance, surface air temperature is expected to increase everywhere across the country. The temperature increase, which may reach 2.5°C along the coast and 3.5°C in the far interior in the near future, is projected to increase by 5.0°C along the coast and by more than 6.0°C in the interior by the end of the century. Projected rainfall changes are associated with large uncertainties, ranging from decreased rainfall over the entire country to wetting in the eastern parts of the country and drying in the western parts. However, an increasing number of studies have highlighted that projected climate change may influence the hydrological cycle and water yield in South African river catchments by intensifying floods and droughts, enhancing evapotranspiration, and changing soil moisture, runoff, and water quality.

Land-use/land-cover (LULC) changes can play a crucial role in influencing the hydrology of a basin. They may have positive or negative impacts on the water cycle and water yield in the basin by influencing processes like evapotranspiration, vegetation interception, and surface infiltration. However, the magnitude and direction of these hydrological impacts depend on the type and extent of the land-use changes. For instance, forestation may reduce soil moisture and

surface runoff, while urbanisation and human settlement may give rise to higher storm flow and enhanced discharge peaks. While some studies have documented hydrological responses to land-use changes in South African river basins, no study has investigated how these responses can be used to mitigate climate change impacts on hydrological droughts in these basins.

On the basis of the above, the specific objectives of this study are:

1. To calibrate, evaluate, and apply a hydrological model over three selected river basins in South Africa.
2. To investigate the influence of bias correction of climate simulation datasets on the quality of hydrological simulation over the river basins.
3. To project the impacts of future climate change on hydrological droughts in the river basins.
4. To explore and quantify the extent to which LULC changes can reduce the impacts of droughts in these river basins.

Methods

We selected three South African river basins for the study, namely: the Vaal River basin, the Limpopo River basin and the Western Cape River basins. These river basins play crucial roles in the socio-economic activities of the country, but they are also hot-spots of droughts. Many studies have documented the vulnerability of socio-economic activities in these basins to droughts. Various drought indices were employed to characterise droughts. Multiple climate datasets (i.e. the Global Meteorological Forcing Dataset (GMFD) and COordinated Regional Downscaling EXperiment (CORDEX)) were analysed, and a series of hydrological simulations were performed over the river basins. For the hydrological simulations, a process-based hydrological model called the Soil and Water Assessment Tool Plus (SWAT+) (Arnold et al., 2012) was coupled with the GMFD observation dataset and the CORDEX simulation dataset. We calibrated and evaluated SWAT+ over the basin and investigated the capability of a well-known bias-correction method called Quantile Delta Mapping (QDM) (Cannon et al., 2015, 2018) to reduce the biases and uncertainty in the hydrological simulations. The impacts of climate change on future hydroclimatic variables and drought frequency were projected at four global warming levels (GWLs), and the extent to which LULC change scenarios (e.g. expansion of forests, grassland, cropland, cropland/grassland mosaic, barren land) can influence the projections were quantified. These extreme but viable LULC changes are consistent ongoing LULC change trends over the basins.

Results and conclusion

The results of the study are presented in five sections. The first section (Section 3.1) presents the outcome of the SWAT+ calibration and validation over the three river basins, the second (Section 3.2) shows the effects of bias correction of CORDEX datasets on hydrological simulations over the basins, while each of the last three sections (Sections 3.3, 3.4 and 3.5) focuses the extent to which LULC changes can mitigate impacts of climate changes over each of the basins (VRB, LRB and WRB, respectively).

Calibration and validation of hydrological model (SWAT+) over the river basins

The SWAT+ model gives realistic simulations of streamflow over the river basins, albeit with some notable biases. Over the VRB, it reproduces the annual cycle of the observed streamflow, captures the timing and magnitude of most peak flows, and replicates the interannual variability of the observed peaks at four hydrological stations (i.e. C3H007, C5H016, C2H003, and C9H009) during the calibration (1971-1980) and validation (1981-2000) periods. The coefficient of correlation (R) between the observed and simulated streamflow ranges between 0.5 and 0.9 over all the stations. Over the LRB, the SWAT+ model also captures the temporal variability of the streamflow at four hydrological stations (i.e. A2H059, A2H029, B3H017 and B7H015) during the calibration period (1988-1998) and validation period (1999-2009). The coefficient of correlation between the observed and simulated streamflows is high ($R > 0.6$) at most stations. Over the WCRB, the model evaluation shows good agreement between the simulated and observed streamflows at four hydrological stations (i.e. G1H013, H7H006, E2H003, and J1H019) during the calibration (1980-1990) and validation (1991-2005) periods. The simulated streamflow also tracked the observed values in reproducing the seasonal and annual variations of the streamflow. In general, the model provides a good representation of hydrological processes and captures the spatial and temporal characteristics of streamflow in all the river basins. The biases in the SWAT+ simulations may be attributed to several factors, such as shortcomings in the SWAT+ model or the model setup over each river basin. Nevertheless, the overall good agreement between the SWAT+ simulation and observation over the river basins is quite encouraging and shows that SWAT+ is indeed suitable for hydrological studies over the basins.

Influence of bias correction of CORDEX datasets on hydrological simulations over the river basins

The SWAT+ simulation with the original CORDEX dataset gives realistic simulations of hydrological variables over all the river basins. It reproduces the spatial distribution of the variables, as in the simulation forced with the observed datasets (GMFD). The coefficient of correlation between the two hydrological simulations is high ($R \geq 0.5$) over all three basins. Nevertheless, there are substantial biases in the hydrological simulation with the original CORDEX dataset due to the biases in the dataset. The bias correction of the CORDEX dataset before using this dataset as input into the SWAT+ model reduces biases in the simulated hydrological variables. It reduces these biases by more than 50% and increases the coefficient

of correlation between SWAT+ simulations (with GMFD and CORDEX forcing) substantially ($R \geq 0.75$) over all the basins.

Using land-use changes to mitigate future impacts of climate change on hydrological droughts in the Vaal River basin

The LULC change scenarios investigated over the Vaal River basin include the expansion of grassland, cropland, cropland/grassland mosaic, and barren land. The future projection with the present-day LULC pattern over the basin shows an increasing trend in temperature and potential evaporation with no trend in precipitation and hydrological variables. However, the spatial distribution of the projections shows a uniform increase in temperature across the basin with a decrease in precipitation, soil water, percolation, surface runoff and streamflow over most parts of the basin. The LULC change scenarios alter the impacts of the climate changes on the hydrological variables and drought. For instance, the expansion of grassland reduces the climate change impacts on soil water, percolation, and the associated drought frequency, although the magnitude of the reduction is small compared to the climate change impacts. Conversely, it enhances the climate change impacts on runoff, water yield, streamflow, and the associated drought frequency. In contrast, the other LULC change scenarios (i.e. expansion of other cropland, cropland/grassland mosaic and barren land) mitigate the impacts of climate change on runoff, water yield, streamflow, and the associated drought frequency, but enhance the climate change impacts on soil water, percolation, and the associated drought frequency.

Using land-use change to mitigate future impacts of climate change on hydrological droughts in the Limpopo River basin

The LULC change scenarios investigated over the Limpopo River include the replacement of savanna with forest (i.e. invasion of trees or bush encroachment) and the expansion of grassland, cropland, and cropland/grassland mosaic. With the present-day LULC pattern, the simulations project that the warming rate over Limpopo (5°C in 2099) may be higher than the global warming rate (4°C in 2100), but no trend exists in the precipitation and hydrological variables. However, the spatial distribution of the rainfall projection shows a decrease in precipitation and drying over the eastern part of the basin, and an increase in precipitation and hydrological variables over the southern part. Hence, it appears that climate change increases the frequency of hydrological droughts over the basin. The replacement of savanna and the expansion of grassland scenarios mitigate the impacts of climate change on the frequency of soil moisture droughts because they increase soil moisture. However, they aggravate the impacts of climate change on the frequency of runoff and streamflow droughts, as they further decrease runoff and streamflow over the basin. The influences of expansion of cropland and grassland/cropland scenarios are in the opposite direction to that of replacement of savanna and the expansion of grassland scenarios.

Using land-use change to mitigate future impacts of climate change on hydrological droughts in the Western Cape River basins

The LULC change scenarios considered for this region are the spread of forest, the restoration of shrubland, the expansion of cropland, and the restoration of grassland. With the present-day LULC pattern over the basin (SWAT+ default), future projections also show an increase in temperature and potential evaporation, but a decrease in precipitation and all the hydrological variables. The drying occurs across the basin, and the magnitude of the drying increases with higher GWLs. The spread of forest enhances the climate change impacts on runoff (by further decreasing runoff) and reduces the climate change impacts on streamflow and on streamflow droughts (by increasing the streamflow). The restoration of shrubland enhances the climate change impacts on runoff and streamflow and the associated droughts (by decreasing both variables). The expansion of cropland and the restoration of grassland produce more complex changes, featuring increases and decreases in hydrological variables in different parts of the basins. However, the impacts of all these LULC changes are small compared to the climate change impacts.

Findings from this study show that, while LULC change scenarios can reduce the impacts of climate change on some hydrological droughts in the river basins, they can also enhance the impacts on other hydrological droughts. Nevertheless, the impacts of the LULC change scenarios are small compared to the climate change impacts. The study has provided a framework for investigating the efficiency of land-use changes in mitigating future climate change impacts on other river basins.

Recommendations

- Results of this study suggest that, while these extreme LULC change scenarios could either mitigate or aggravate the climate change impacts on hydrological drought frequency over the basins, the magnitudes of the impacts are in most cases less than 30% of the climate change impacts. This implies that LULC changes may not be sufficient to offset the climate change impacts over the basins; hence, there is a need to explore other climate change mitigation options in these areas. In addition, as all the LULC changes reduce the climate change impacts on one hydrological drought, while aggravating the impacts on another, there is a need to weigh the pros and cons of any LULC change before implementing it.
- The approach used in this study only offers insight into the potential hydrological impacts of using LULC changes to mitigate droughts in the river basins. It is by no means intended to be prescriptive about LULC activities for a particular river basin, but it may assist stakeholders and decision makers in making better decisions on land management and water resource planning in a future impacted by drought due to climate change.
- For simplicity and ease of interpretation, all the LULC change experiments in this study have assumed that the future climate projection would sustain the prescribed LULC patterns, so the vegetation did respond to the climate variability and change. This may

not always be the case in practice. Hence, there is a need to extend the study to perform more sophisticated experiments that would enable vegetation to respond to future atmospheric conditions. The results of such experiments could alter the magnitude of the LULC changes obtained in the present study.

- Solar radiation management (SRM) has been proposed as a global and more effective option to mitigate climate change impacts. SRM aims to eliminate global warming by artificially reflecting a small amount of inbound sunlight out into space. However, although SRM is still in its early stages of research, controversy exists because its full effect on different components of the earth system is unknown. There is a need to investigate the potential impacts of SRM on the hydrological drought over the basins focused on in this study and to compare the results with those of LULC changes obtained in the present study. This will provide an opportunity for comparing global and local climate change mitigation strategies over the basins.

Acknowledgments

The authors thank Dr B Petja for the efficient management of the study and interest in the work.

The Project Reference Group are also gratefully thanked for their guidance during the study.

The Reference Group members were:

Dr OJ Botai	:	South African Weather Service
Prof GA Ekama	:	University of Cape Town
Dr C Mapiye	:	Stellenbosch University
Dr E Mwendera	:	The Agricultural Research Council
Mr J Roberts	:	Department of Water and Sanitation
Dr K Winter	:	University of Cape Town
Prof G Wolfaardt	:	Stellenbosch University
Dr A Adeola	:	South African Weather Service
Mr C Moseki	:	Department Water Affairs and Sanitation
Mr AB Neswiswi	:	Department Water Affairs and Sanitation

Capacity building

The following postgraduate students were supported from this study:

1. Myra Naik (PhD thesis; to be submitted to the University of Cape Town).
2. Nokwethaba Z. Makhanya (MSc thesis; submitted to the University of Cape Town).
3. Tlakale Mogebeisa (MSc thesis; submitted to the University of Cape Town).
4. Rhoda Adaramola (MSc thesis; graduated from the University of Cape Town).
5. Mariam Nguvava (PhD thesis; graduated from the University of Cape Town).

Knowledge dissemination

Findings and outputs from this study have been used in the following publications:

A. Published

1. Abiodun, B.J., Makhanya, N., Petja, B., Abatan, A.A. and Oguntunde, P.G. (2019). Future projection of droughts over major river basins in Southern Africa at specific global warming levels. *Theoretical Applied Climatology*, 137, pp.1785-1799. <https://doi.org/10.1007/s00704-018-2693-0>
2. Abiodun, B.J., Mogebeisa, T.O., Petja, B., Abatan, A.A. and Roland, T.R. (2020). Potential impacts of specific global warming levels on extreme rainfall events over Southern Africa in CORDEX and NEX-GDDP ensembles. *International Journal of Climatology*, 40(6), pp. 3118-3141. <https://doi.org/10.1002/joc.6386>.
3. Akinyemi, F.O. and Abiodun, B.J. (2019). Potential impacts of global warming levels 1.5°C and above on climate extremes in Botswana. *Climatic Change*, 154, pp. 387-400. <https://doi.org/10.1007/s10584-019-02446-1>.
4. Naik, M. and Abiodun, B.J. (2019). Projected changes in drought characteristics over the Western Cape, South Africa. *Meteorological Applications*, 27(1), p. e1802. <https://doi.org/10.1002/met.1802>.
5. Nguvava, M., Abiodun, B.J. and Otieno, F. (2019). Projecting drought characteristics over East African basins at specific global warming levels. *Atmospheric Research*, 228, pp. 41-54. <https://doi.org/10.1016/j.atmosres.2019.05.008>.

B. Submitted (under review) or to be submitted.

1. Abiodun, B.J., Abatan, A.A., Petja, B., Nguvava, Naik, M., Mogebeisa T., Makhanya, N. and Yocgo, R. (2021). Using land cover changes to reduce climate change impacts on hydrological droughts in the Vaal River basin (submitted to *Regional Environmental Change*).
2. Naik, M. and Abiodun, B.J. (2021). Can land-use change mitigate future impacts of climate change on hydrological droughts in the Western Cape (South Africa)? (Submitted to *Theoretical Applied Climatology*).
3. Makhanya, N., Abiodun, B.J. and Wolski, P. (2021). Potential impacts of climate change and land-use change on hydrological droughts in the Limpopo River basin (to be submitted to *Science of the Total Environment*).
4. Mogebeisa, T. and Abiodun, B.J. (2021). Potential impacts of climate change on hydrological extremes in the Incomati River basin (to be submitted to *Natural Hazards*).
5. Nguvava, M. and Abiodun, B.J. (2021). Potential impacts of climate change and land cover change on hydrological droughts in Rufiji basin, Tanzania (to be submitted to *Science of the Total Environment*).

This page was intentionally left blank

Table of Contents

Executive Summary	iii
Introduction	iii
Methods	iv
Results and conclusion	v
Recommendations	vii
Acknowledgments.....	viii
Capacity building.....	viii
Knowledge dissemination.....	ix
List of Figures.....	xiv
List of Tables	xix
List of Acronyms	xx
Chapter 1: Introduction.....	1
1.1 Background.....	1
1.2 Impacts of droughts on the river basins	1
1.3 Climate change and droughts.....	2
1.4 Impacts of land use/land cover changes in the river basins	2
1.5 Study aim and objectives	3
1.6 Organisation of the report	3
Chapter 2: Methodology	5
2.1 Introduction.....	5
2.2 Study domain	5
2.2.1 The Vaal River basin	6
2.2.2 The Limpopo River basin	6
2.2.3 The Western Cape River basins	7
2.3 Data.....	8
2.4 Methods.....	9
2.4.1 Characterising droughts	9
2.4.2 Bias correction of CORDEX simulation datasets	11
2.4.3 Hydrological modelling	12
2.4.4 Description of the hydrological model: SWAT+.....	15
2.5 Summary	17
Chapter 3: Calibration and validation of hydrological model (SWAT+) over the river basins	18
3.1 Introduction.....	18
3.2 Calibration and validation experiments	18
3.3 Calibration and validation over the Vaal River basin	25
3.4 Calibration and validation over the Limpopo River basin.....	26

3.5 Calibration and validation over the Western Cape River basins.....	28
3.6 Summary	29
Chapter 4: Influence of bias correction of CORDEX datasets on hydrological simulations over the river basins	31
4.1 Introduction.....	31
4.2 Bias-correction experiments	31
4.3 Influence of bias correction in the Vaal River basin.....	31
4.4 Influence of bias correction in the Limpopo River basin.....	35
4.5 Influence of bias correction in the Western Cape River basins	38
4.6 Summary	41
Chapter 5: Using land-use change to mitigate future impacts of climate change on hydrological droughts in the Vaal River basin.....	43
5.1 Introduction.....	43
5.2 Land-use change experiments.....	43
5.3 Impacts of climate change	46
5.4 Impacts of LULC changes	51
5.5 A comparison of impacts of climate and LULC changes	53
5.6 Summary	56
Chapter 6: Using land-use changes to reduce hydrological droughts in the Limpopo River basin	58
6.1 Introduction.....	58
6.2 Land-use change experiments.....	58
6.3 Impacts of climate change	61
6.4 Impacts of LULC changes	65
6.5 A comparison of impacts of climate and LULC changes	66
6.6 Summary	68
Chapter 7: Using land-use change to mitigate future impacts of climate change on hydrological droughts in the Western Cape River basins	70
7.1 Introduction.....	70
7.2 Land-use change experiments.....	70
7.3 Impacts of climate change	73
7.4 Impacts of LULC changes	79
7.5 A comparison of the impacts of land-use change with climate change projections.....	82
7.6 Summary	86
Chapter 8: Conclusion and recommendations	87
8.1 Conclusion	87
8.2 Recommendations.....	88

References.....	90
Appendix.....	100

List of Figures

Figure 2.1: Map of Southern Africa, showing the location of the basins used in the study: the Vaal River basin, the Limpopo River basin and the Western Cape River basins (Olifants, Gouritz, Breede and Berg).....	5
Figure 2.2: A comparison between catchment delineation in SWAT and SWAT+.....	17
Figure 3.1: The characteristics of the Vaal River basin used in the study: (a) the topography of the region (i.e. DEM), streams, streamflow observation stations (i.e. C2H007, C9H009, C5H016 and C2H003); (b) the SWAT+ delineation of the basin to sub-basins and channels; (c) soil types and (d) LULC types: Urban residential medium density (URMD), Dry cropland and pasture (CRDY), Cropland/grassland mosaic (CRGR), Cropland/woodland mosaic (CRWO), Grassland (GRAS), Shrubland (SHRB), Savanna (SAVA), Deciduous broadleaf forest (FODB), Evergreen broadleaf forest (FOEB), Mixed Forest (FOMI), Water (WATR), and Bare ground/sparse vegetation (BSVG). The percentage of each LULC type is indicated in brackets.....	20
Figure 3.2: The characteristics of the Limpopo River basin used in the study: (a) the topography of the region (i.e. DEM), streams, streamflow observation stations (i.e. A2H059, A6H029, B3H017 and B7H015); (b) the SWAT+ delineation of the basin to sub-basins and channels; (c) soil types and (d) LULC types: Urban residential medium density (URMD), Dry cropland and pasture (CRDY), Cropland/grassland mosaic (CRGR), Cropland/woodland mosaic (CRWO), Grassland (GRAS), Shrubland (SHRB), Savanna (SAVA), Deciduous broadleaf forest (FODB), Evergreen broadleaf forest (FOEB), Mixed forest (FOMI), Water (WATR), Bare ground/sparse vegetation (BSVG). The percentage of each LULC type is indicated in brackets.....	21
Figure 3.3: The characteristics of the Western Cape River basins used in the study: (a) the topography of the region (i.e. DEM), streams, streamflow observation stations (i.e. E2H003, G1H013, H7H006, and J1H019); (b) the SWAT+ delineation of the basin to sub-basins and channels; (c) soil types and (d) LULC types: Urban residential medium density (URMD), Dry cropland and pasture (CRDY), Cropland/grassland mosaic (CRGR), Cropland/woodland mosaic (CRWO), Grassland (GRAS), Shrubland (SHRB), Savanna (SAVA), Deciduous broadleaf forest (FODB), Evergreen broadleaf forest (FOEB), Mixed forest (FOMI), Water (WATR), and Bare ground/sparse vegetation (BSVG). The percentage of each LULC type is indicated in brackets.....	22
Figure 3.4: The convergence of SWAT+ simulations during the calibration over the river basins: (a) VRB, (b) LRB and (c) WRB.....	25
Figure 3.5: Evaluation of SWAT+ simulated streamflow at four hydrological stations (C3H007, C5H016, C2H003 and C9H009) in the Vaal River basin during the calibration and evaluation periods. The values of the statistical evaluation metrics (i.e. NSE, PBIAS, RMSE, and R) are indicated.....	26
Figure 3.6: Evaluation of SWAT+ simulated streamflow at four hydrological stations (A2H059, A6H029, B3H017 and B7H015) in the Limpopo River basin during the calibration and evaluation periods. The values of the statistical evaluation metrics (i.e. NSE, PBIAS, RMSE, and R) are indicated.....	27

Figure 3.7: Evaluation of SWAT+ simulated streamflow at four hydrological stations (G1H013, H7H006, E2H003 and J1H019) in the Western Cape River catchments during the calibration and evaluation periods. The values of the statistical evaluation metrics (i.e. NSE, PBIAS, RMSE, and R are indicated.	29
Figure 4.1: The spatial distribution of the climate variables over the Vaal River basin, as depicted by GMFD, original CORDEX (CORDEX_ORG) and QDM bias-corrected CORDEX (CORDEX_QDM) datasets, and the biases of the CORDEX datasets (with reference to GMFD). The associated correlation (R), percentage bias (PBIAS) and root mean square error (RMSE) are indicated.	33
Figure 4.2: Same as Figure 4.1, except for hydrological variables.....	34
Figure 4.3: The spatial distribution of the climate variables over the Limpopo River basin, as depicted by GMFD, original CORDEX (CORDEX_ORG) and QDM bias-corrected CORDEX (CORDEX_QDM) datasets, and the biases of the CORDEX datasets (with reference to GMFD). The associated correlation (R), percentage bias (PBIAS) and root mean square error (RMSE) are indicated.	37
Figure 4.4: Same as Figure 4.3, except for hydrological variables.....	38
Figure 4.5: The spatial distribution of the climate variables over the Western Cape River basins, as depicted by GMFD, original CORDEX (CORDEX_ORG) and QDM bias-corrected CORDEX (CORDEX_QDM) datasets, and the biases of the CORDEX datasets (with reference to GMFD). The associated correlation (R), percentage bias (PBIAS) and root mean square error (RMSE) are indicated.	40
Figure 4.6: Same as Figure 4.5, except for hydrological variables.....	41
Figure 5.1: The LULC patterns used in the LULC change experiments for the Vaal River basin: (a) CtrLand, (b) GrLand, (c) CrLand, (d) CrGrLand and (e) BrLand. The experiments are described in Table 5.1. The LULC types are: Bare ground/sparse vegetation (BSVG), Water (WATR), Evergreen broadleaf forest (FOEB), Deciduous broadleaf forest (FODB), Savanna (SAVA), Shrubland (SHRB), Grassland (GRAS), Cropland/woodland mosaic (CRWO), Cropland/grassland mosaic (CRGR), Dry cropland and pasture (CRDY), Urban residential medium density (URMD). The percentage of each LULC type is indicated in brackets.....	45
Figure 5.2: Temporal variations of the changes in hydroclimatic variables over the Vaal River basin in the period 1971-2099 under the RCP8.5 climate scenario. The changes are calculated with reference to the present-day climate (1971-2000). The solid lines represent the multi-model ensemble mean of selected climate models, and the spreads represent the range of selected climate models.	47
Figure 5.3: Spatial distribution of the projected changes in temperature ($^{\circ}\text{C}$), precipitation (mm month^{-1}), potential evapotranspiration (PET, mm month^{-1}) and evapotranspiration (ET, mm month^{-1}) over the Vaal River basin at different global warming levels (GWL1.5, GWL2.0, GWL2.5, and GWL3.0). The vertical strip () indicates where at least 80% of the simulations agree on the sign of the changes, while the horizontal strip (–) indicates where at least 80% of the simulations agree that the projected change is statistically significant (at 99% confidence level). The cross (+) shows where both conditions are satisfied, hence the change is robust.	49

Figure 5.4: Same as Figure 5.3, except for ET/PET (%), soil water (mm month ⁻¹), surface runoff (Runoff, m ³ s ⁻¹) and percolation (mm month ⁻¹).	50
Figure 5.5: Same as Figure 5.3, but for channel variables: precipitation (mm month ⁻¹), stream ET (mm month ⁻¹), and streamflow (m ³ s ⁻¹).	51
Figure 5.6: Impacts of LULC changes on hydrological variables over the Vaal River basin: CN (unitless), soil water (mm month ⁻¹), surface runoff (Runoff, m ³ s ⁻¹) and streamflow (m ³ s ⁻¹). The vertical strip () indicates where at least 80% of the simulations agree on the sign of the changes, while the horizontal strip (–) indicates where at least 80% of the simulations agree that the projected change is statistically significant (at 99% confidence level). The cross (+) shows where both conditions are satisfied, hence the change is robust.	52
Figure 5.7: A comparison of the impacts of climate change (CChange) and LULC change (FrLand, GrLand, CrLand, and CrGrLand) on hydrological variables: ET, ET/PET, soil water (SW), percolation (PERC), Runoff, water yield (WYLD), and streamflow (SFlow) over the Vaal River basin at different global warming levels (GWL1.5, GWL2.0, GWL2.5 and GWL3.0). The present-day climatological value for each variable is indicated in brackets.	55
Figure 5.8: A comparison of the impacts of climate change (CChange) and LULC change (FrLand, GrLand, CrLand, and CrGrLand) on the frequency of droughts (SPEI, SPI, SWI, PERCI, RFI, WYLDI and SFI) over the Vaal River basin at different global warming levels (GWL1.5, GWL2.0, GWL2.5 and GWL3.0). The present-day climatological value for each variable is indicated in brackets.	56
Figure 6.1: The LULC patterns used in the LULC change experiments for the Limpopo River basin: (a) CtrLand, (b) FrLand (c) GrLand (d) CrLand and (e) CrGrLand. The land-use types are urban residential medium density (URMD), cropland/dryland and pasture (CRDY), cropland/grassland mosaic (CRGR), cropland/woodland mosaic (CRWO), grassland (GRAS), shrubland (SHRB), savanna (SAVA), forest – deciduous broadleaf (FODB), forest – evergreen broadleaf (FOEB), forest – mixed (FOMI), water (WATR), and Bare ground/sparse vegetation (BSVG). The percentage of each LULC type is indicated in brackets.....	60
Figure 6.2: Temporal variation of the changes in hydroclimatic variables over the Limpopo River basin in the period 1971-2099 under the RCP8.5 climate scenario. The changes are calculated with reference to the present-day climate (1971-2000). The solid lines represent the multi-model ensemble mean of selected climate models, and the spreads represent the range of selected climate models.	61
Figure 6.3: Spatial distribution of the projected changes in temperature (°C), precipitation (mm month ⁻¹), potential evapotranspiration (PET, mm month ⁻¹) and evapotranspiration (ET, mm month ⁻¹) over the Limpopo River basin at different global warming levels (GWL1.5, GWL2.0, GWL2.5, and GWL3.0). The vertical strip () indicates where at least 80% of the simulations agree on the sign of the changes, while the horizontal strip (–) indicates where at least 80% of the simulations agree that the projected change is statistically significant (at 99% confidence level). The cross (+) shows where both conditions are satisfied, hence the change is robust.	62

Figure 6.4: Same as Figure 6.2, except for ET/PET (%), soil water (mm month ⁻¹), surface runoff (Runoff; m ³ s ⁻¹) and percolation (mm month ⁻¹).....	63
Figure 6.5: Same as Figure 6.3, but for channel variables: precipitation (mm month ⁻¹), stream ET (mm month ⁻¹), and streamflow (m ³ s ⁻¹).	65
Figure 6.6: Impacts of LULC changes on hydrological variables over the Limpopo River basin: CN (unitless), soil water (mm month ⁻¹), surface runoff (Runoff, m ³ s ⁻¹) and streamflow (m ³ s ⁻¹). The vertical strip () indicates where at least 80% of the simulations agree on the sign of the changes, while the horizontal strip (–) indicates where at least 80% of the simulations agree that the projected change is statistically significant (at 99% confidence level). The cross (+) shows where both conditions are satisfied, hence the change is robust.	66
Figure 6.7: A comparison of the impacts of climate change (CChange) and LULC change (FrLand, GrLand, CrLand, and CrGrLand) on hydrological variables: ET, ET/PET, soil water (SW), percolation (PERC), Runoff, water yield (WYLD), and streamflow over the Limpopo River basin at different global warming levels. The present-day climatological value for each variable is indicated in brackets.	67
Figure 6.8: A comparison of the impacts of climate change (CChange) and LULC change (FrLand, GrLand, CrLand, and CrGrLand) on the frequency of droughts (SPEI, SPI, SWI, PERCI, RFI, WYLDI and SFI) over the Limpopo River basin at different global warming levels (GWL1.5, GWL2.0, GWL2.5 and GWL3.0). The present-day climatological value for each variable is indicated in brackets.	68
Figure 7.1: The LULC patterns used in the LULC change experiments for Western Cape River basins: (a) CtrLand (b) FrLand, (c) SrLand (d) CrLand (e) GrLand. The land-use types are urban residential medium density (URMD), cropland/dryland and pasture (CRDY), cropland/grassland mosaic (CRGR), cropland/woodland mosaic (CRWO), grassland (GRAS), shrubland (SHRB), savanna (SAVA), forest – deciduous broadleaf (FODB), forest – evergreen broadleaf (FOEB), forest – mixed (FOMI), water (WATR), bare ground/sparse vegetation (BSVG). The percentage of each LULC type is indicated in brackets.	72
Figure 7.2: Temporal variation of the changes in hydroclimatic variables over the Western Cape River basins in the period 1971-2099 under the RCP8.5 climate scenario. The changes are calculated with reference to the present-day climate (1971-2000). The solid lines represent the multi-model ensemble mean of selected climate models, and the spreads represent the range of selected climate models.	74
Figure 7.3: Spatial distribution of the projected changes in temperature (°C), precipitation (mm/ month ⁻¹), potential evapotranspiration (PET, mm month ⁻¹) and evapotranspiration (ET, mm month ⁻¹) over the Western Cape River basins at different global warming levels (GWL1.5, GWL2.0, GWL2.5, and GWL3.0). The vertical strip () indicates where at least 80% of the simulations agree on the sign of the changes, while the horizontal strip (–) indicates where at least 80% of the simulations agree that the projected change is statistically significant (at 99% confidence level). The cross (+) shows where both conditions are satisfied, hence the change is robust.	76

Figure 7.4: Same as Figure 7.3, except for ET/PET (%), soil water (mm month ⁻¹), surface runoff (Runoff, m ³ s ⁻¹) and percolation (mm month ⁻¹).	78
Figure 7.5: Same as Figure 7.3, but for channel variables: precipitation (mm month ⁻¹), stream ET (mm month ⁻¹), and streamflow (m ³ s ⁻¹).	79
Figure 7.6: Impacts of LULC changes on hydrological variables over the Western Cape River basins: CN (unitless), soil water (mm month ⁻¹), surface runoff (Runoff, m ³ s ⁻¹) and streamflow (m ³ s ⁻¹). The vertical strip () indicates where at least 80% of the simulations agree on the sign of the changes, while horizontal strip (–) indicates where at least 80% of the simulations agree that the projected change is statistically significant (at 99% confidence level). The cross (+) shows where both conditions are satisfied, hence the change is robust.	80
Figure 7.7: A comparison of the impacts of climate change and LULC change (FrLand, SrLand, CrLand, and GrLand) on hydrological variables: ET, ET/PET, soil water (SW), percolation (PERC), Runoff, water yield (WYLD), and streamflow over the Western Cape River basin at different global warming levels. The present-day climatological value for each variable is indicated in brackets.	83
Figure 7.8: A comparison of the impacts of climate change (CChange) and LULC change (FrLand, GrLand, CrLand, and CrGrLand) on the frequency of droughts (SPEI, SPI, SWI, PERCI, RFI, WYLDI and SFI) over the Western Cape River basins at different global warming levels (GWL1.5, GWL2.0, GWL2.5 and GWL3.0). The present-day climatological value for each variable is indicated in brackets.	85

List of Tables

Table 2.1: The CMIP5 GCM simulations used in the study and the corresponding 30-year period for various GWLs (1.5°C, 2°C, 2.5°C and 3.0°C) under the RCP8.5 scenario. All the GCM simulations were downscaled with the RCA4 model in the CORDEX (Déqué et al., 2017) and bias-corrected.....	9
Table 2.2: The description of drought indices used to characterise meteorological, and hydrological droughts in study. All of the indices were calculated with monthly data at a 12-month scale.....	10
Table 2.3: Classification of drought indices (for SPI, SPEI, SWI, RFI, SFI, WYLDI, and PERCI). The definitions of the drought indices are summarised in Table 2.2.....	11
Table 2.4: Characteristics of empirical, conceptual, and physically based models.....	13
Table 2.5: Primary differences of functionalities between SWAT and SWAT+.....	16
Table 3.1: Simulations used in the calibration and validation experiments over the selected river basins (VRB, LRB, and WRB). The indicated simulation periods begin after a five-year model spin-up.....	19
Table 3.2: Selected model parameters for the SWAT+ calibration and their associated best values based on IPEAT+ optimisation using a range of $\pm 30\%$ change in the default values.....	23
Table 5.1: Summary of LULC change experiments in the Vaal River basin.....	44
Table 6.1: Summary of LULC change experiments in the Limpopo River basin.....	59
Table 7.1: Summary of LULC change experiments in the Western Cape River basins.....	71

List of Acronyms

Acronyms	Meaning
ACRU	ACRU (Agricultural Catchments Research Unit)
BrLand	Barren land restoration
BSN	Define acronym
BSVG	Bare ground/sparse vegetation
BUHI	Botswana Upper High Influence
CMIP5	Coupled Model Intercomparison Project Phase 5
CN	Curve Number
CORDEX	COordinated Regional Downscaling EXperiment
CRDY	Dry cropland and pasture
CRGR	Cropland/grassland mosaic
CrGrLand	Crop and grassland restoration
CrLand	Cropland restoration
CRWO	Cropland/woodland mosaic
CtrlLand	Control experiment
CWB	Climate Water Balance
DEM	Digital Elevation Model
DWAF	Department of Water Affairs
DWS	Department of Water and Sanitation
ET	Evapotranspiration
FAO	Food and Agriculture Organization
FODB	Deciduous broadleaf forest
FOEB	Evergreen broadleaf forest
FOMI	Mixed forest
FrLand	Forest restoration land
FWI	Fire Weather Index
GCM	Global Climate Model

GIS	Geographical Information System
GMFD	Global Meteorological Forcing Dataset
GNP	Gross National Product
GRAS	Grassland
GrLand	Grassland restoration
GW	Ground Water
GWLs	Global Warming Levels
HG	Hargreaves Method
HRUs	Hydrological Response Units
IPEAT+	Integrated Parameter Estimation and Uncertainty Analysis Tool Plus
ITCZ	InterTropical Convergence Zone
LRB	Limpopo River basin
LULC	Land use/land cover
MBC	Multivariate bias-correction
NCEP/NCAR	National Centers for Environmental Prediction-National Center for Atmospheric Research
NSE	Nash-Sutcliffe Efficiency
PBIAS	Percent Bias
PERCI	Percolation Index
PET	Potential evapotranspiration
PM	Penman-Monteith
QDM	Quantile Delta Mapping
R	Coefficient of Correlation
RCA4	Rosby Centre Regional Climate Model 4
RCM	Regional Climate Model
RCP	Representative Concentration Pathway
RFI	Runoff Index
RMSE	Root Mean Square Error
SADC	Southern African Development Community
SAVA	Savanna

SFI	Streamflow Index, calculated based on streamflow
SHRB	Shrubland
SOL	SWAT Soil Input
SPEI	Standardized Precipitation Evapotranspiration Index
SPI	Standardized Precipitation Index
SrLand	Shrubland restoration
SRM	Solar Radiation Management
SRTM	Shuttle Radar Topography Mission
SWAT	Soil and Water Assessment Tool
SWAT+	Soil and Water Assessment Tool Plus
SWI	Soil Water Index
TWT	Theewaterskloof
USDA-ARS	United States Department of Agriculture-Agricultural Research Service
UNESCO	United Nations Educational, Scientific and Cultural Organization
URMD	Urban residential medium density
USDA-ARS	United States Department of Agriculture-Agricultural Research
VRB	Vaal River basin
WATR	Water
WCRP	World Climate Research Program
WCWSS	Western Cape Water Supply System
WRB	Western Cape River basins
WYLDI	Water Yield Drought Index

Chapter 1: Introduction

1.1 Background

River basins form the backbone of socio-economic activities in South Africa because they provide water to support activities, such as agriculture, fisheries, livestock, forest products, mining, industry, power generation, and tourism. For instance, the Vaal River basin (VRB) accounts for more than 24% of the country's gross national product (GNP) and serves more than 45% of the nation's population (Braune and Rogers, 1987; DWAF, 2003). Through the storage of water in dams, this basin supports urban services and accommodates a range of water-based leisure activities like swimming, boating, water skiing, and yachting. The Limpopo River basin (LRB) accounts for 24% of national mining output, 7% of national agriculture, 6% of national construction, and 2% of national manufacturing (REB, 2016). Agricultural produce from the LRB makes up a huge portion of South Africa's national exports. The LRB also provides fertile soil for cultivating a variety of South African crops, like avocados, mangoes, papayas, tomatoes, and potatoes (Limpopo Business, 2017). A large proportion of the crops grown in this basin are high-value crops (e.g. citrus, bananas, and grapes), which are exported (Limpopo Business, 2017). The LRB is also home to 18% of the country's goats and 7% of the cattle and produces 6.8% of the country's eggs (Limpopo Business, 2017). The basin accommodates some of the world's largest thermal power generating stations, such as Medupi and Matimba, which is the largest direct dry-cooled power station in the world (Eskom, 2020). Furthermore, the LRB attracts tourists from around the world to see the majestic Victoria Falls and the Big Five in the Kruger National Park. The Western Cape River basins (WRB) also have rich soil for viticulture, fruit farming, and wheat cultivation, and support biodiversity that attracts both local and international tourists throughout the year. However, given ongoing rapid urbanisation and population growth, the water demand from these river basins (VRB, LRB, and WRB) is likely to escalate in the future. Hence, for sustainable development of socio-economic activities in South Africa, there is a need to ensure that these river basins are healthy.

1.2 Impacts of droughts on the river basins

Drought poses a direct threat to socio-economic activities in South Africa because of its devastating impacts on the river basins. Droughts, which usually stress water resources, pose a big challenge to water resource management and devastate the socio-economic activities of the riparian communities. For instance, in the 1980s, severe hydrological droughts reduced the streamflow in the VRB and resulted in the imposition of more than 30% water restrictions on urban and industrial use (Braune and Rogers, 1987). As part of measures to minimise the impacts of hydrological droughts in the basin, water transfer schemes (like the Lesotho Highlands Water Project and the Tugela-Vaal Water Transfer Scheme) have been developed to channel water into the Vaal River from other basins. In the 1990s, a severe drought destroyed crops in the LRB, induced a water shortage that affected millions of people and disrupted socio-economic activities in South Africa (Benson and Clay, 1998). The country suffered a GDP loss

of 1.8% (about US\$500 million) (Davis and Vincent, 2017). The South African region endured the lowest recorded annual rainfall of 403 mm and the hottest recorded temperatures over the last ten years (Davis and Vincent, 2017). In 2015-2016, the LRB experienced its worst drought since 1930 due to the strong 2015-2016 El Niño event. Dam levels in Limpopo were down to about 22% (Otter, n.d.) and the province was declared a drought disaster area. More recently, a severe drought that affected the WRB drastically reduced the dam water level in Cape Town (Africa's most attractive tourist city), leading to water restrictions for the millions of people in the city (Blamey et al., 2019; Odoulami et al., 2021; Omar and Abiodun, 2020; Sousa et al., 2018; Wolski, 2018). Hence, there is clearly a need for more studies on how to manage drought risks over these basins.

1.3 Climate change and droughts

Several studies have reported an increasing trend in drought activities (in terms of their severity, frequency, and persistence) in Africa over the last decades (Omar and Abiodun, 2020; Padrón et al., 2020; Spinoni et al., 2019) and attributed the trend to global warming (e.g. Bellprat et al., 2015; Funk et al., 2018; Otto et al., 2018; Pascale et al., 2020; Uhe et al., 2018). These trends may continue into the future (Abiodun et al., 2019; Cook et al., 2020; Spinoni et al., 2019). Dai et al. (2018) showed that the warming associated with climate change adds extra heat into the atmosphere, and that most of this heat goes into drying the continent. Hence, the warming would amplify the evaporative demand of the atmosphere, trigger natural droughts more quickly, and make such droughts more intense and longer-lasting. South Africa is projected to become generally drier under this warming, with an associated increase in dry spells and droughts (Abiodun et al., 2019; Abiodun et al., 2020; Cook et al., 2020; Dosio et al., 2019; Maúre et al., 2018). Abiodun et al. (2019) projected an increase in drought intensity and frequency over the major river basins in Southern Africa at various global warming levels (GWLs). Climate change would negatively impact water availability for crops and pastures, with a greater chance of failed harvests and reduced livestock feeds. In addition, the adequate provision of water for livestock production could become more difficult under climate change. Moreover, given ongoing rapid urbanisation and population growth, there is a concern that climate change may enhance the severity and impacts of hydrological droughts in the future. Hence, there is a need to quantify and minimise the potential impacts of climate change on hydrological droughts and on socio-economic activities.

1.4 Impacts of land-use/land-cover changes in the river basins

Land use/land cover (LULC) can have profound effects on the water cycle and water yield in a basin (e.g. Falkenmark et al., 1999; Koneti et al., 2018; Li et al., 2007 and 2018; Lumsden et al., 2003). The LULC changes, which influence hydrological processes, such as evapotranspiration, interception, and infiltration, can alter the partitioning of rainwater into surface and subsurface flows (Falkenmark et al., 1999). In addition, LULC changes can have both negative and positive impacts on water yield, depending on the type and degree of LULC changes (Lumsden et al., 2003). For example, while forestation may reduce runoff and decrease

streamflow, human settlement may enhance runoff and increase streamflow. Li et al. (2018) showed that an expansion of the built-up area in Jing-Jin-Ji (China) produced up to a 5.1% increase in total water yield. Setyorini et al. (2017) also showed that the conversion of forest to grassland, cropland, and urban area in the Upper Brantas basin (Indonesia) increased evapotranspiration, surface runoff, and streamflow, but decreased groundwater and lateral flow. Koneti et al. (2018) confirmed that urbanisation and the expansion of cropland at the expense of forest in the Godavari River basin (India) increased runoff and streamflow but decreased evapotranspiration and infiltration. All these studies agreed that the impacts of a LULC change depend on the biophysical characteristics of the LULC change. In general, an increase in vegetated land lowers water yield due to a higher rate of evapotranspiration and water infiltration, while an increase in bare land and built-up areas enhances water yield because of their impermeable surface. Li et al. (2007) shed light on this in their numerical study of West Africa. They showed that, while removal of vegetation (i.e. forest, grassland, and savanna) can increase water yield, this increase may be non-linear and may exhibit a threshold effect. Simply stated, below a certain threshold, the LULC changes may produce no significant impacts; but above the threshold, the impact may increase dramatically (Li et al., 2007). Nevertheless, while all these studies have documented how LULC changes can influence the hydrological cycles and water yield in a basin, there is still a dearth of information on how and to what extent LULC changes can be used to reduce the impacts of climate change on drought in river basins in South Africa. Such information will be valuable in formulating appropriate LULC policies to mitigate the impacts of climate change on water yields and hydrological droughts in the future.

1.5 Study aim and objectives

This study aims to examine and explore the extent to which land-use changes can be applied in reducing the impacts of climate change on hydrological droughts in three South African river basins, namely, the Vaal River basin (VRB), the Limpopo River basin (LRB) and the Western Cape River basins (WRB).

The objectives of this study are:

1. To calibrate, evaluate and apply a hydrological model over the selected river basins in South Africa.
2. To investigate the influence of bias correction in the climate simulation datasets on the quality of hydrological simulations over the river basins.
3. To project the impacts of future climate change on hydrological variables and drought characteristics in the river basins.
4. To explore and quantify the extent to which LULC changes can reduce impacts of droughts in the river basins.

1.6 Organisation of the report

Chapter 2 outlines the methodology of this study. This includes the description of the selected river basins, datasets, hydrological model (SWAT+), and analysis methods. Chapter 3 presents

the calibration and validation of the SWAT+ over the river basins. Chapter 4 provides an insight into how bias correction of climate variables influences the quality of hydrological simulation over the basins. Chapters 5 to 7 present the future projection of hydrological variables and droughts over the river basins and show how various land-use changes can influence these projections. Chapter 8 provides concluding remarks and recommendations for further research.

Chapter 2: Methodology

2.1 Introduction

This chapter gives a compressive description of the methodology of the. It describes the study domain, research datasets, and analysis methods used in the subsequent chapters (3 to 7). However, the methods described here are those used for analysis in two or more of the chapters. The methods that are unique to a chapter are discussed in the chapter.

2.2 Study domain

The focus of this study is on three river basins in South Africa, namely: the Vaal River basin (VRB), the Limpopo River basin (LRB) and the Western Cape River basins (WCRB). These basins were chosen because of their economic importance coupled with their vulnerability to droughts. They are all renowned drought hot-spots in Southern Africa.

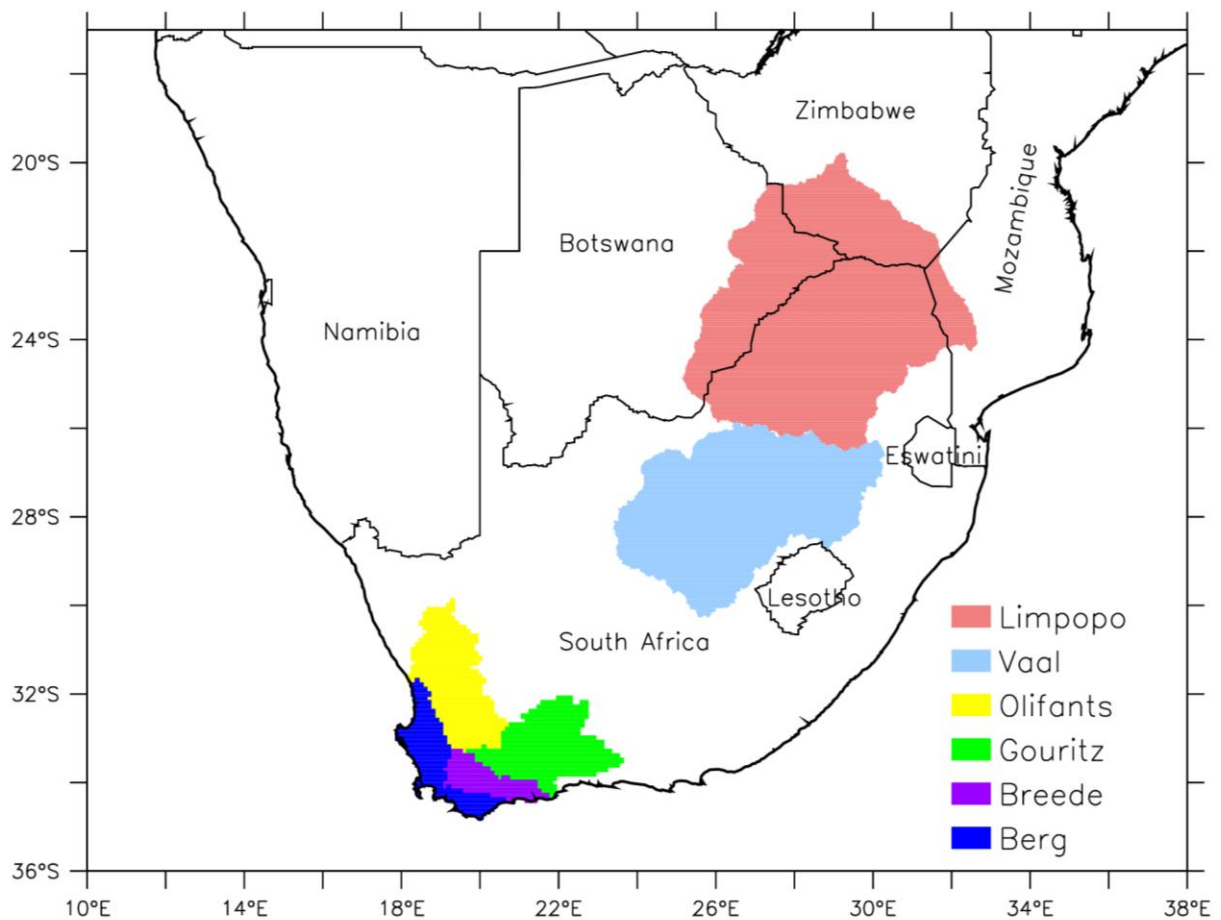


Figure 2.1: Map of Southern Africa, showing the location of the basins used in the study: the Vaal River basin, the Limpopo River basin and the Western Cape River basins (Olifants, Gouritz, Breede and Berg).

2.2.1 The Vaal River basin

The Vaal River basin (26°-30° S, 23.5°-30° E; VRB), located in the north-east of South Africa (Fig. 2.1), is the heartbeat of many socio-economic activities in South Africa. The Vaal River, perceived to be the most ‘hardworking’ river in South Africa (Otieno et al., 2009; Van Vuuren, 2008), meanders through the economic heartland of the water-stressed country to provide water for industries, mining, irrigation, power generation, and about 12 million people (DWAF, 2003). As a result, it accounts for more than 24% of the country’s GNP and serves more than 45% of the nation’s population (Braune and Rogers, 1987; DWAF, 2003). Through storage of water in dams, the river provides about USD100 billion/year support to urban services and agricultural production (Jury, 2016), in addition to accommodating a range of water-based leisure activities (like swimming, boating, water skiing, and yachting) that attract local and international tourists throughout the year. It also serves as a hub for several inter-basin water transfers. Nevertheless, the streamflow in the Vaal River is highly erratic due to large rainfall variability and excessive evaporation, which often induce hydrological droughts in the basin.

The VRB covers an area of about 196,000 km², and the river itself is about 1300 km long, flowing westward from its source in the Mpumalanga Province (at Ermelo – 26.5° S, 30.0° E – on the western slopes of the Drakensberg range) to join the Orange River (near Douglas – 29.1° S, 23.8° E), which flows into the Atlantic Ocean. The main tributaries of the river originate near the Eastern Escarpment Mountains. The major dams along the Vaal River include the Vaal Dam (2200 million m³ at 26.9° S, 28.1° E) and the Bloemhof Dam (1200 million m³ at 27.7° S, 25.7° E). The climate of the basin is subtropical dry savanna with the mean annual evaporation (about 1300 mm) exceeding the annual precipitation (about 600 mm) (Jury, 2016). The precipitation varies from about 1000 mm in the east to about 300 mm in the west (Akanbi et al., 2021). Its annual mean temperature is about 15°C, ranging from 9°C in August to 24°C in January (Akanbi et al., 2021). The dominant land cover in the basin is grassland (54%), cropland/grassland mosaic (29.3%), and cropland (18%) with a trace of savanna (3.4%). The predominant land use is agriculture, of which dry-land commercial cultivation is the largest practice. Although the Vaal River is the most developed and most regulated river in South Africa, hydrological drought poses a big challenge to water resource management in the basin. For instance, in the 1980s, severe hydrological droughts reduced the streamflow in the basin and resulted in the imposition of more than 30% water restrictions on urban and industrial use (Braune and Rogers, 1987).

2.2.2 The Limpopo River basin

The Limpopo River basin (25° E – 35° E, 19° S – 27° S; LRB), located in the south-east of Southern Africa, is one of the most economically important river basins in Southern Africa (Figure 2.1). This complex transboundary basin sustains 18.8 million people across four adjoining riparian countries (South Africa, Botswana, Mozambique, and Zimbabwe) and supports the economies of these nations (Merz et al., 2020; Trambauer et al., 2015). It also contributes to the economy of the entire Southern African Development Community (SADC)

region by supporting a wide range of socio-economic activities, such as mining, industry, agriculture, and tourism.

The LRB drains an area of approximately 415 000 km², and the river itself extends more than 1750 km in length. The topography of the LRB ranges from about 2300 m above sea level (m.a.s.l) in the highveld regions in South Africa to less than 7 m.a.s.l on the vast floodplains of the Mozambican part of the catchment. The basin comprises generally level or undulating fields between ranges of hills and mountains. The exceptions to the generally flat landscape are the northward streaming tributaries of the Limpopo, which are found in the mountainous regions of South Africa, including the Waterberg, Strydpoort Mountains, and the Drakensberg range in the south-eastern part of the basin. The climate of the LRB varies considerably, ranging from predominantly arid in the west to semi-arid and temperate in the central zones, to tropical rainy conditions along the coastal plain of Mozambique, and tropical dry savannah towards the Indian Ocean (Food and Agriculture Organization (FAO), 2004; Seibert et al., 2017; Trambauer et al., 2015). Rainfall over the basin is largely influenced by the movement of the InterTropical Convergence Zone (ITCZ), which gives rise to two distinct rainfall seasons. These include a warm wet season during the summer (December-February) and a cold dry season during winter (June-August). Temperatures over the basin range from 18°C to 34°C in summer and 5°C to 26°C in winter (Gyamfi et al., 2016). Evaporation over the basin is 1970 mm/year on average, with a range of 800 to 2400 mm/year (FAO, 2004). However, drought poses a big threat in the basin. For example, drought caused widespread crop destruction in the basin in 1992-1993 and induced massive agricultural and economic losses in the riparian countries.

2.2.3 The Western Cape River basins

The Western Cape Province (30° S – 35° S; 17° E – 25° E) lies in the southernmost part of South Africa (Figure 2.1). The economic activities in the province include manufacturing, construction, mining, and agriculture. The Western Cape River basins (WRB) consist of four river systems: the Breede (12,348 km²), Berg (7,715 km²), Gouritz (45,715 km²) and Olifants (46,220 km²). These river catchments are rich in biodiversity and have high ecological importance. The Breede and Berg, which are located entirely within the Western Cape, are arguably the most important of these. Six major dams within these two basins form part of the Western Cape Water Supply System (WCWSS). These networks of pump stations and pipelines are key, since they support industry and tourism in the Cape Town metropolitan area and supply drinking and domestic water for use in the City of Cape Town, as well as water for irrigation on surrounding farms (e.g. viticulture and fruit farming under irrigation and rain-fed wheat cultivation) (Statistics South Africa, 2010).

The climate conditions across the Western Cape are temperate Mediterranean with warm dry summers and mild moist winters. Average summer temperatures range from 15°C to 27°C, while winter temperatures range from 5°C to 22°C (Hurry and Van Heerden, 1982; Kruger, 2004; Tyson, 1986). The Western Cape is one of South Africa's driest regions, receiving only ~350 mm of rain annually, well below the national annual average of ~500 mm (Dennis and Dennis, 2012). Much of the rainfall occurs during the austral winter months (extending from

about May to September), and is typically received from cold fronts and associated extratropical cyclones, or occasional westerly disturbances, such as cut-off lows. Rainfall is, however, highly heterogeneous and varies considerably, from semiarid areas to relatively wet areas on the windward slopes of mountains (Blamey et al., 2019). Annual precipitation ranges from ~300 mm to more than 900 mm, although some areas receive extreme rainfall, i.e. as low as 60 mm and as high as 3345 mm (Botai et al., 2017). The Western Cape recently experienced one of the most severe droughts in its history. It was a multi-year drought, and rare in that it manifested across four drought classes: meteorological, agricultural, hydrological, and socio-economic. The drought was characterised by below normal rainfall over three consecutive years (2015-2017).

2.3 Data

Three types of datasets are used in this study, namely: the geographical information system (GIS), hydrological, and climate datasets. The GIS consists of the basin shapefile data, topography data (digital elevation model (DEM); 90-metre resolution; obtained from the Shuttle Radar Topography Mission (SRTM): <https://srtm.csi.cgiar.org>), soil type data (obtained from the Waterbase; <http://www.waterbase.org>), and LULC data (obtained from the Waterbase; <http://www.waterbase.org>). The GIS datasets are used to characterise the basin in the hydrological modelling. The hydrological dataset comprises a daily streamflow dataset obtained from the Department of Water and Sanitation (DWS) (<https://www.dws.gov.za/Hydrology/>). The streamflow data at the hydrological stations were utilised for the calibration and validation of the hydrological model over the basins.

The climate observation dataset is the Global Meteorological Forcing Dataset (GMFD), which is a combination of the global observational dataset and the National Centers for Environmental Prediction – National Center for Atmospheric Research (NCEP/NCAR) reanalysis dataset (Sheffield et al., 2006). The GMFD was developed for global land surface modelling at 1.0° high spatial resolution and at a 3-hourly time step between 1948 and 2000. We use GMFD daily data (precipitation, minimum temperature, maximum temperature, solar radiation, wind speed, and relative humidity) as climate input data in calibrating the hydrological model and in evaluating the climate simulation dataset.

The climate simulation dataset is from the COordinated Regional Downscaling EXperiment (CORDEX) (Giorgi et al., 2009). CORDEX was established by the World Climate Research Program (WCRP) to produce regional climate simulations worldwide. The CORDEX datasets used in this study comprise a 50 km resolution simulation from a regional climate model (RCM) called the Rossby Centre Regional Climate Model 4 (RCA4) that downscaled seven Coupled Model Intercomparison Project Phase 5 (CMIP5) (Taylor et al., 2012) Global Climate Model (GCM) simulations for past and future climates (Table 2.1). Detailed information about the downscaling is reported in Déqué et al. (2017). To minimise the systematic bias in the CORDEX dataset, we applied bias correction to the dataset using the Quantile Delta Mapping (QDM) technique (Cannon et al., 2015) as implemented in the QDM R-package (<https://rdrr.io/cran/MBC/man/QDM.html>). The bias-corrected CORDEX dataset

(seven-member ensemble) served as the input climate data for the hydrological model in simulating the past and future hydrology over the basin.

Table 2.1: The CMIP5 GCM simulations used in the study and the corresponding 30-year period for various GWLs (1.5°C, 2°C, 2.5°C and 3.0°C) under the RCP8.5 scenario. All the GCM simulations were downscaled with the RCA4 model in the CORDEX (Déqué et al., 2017) and bias-corrected.

GCMs	Period of Global Warming Levels (GWLs)			
	1.5°C	2°C	2.5°C	3°C
CanESM2	1999-2028	2012-2041	2024-2053	2034-2063
CNRM-CM5	2015-2044	2029-2058	2041-2070	2052-2081
CSIRO-Mk3-6-0	2018-2047	2030-2059	2040-2069	2050-2079
IPSL-CM5A-MR	2002-2031	2016-2045	2027-2056	2036-2065
MIROC5	2019-2048	2034-2063	2047-2076	2058-2087
MPI-ESM-LR	2004-2033	2021-2050	2034-2063	2046-2075
NorESM1-M	2019-2048	2034-2060	2047-2076	2059-2088

2.4 Methods

This section details the methods used in analysis data in the study. It starts describes the indices used to characterize meteorological and hydrological droughts and explains the bias-correction technique used in the study. It also gives a general description of hydrological modelling concepts and provide a detailed information on the hydrological model (SWAT+) used in the study.

2.4.1 Characterising droughts

We used seven standardised drought indices to characterise droughts (Table 2.2). The use of standardised indices has become increasingly popular in drought assessment since the introduction of the Standardized Precipitation Index (SPI) by McKee et al. (1993). A major advantage of standardised indices is their comparability among time, space, and variables. The calculation procedure is the same, independently of the input variable used (i.e. runoff, streamflow, or soil moisture). Meteorological drought is characterised using SPI and SPEI (Standardized Precipitation Evapotranspiration Index), while hydrological drought is identified using the SWI, RFI, SFI and WYLDI over the LRB. SPI is formulated by fitting long-term precipitation (P) records to a gamma probability density function, which is transformed to a normal distribution. The transformed probability gives the SPI values, which mainly vary from -2 to 2 (Mckee et al., 1993). Details of the equation formulation and calculation for the drought index are specified in previous studies (Edwards and McKee, 1997; McKee et al., 1993). Like

SPI, SPEI is a probability-based function calculated that uses climatic water balance data instead of precipitation data (Vicente-Serrano et al., 2010). The advantage of using SPEI is the inclusion of the atmospheric water demand, potential evapotranspiration (PET), which has been shown to play a crucial role in drought severity (Meque and Abiodun, 2014; Ujeneza and Abiodun, 2014). The climate water balance (CWB_i) for the month i is calculated as:

$$CWB_i = P_i - PET_i$$

Table 2.2: The description of drought indices used to characterise meteorological, and hydrological droughts in study. All of the indices were calculated with monthly data at a 12-month scale.

Drought indices	Description	Drought type
SPI	Standardized Precipitation Index, calculated based on precipitation	Meteorological drought
SPEI	Standardized Precipitation Evapotranspiration Index, calculated based on climate water balance (CWB) (precipitation minus potential evapotranspiration)	Meteorological drought
SWI	Soil Water Index, calculated based on soil moisture	Hydrological drought
RFI	Runoff Index, calculated based on surface runoff	Hydrological drought
SFI	Streamflow Index, calculated based on streamflow	Hydrological drought
WYLDI	Water Yield Index, calculated based on water yield	Hydrological drought
PERCI	Percolation Index, calculated based on percolation	Hydrological drought

In this study, PET was obtained using the Hargreaves method (HG; Hargreaves and Samani, 1985). However, the Penman-Monteith (PM) method is better suited for the calculation of PET, as it is based on fundamental physical principles. Due to its comprehensive theoretical base, the PM method is usually preferred for calculation of PET (Monteith, 1965). However, the PM method requires several climate variables (i.e. air temperature, relative humidity, solar radiation, and wind speed), for some of which there is no reliable data for the study region. Owing to its basis on fundamental physical principles, the PM method is better suited for the calculation of PET. However, the PM method requires several climate variables (air temperature, relative humidity, windspeed, and net radiation), which are available only for a

limited number of CORDEX simulations over the basin. Beguería et al. (2014) recommended the use of HG for calculating PET where the data is scarce to use the PM method. Similarly, the Runoff Index (RFI), Streamflow Index (SFI) and Soil Water Index (SWI) are essentially based on the methodology for calculating SPI, which involves fitting a distribution to the time series of runoff, streamflow or soil moisture and transforming it to a normal distribution. Input data for computation of RFI, SFI and SWI were derived from the hydrological SWAT+ model. The advantage of this parameter is that it offers the possibility of quantifying most of the hydrological components with high importance for water resource use systems. The classification for all the above-mentioned indices is outlined in Table 2.3.

Table 2.3: Classification of drought indices (for SPI, SPEI, SWI, RFI, SFI, WYLDI, and PERCI). The definitions of the drought indices are summarised in Table 2.2.

Drought indices values	Classification
2.00 and more	Extremely wet
1.50 to 1.99	Very wet
1.00 to 1.49	Moderately wet
0.00 to 0.99	Near normal
0.00 to -0.99	Mild drought
-1.00 to -1.49	Moderate drought
-1.50 to -1.99	Severe drought
-2.00 or more	Extreme drought

2.4.2 Bias correction of CORDEX simulation datasets

It is well known that climate models (global and regional) are viable tools for simulating climate systems. However, numerous studies have shown that the outputs of global and regional climate models can differ significantly from observational reference data (Maraun, 2016; Randall et al., 2007). Hence, the climate model outputs are usually bias corrected statistically before they are used in hydrological simulations (Ehret et al., 2012; Maraun, 2016). Bias correction (a method applied to statistically match climate simulations to observation data to better capture the local- and regional-scale features) is particularly useful in analyses of drought conditions. Some studies have shown how bias correction is important for climate model outputs that are intended to analyse future drought over the United States and over Australia (Johnson and Sharma, 2015). This is because bias correction may improve the consensus amongst climate models in ensemble simulations and/or moderate the future drought frequency associated with the climate change signal. For example, Mbaye et al. (2018) showed that climate simulations for extreme precipitation and temperature over the Senegal River basin are sensitive (in

magnitude) to bias correction. However, no studies have investigated the sensitivity of future climate projection over Southern Africa to bias correction.

Many empirical statistical techniques have been developed to downscale climate model outputs for impact studies. For hydrological impact studies, the QDM approach is a common and often recommended approach (Chen et al., 2013; Gudmundsson et al., 2012; Teutschbein and Seibert, 2012). The QDM approaches correct biases in the entire distribution of modelled variables such that the distribution of the modelled variables matches that of the observation data (Cannon, 2016). However, QDM approaches correct the climate variables independently from one another, thereby neglecting the spatial and inter-variable correlations, which may alter the quality of the corrections (Wilcke et al., 2013). Meanwhile, the interdependence of key climate variables, such as air temperature and precipitation, are important when modelling multivariate drought indices, such as SPEI (Cannon, 2016). Several studies have shown that, while univariate quantile mapping retains the inter-variable dependencies as represented by the raw climate model output data, it is however unable to capture the local interdependencies in observations (Wilcke et al., 2013).

To account for interdependencies, multivariate bias-correction (MBC) approaches have been developed to allow for the preservation of the interdependence of climate variables found in the target observation data throughout the bias-correction process (Cannon, 2016; Li et al., 2014). The MBC approach also corrects the biases in climate model outputs by adjusting marginal distribution, using quantile mapping that can preserve the dependence structure between multiple variables projected changes in simulated quantiles to a certain extent (Cannon, 2018). In applications that require multiple variables, it is desirable not just to correct the marginal distributions of the individual variables, but also to preserve and, if possible, correct the relationships between variables. For instance, Cannon (2018) presents a highly flexible multivariate bias-adjustment method and demonstrates its effectiveness on a modelled multivariate hazard indicator. By adjusting biases and dependencies between temperature, precipitation, relative humidity and wind speed, the method substantially reduces biases in the five-dimensional Fire Weather Index (FWI), outperforming univariate bias-adjustment approaches. Nevertheless, it is still largely unknown how widely used statistical bias-correction methods affect modelled impacts that depend on multiple drivers, such as the drought index SPEI. However, in this study, we used the QDM bias-correction method to correct the CORDEX dataset.

2.4.3 Hydrological modelling

Hydrological modelling is an act of using mathematical equations to represent complex hydrological processes with the aim of providing or predicting the spatial and temporal distribution of hydrological variables over large areas or basins. In other words, a hydrological model uses simplified equations to represent complex hydrological reality (Sorooshian et al., 2008). A hydrological model consists of various equations and parameters that describe the characteristics of the process represented by the model. For example, a runoff model consists of a set of equations that estimates runoff as a function of various parameters used to describe

watershed characteristics. The two most important inputs required for a hydrological model are rainfall data and drainage area, followed by watershed characteristics, like soil properties, vegetation cover, watershed topography, soil moisture content, and characteristics of the groundwater aquifer. As hydrological models are now considered an important and necessary tool for water and environment resource management, several hydrological models have been developed across the world, not only to understand and predict various hydrological processes, but also to study the impacts of climate, soil properties and land cover changes on hydrology and water resources (Devia et al., 2015). Hydrological models can be classified as empirical, conceptual, and physically based models. These classifications are described below and summarised in Table 2.4.

Table 2.4: Characteristics of empirical, conceptual, and physically based models.

Empirical model	Conceptual model	Physically based model
Data based or metric or black box model	Parametric or grey box model	Mechanistic or white box model
Involve mathematical equations, and derive value from available time series	Based on modelling of reservoirs, and include semi-empirical equations with a physical basis	Based on spatial distribution, evaluation of parameters describing physical characteristics
Little consideration of features and processes of system	Parameters are derived from field data and calibration	Require data about initial state of model and morphology of catchment
High predictive power, and low explanatory depth	Simple and can be easily implemented in computer code	Complex model, requiring human expertise and computation capability
Cannot be generated to other catchments	Require large hydrological and meteorological data	Suffer from scale related problems
Valid within the boundary of a given domain	Calibration involves curve fitting, making physical interpretation difficult	Valid for a wide range of situations

2.4.3.1 Empirical models

Empirical models are observation-oriented models. They are built only on information from existing data without considering the features and processes of the hydrological system. Hence, these models are called data-driven models. Their mathematical equations are derived from concurrent input and output time series and not from the physical processes of the catchment. A unit hydrograph is a good example of empirical models. For empirical models, statistically based methods (like regression and correlation) are used to find the functional relationship between inputs and outputs. Machine learning techniques (like artificial neural networks and fuzzy regression) can also be used to develop empirical models. The main shortcoming of these models is that they are only valid within the physical/geographical boundaries.

2.4.3.2 Conceptual models

Conceptual models describe all the component hydrological processes and consist of several interconnected reservoirs that represent the physical elements in a river basin. As in reality, the model catchments are recharged by rainfall, infiltration and percolation, and they are emptied by evaporation, runoff, drainage, etc. These models use semi-empirical equations. So, their model parameters are assessed not only from field data but also through calibration. Large numbers of meteorological and hydrological records are required for calibration of these models. The calibration involves curve fitting, which makes the interpretation difficult, and hence the effect of land-use change cannot be predicted with much confidence. However, many conceptual models are now being developed with varying degrees of complexity. The well-known Pitman model, developed at the Center for Water Resources Research, Rhodes University Rhodes in Grahamstown in South Africa (Hughes, et al., 2006), is a good example of a conceptual model.

2.4.3.3 Physically based models

The physically based model is a mathematically idealised representation of the real phenomenon. These are also called mechanistic models because they include the principles of physical processes. They use state variables, which are measurable and are functions of both time and space. The hydrological processes of water movement are represented by finite difference equations. Extensive hydrological and meteorological data is not required for their calibration, but the evaluation of many parameters describing the physical characteristics of the catchment is required (Abbott et al., 1986). In these models, a huge amount of data (such as soil moisture content, initial water depth, topography, topology, dimensions of river network, etc.) is required. Physically based models can overcome many defects of the other two types of models (i.e. empirical and conceptual models) because their parameters can have physically interpreted. In addition, they can provide large amounts of information even outside the boundary, and they can be applied to a wide range of situations. Examples of these models include the ACRU model, Department of Agricultural Engineering at the University of KwaZulu-Natal, Pietermaritzburg, Republic of South Africa (Schulze, 1995). A physically based model (called SWAT+) was used for the present study.

2.4.4 Description of the hydrological model: SWAT+

The hydrological model used in the study is called the SWAT+ model. The SWAT+ is an improved version of the Soil and Water Assessment Tool (SWAT). The SWAT model is a spatially distributed, continuous-time and process-based hydrological model for performing a wide variety of watershed-scale applications. The SWAT model, well known for providing scientifically credible solutions, was developed by the United States Department of Agriculture-Agricultural Research Service (USDA-ARS) in the early 1990s. This model is made up of several components, with major ones including weather, hydrology, soil temperature and properties, plant growth, nutrients, pesticides, bacteria and pathogens, and land management (Arnold et al., 2012). Hence, it can be used to simulate hydrological (e.g. surface and subsurface flows), sediment, and nutrient/pesticide processes. Changing management practices can be reasonably simulated by many governing functions. SWAT simulates processes based on sub-basins, which are further divided into Hydrological Response Units (HRU). The HRU represents an area of homogenous land use, management, and soil characteristics of the sub-basin. In HRUs, designated land use, soil type, and slope information can be grouped into files for each sub-basin. The results from the HRU are scaled to cover the whole respective sub-basin. The generalisation is a process during which HRU influences the results, but also enables the model to simulate large areas, while still maintaining detailed physical processes. All calculations and flow routings are performed on the basis of HRUs using daily time steps, even though the results can be outputted as monthly or yearly values. SWAT processes are simulated based on the water balance equation (Neitsch et al., 2005):

$$SW_t = SW_0 + \sum_{i=1}^t (R_{day\ i} - Q_{surf\ i} - E_{a\ i} - W_{seep\ i} - Q_{gw\ i}) \quad (1)$$

Where t is time in days, SW_t is the final moisture content of the soil, SW_0 is the initial moisture content of soil on day i , and R_{day} , Q_{surf} , E_a , W_{seep} , and Q_{gw} are daily amounts (mm) of rainfall, surface runoff, evapotranspiration, water transferred from the soil profile into the gas zone, and the return flow respectively. The water balance has direct impacts on plant growth and the movement of nutrients and sediments in the soil basin. Based on the goal of the present study, we will concentrate on the climate, hydrology, and vegetation components of the SWAT model.

The outputs at the HRU level are aggregated at the sub-basin level, and eventually delivered from the upstream to the downstream sub-basin via channel routing. This approach was useful back in the time when computational speed was still quite slow. Conversely, users can assign one HRU to each sub-basin, so that the SWAT project will be closer to a physically based model (instead of semi-physically-based), given modern computer technology.

The SWAT model has been applied globally to various subjects, such as the Great Lakes in the United States, the Yellow River basin in China, the Blue Nile basin in Africa, and the LRB in South Africa (Querner and Zanen, 2013). Although the SWAT model has become widely used across the globe, many studies have also revealed limitations and identified specific model development needs. Numerous additions and modifications of the model and its individual

components have made the code increasingly difficult to manage and maintain. To face present and future challenges in water resources modelling, the SWAT code has thus undergone major modifications over the past few years, resulting in SWAT+, which is a completely revised version of the model.

The SWAT+ model, the new generation of the SWAT model, was developed to make the model more flexible and advanced. The major improvement of SWAT+ over SWAT is that the model has been reconstructed in the form of independent modules (objects), so that it is much easier in terms of model maintenance and the corresponding development as well. In addition to modularisation, there are also some key developments to enhance the performance of the model. For example, new functionalities of aquifers and reservoir operation rules are available in SWAT+. Aquifers used to be controlled exclusively in HRUs. Now the corresponding aquifer boundaries can be defined flexibly without following the limitations of HRUs. Reservoir functions were one of the primary problems of the SWAT model. Reservoir releases may play a significant role in watershed responses. With SWAT+, users can now assign detailed operation rules effortlessly so that reservoir simulation outputs can be much closer to actual operational routines. The primary differences between the SWAT+ and SWAT models are summarised in Table 2.5. There are other spatial modules with designated functions: (i) outlets can be used to add/remove water from the watershed; (ii) canal; can be used to conduct water diversion among irrigation regions; (iii) pumps can be extracted from any aquifer to a specified spatial object; (iv) herds can be applied to biomass and the associated grazing conditions; and, (v) water rights can be assigned according to different shares of water demand. More details can also be found in Arnold et al. (2012). The SWAT+ model is thus utilised for this study.

Table 2.5: Primary differences of functionalities between SWAT and SWAT+.

Category	SWAT+	SWAT
Calibration Support	Users can manually calibrate SWAT+ by using calibration.cal	Not Supported
Reservoir Operation	Users can assign operation rules	Not Supported
Coding Flexibility	Easy to modify/upgrade modularised coding structure	Not Supported
Aquifer Boundary	Can be defined flexibly without limitations	Used to be linked with HRUs
Connectivity	Users can define individual watershed objects	Limited spatial flexibility

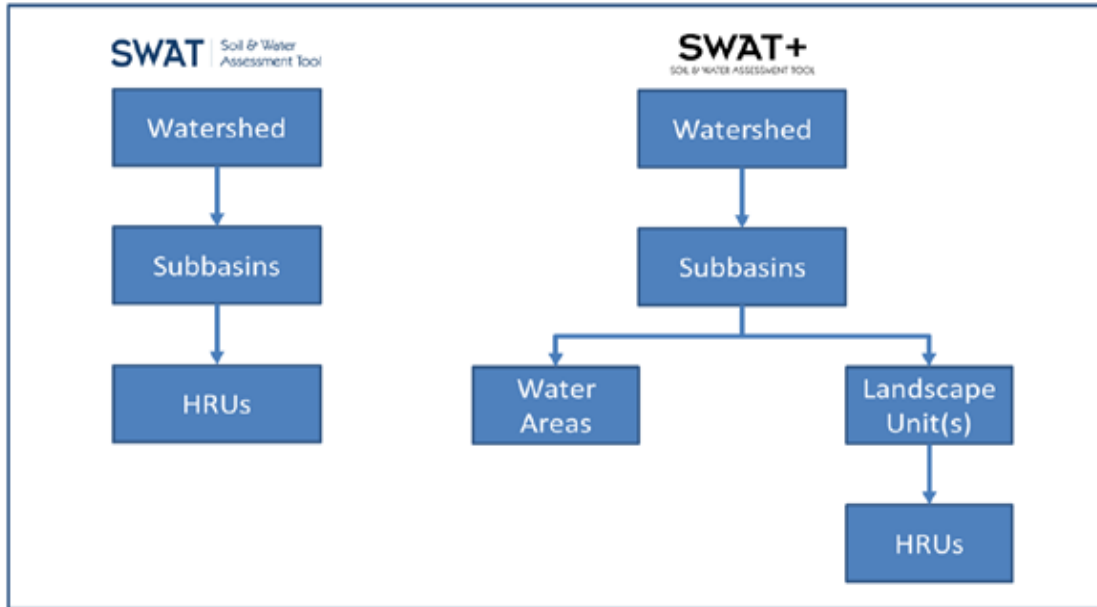


Figure 2.2: A comparison between catchment delineation in SWAT and SWAT+.

We developed and applied two hydro-climatological modelling systems to perform all the experiments in this report. The first system (hereafter, GMFD_SWAT+) couples the GMFD climate observation dataset with the SWAT+ hydrological model and the second system (hereafter, CORDEX_SWAT+) couples the CORDEX climate simulation dataset with the SWAT+ hydrological model. The GMFD_SWAT+ was used for automatic calibration and validation of SWAT+ over the river basins (see Chapter 3). After the calibration, the results of GMFD_SWAT+ were used as the reference for evaluating CORDEX_SWAT+ over the basins (see Chapter 4). The CORDEX_SWAT+ was used to study the influence of bias correction on CORDEX datasets on hydrological simulation over the basins (Chapter 4) and to investigate the impacts of climate change and land-use changes on hydrological droughts over the basins (see Chapters 5, 6 and 7).

2.5 Summary

The chapter has provided information on the study domain (which comprises of three prominent river basins in South Africa: VRB, LRB and WRB) and described the various datasets (i.e. QGIS, hydrological, and climate data) analysed in the study. It has also provided a comprehensive description of the research methods (i.e. drought indices definitions, bias-correction techniques, hydrological modelling concepts and SWAT+ model) that cut across the subsequent chapters. However, it does not cover research methods that are peculiar to a particular chapter; those methods will be presented in the concerned chapter.

Chapter 3: Calibration and validation of hydrological model (SWAT+) over the river basins

3.1 Introduction

Before applying any hydrological model for studies over a particular basin, it is essential to calibrate and validate the model. Model calibration is the process of estimating model parameter values to enable a hydrological model to match observations as much as possible. Model validation is the process of demonstrating that a given site-specific model can make sufficiently accurate simulations (Arnold et al., 2012; Refsgaard, 1997). Validation ensures that the set of calibrated parameters performs reasonably well under an independent dataset, i.e. without any further adjustment at different spatial and temporal scales (Neitsch et al., 2002). This chapter reports our calibration and validation of the SWAT+ model over the three selected river basins.

3.2 Calibration and validation experiments

Over each basin, the SWAT+ was set up to perform two experiments (viz., calibration and validation experiments). The details about simulation setup and time periods for the experiments are provided in Table 3.1. Any SWAT+ simulation requires both the GIS data (topography, soil type, LULC type) and the climate data (temperature, rainfall, humidity, solar radiation, and wind speed). The GIS data used for the SWAT+ calibration and validation over the VRB, LRB and WRB are shown in Figures 3.1, 3.2 and 3.3, respectively. The GMFD dataset was used as the climate input data. Information about the GIS and GMFD datasets is provided in Chapter 2.

Calibration of SWAT+ can be difficult or impossible over large-scale basins like our selected basins. However, the SWAT+ has an auto-calibration tool called IPEAT+ (Integrated Parameter Estimation and Uncertainty Analysis Tool Plus) (Yen et al., 2019) to assist in optimising the calibration process. The IPEAT+ algorithm is very efficient in obtaining the best values for selected model parameters in SWAT+ over a basin with any objective function (Yen et al., 2019). For a quick convergence of the SWAT+ calibration (i.e. to obtain the best model parameter values fast), we used IPEAT+ to run SWAT+ 300 times (i.e. to perform 300 simulations) using ten model parameters (Table 3.2) that changed within $\pm 30\%$ of default values. The 1-NSE (Nash-Sutcliffe model efficiency coefficient) was used as the objective function. Although the calibration converges within the first 150 simulations over the basin, we used 300 simulations to ensure a full convergence (Yen et al., 2019). The best values obtained for the selected model parameters over the basins are shown in Table 3.2. These values were used in the remaining experiments in this report. In the validation experiment, the SWAT+ was applied to perform one simulation over the validation period. The calibration and validation periods vary over the basins because they depend on the availability of reliable streamflow data at the hydrological stations in the basins. The standard statistics metrics [such as Nash-Sutcliffe model efficiency coefficient (NSE), Percentage Bias (PBIAS), Root Mean Square Error

(RMSE), Coefficient of Correlation (R)] were employed in evaluating the simulations during the calibration and validation periods. The results of the calibration and validation experiments are presented and discussed for each basin in the following sections.

Table 3.1: Simulations used in the calibration and validation experiments over the selected river basins (VRB, LRB, and WRB). The indicated simulation periods begin after a five-year model spin-up.

Simulation domain and periods			
Domain	VRB (Figure. 3.1)	LRB (Figure. 3.2)	WRB (Figure. 3.3)
Experiment			
• Calibration	1971-1980	1988-1998	1980-1990
• Validation	1981-2000	1999-2009	1991-2005

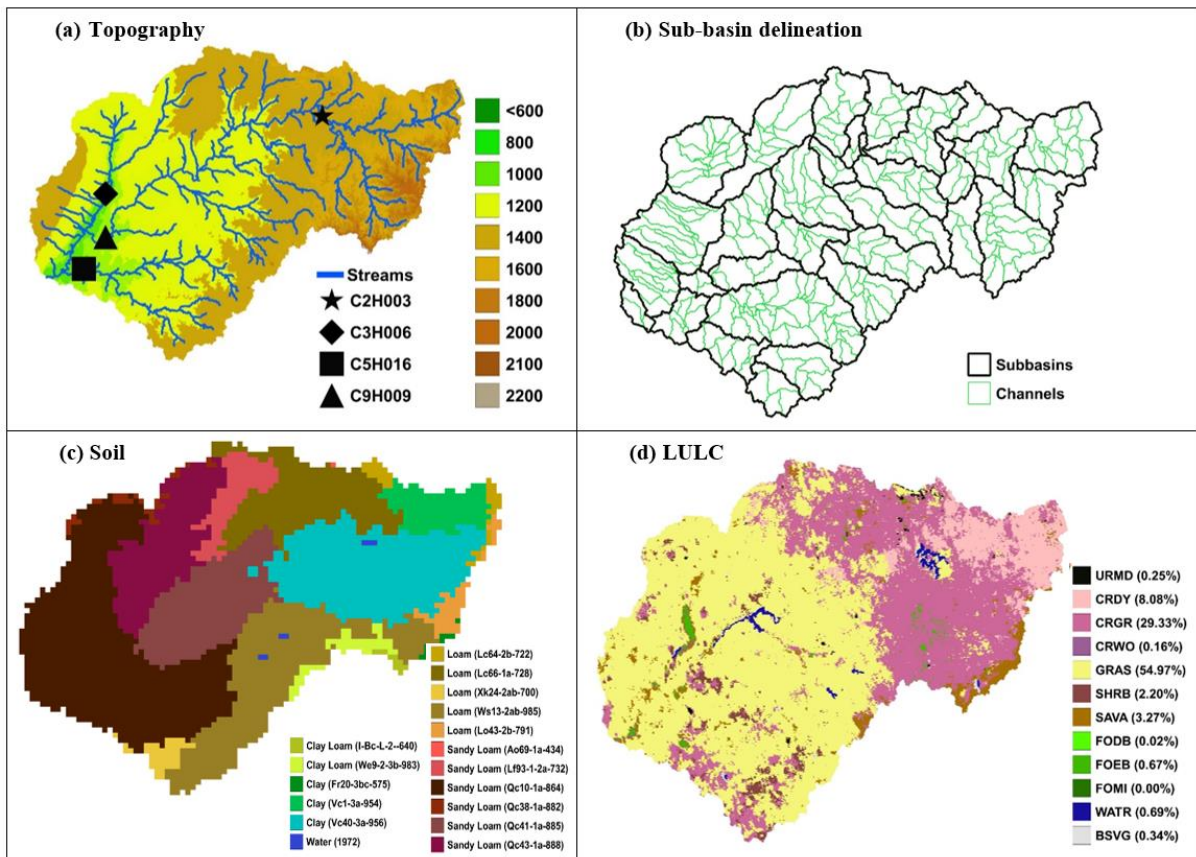


Figure 3.1: The characteristics of the Vaal River basin used in the study: (a) the topography of the region (i.e. DEM), streams, streamflow observation stations (i.e. C2H007, C9H009, C5H016 and C2H003); (b) the SWAT+ delineation of the basin to sub-basins and channels; (c) soil types and (d) LULC types: Urban residential medium density (URMD), Dry cropland and pasture (CRDY), Cropland/grassland mosaic (CRGR), Cropland/woodland mosaic (CRWO), Grassland (GRAS), Shrubland (SHRB), Savanna (SAVA), Deciduous broadleaf forest (FODB), Evergreen broadleaf forest (FOEB), Mixed Forest (FOMI), Water (WATR), and Bare ground/sparse vegetation (BSVG). The percentage of each LULC type is indicated in brackets.

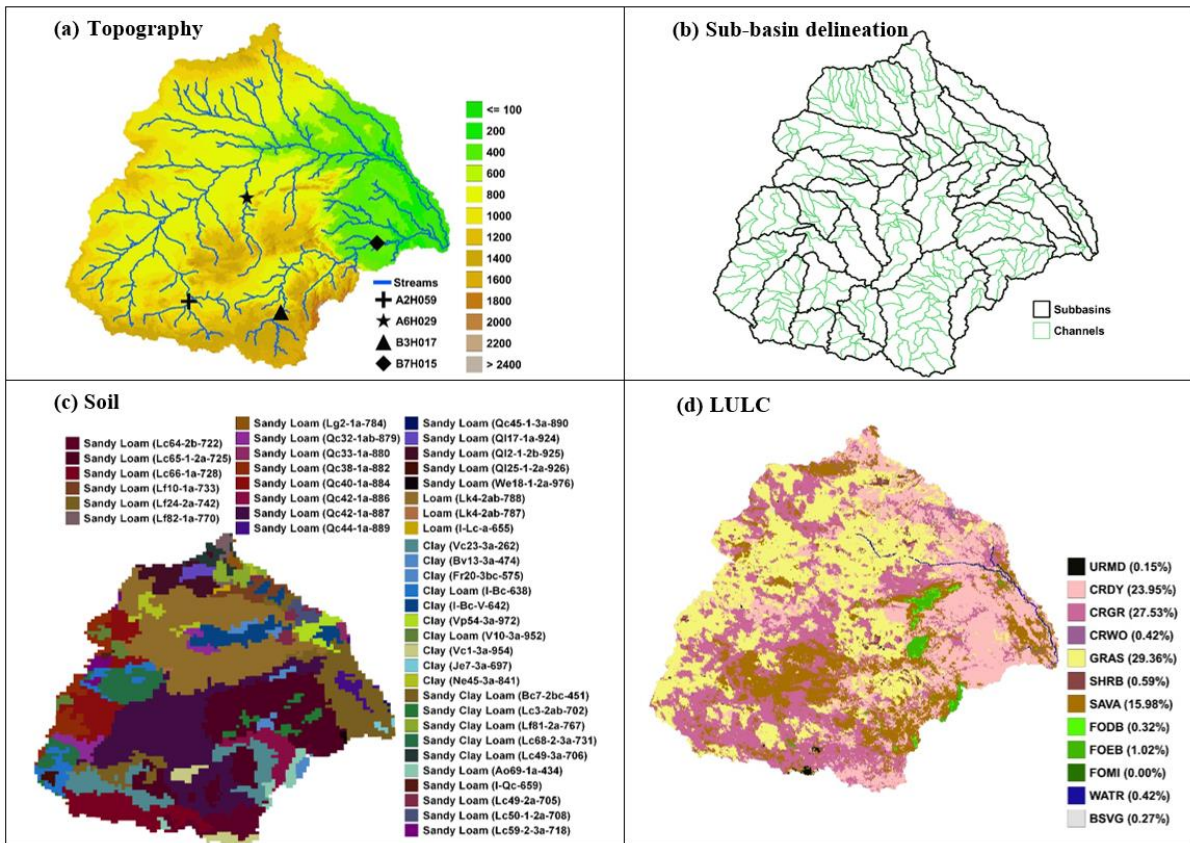


Figure 3.2: The characteristics of the Limpopo River basin used in the study: (a) the topography of the region (i.e. DEM), streams, streamflow observation stations (i.e. A2H059, A6H029, B3H017 and B7H015); (b) the SWAT+ delineation of the basin to sub-basins and channels; (c) soil types and (d) LULC types: Urban residential medium density (URMD), Dry cropland and pasture (CRDY), Cropland/grassland mosaic (CRGR), Cropland/woodland mosaic (CRWO), Grassland (GRAS), Shrubland (SHRB), Savanna (SAVA), Deciduous broadleaf forest (FODB), Evergreen broadleaf forest (FOEB), Mixed forest (FOMI), Water (WATR), Bare ground/sparse vegetation (BSVG). The percentage of each LULC type is indicated in brackets.

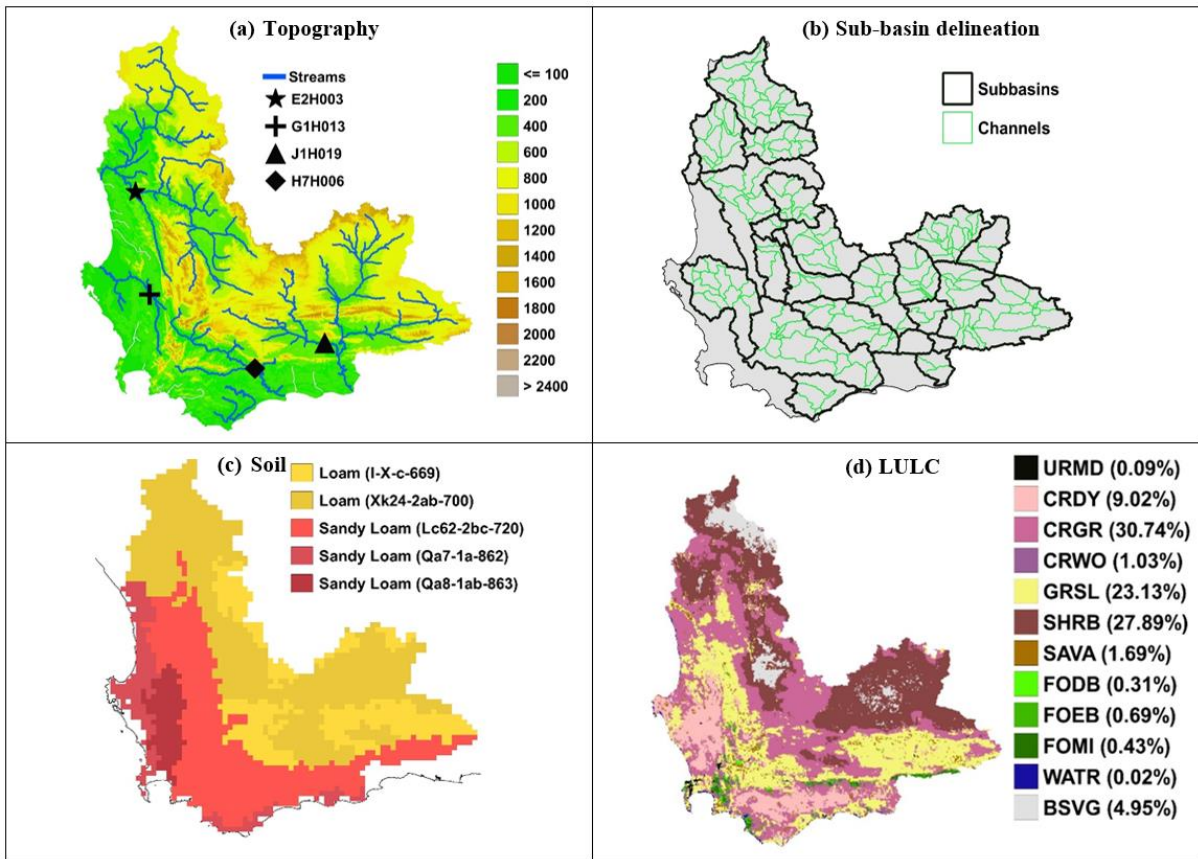
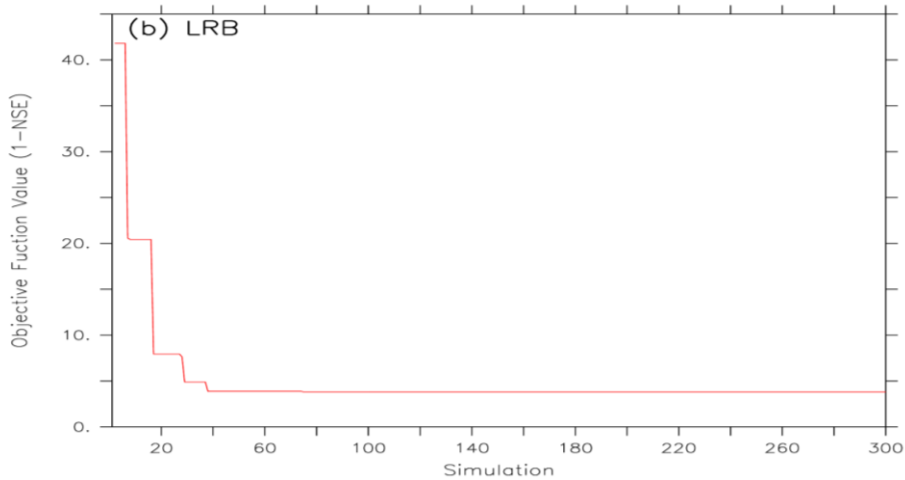
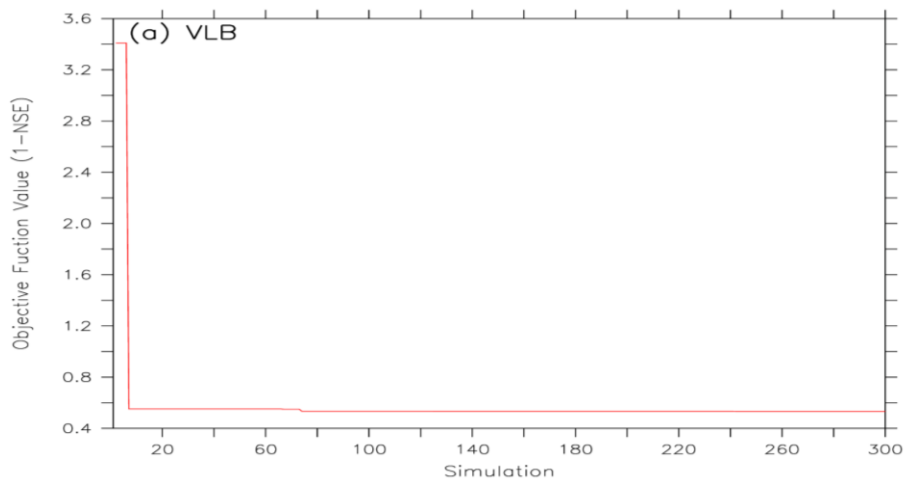


Figure 3.3: The characteristics of the Western Cape River basins used in the study: (a) the topography of the region (i.e. DEM), streams, streamflow observation stations (i.e. E2H003, G1H013, H7H006, and J1H019); (b) the SWAT+ delineation of the basin to sub-basins and channels; (c) soil types and (d) LULC types: Urban residential medium density (URMD), Dry cropland and pasture (CRDY), Cropland/grassland mosaic (CRGR), Cropland/woodland mosaic (CRWO), Grassland (GRAS), Shrubland (SHRB), Savanna (SAVA), Deciduous broadleaf forest (FODB), Evergreen broadleaf forest (FOEB), Mixed forest (FOMI), Water (WATR), and Bare ground/sparse vegetation (BSVG). The percentage of each LULC type is indicated in brackets.

Table 3.2: Selected model parameters for the SWAT+ calibration and their associated best values based on IPEAT+ optimisation using a range of $\pm 30\%$ change in the default values.

Parameter	Description	Unit	Object type	Best value (% change in the default value)		
				VRB	LRB	WRB
CN2	SCS runoff curve number	unit	HRU	-19.3	-29.9	-6.2
ESCO	Soil evaporation compensation factor	unit	HRU	-4.4	-29.7	-1.9
EPCO	Plant evaporation compensation factor	unit	HRU	-29.3	-13.4	-7.4
SOL_AWC	Soil available water storage capacity	mm_H2O/ mm	SOL	16.9	-5.8	8.2
SOL_K	Saturated hydraulic conductivity	mm/hr	SOL	1.0	5.0	12.4
GW_DELAY	Groundwater delay, time required for water leaving bottom of the root zone to reach the shallow aquifer	days	GW	5.2	2.24	1.6
FLO_MIN	Water table depth for return flow	mm	GW	-27.7	28.5	-12.9
REVAP_CO	Groundwater “revap” coefficient	unit	GW	28.5	9.08	12.4

Parameter	Description	Unit	Object type	Best value (% change in the default value)		
				VRB	LRB	WRB
REVAP_MIN	Threshold water depth in shallow aquifer for return to reach to occur	mm	GW	2.1	4.6	0.7
SURLAG	Surface lag coefficient, controls fraction of water entering reach in one day	days	BSN	10.7	14.9	7.6



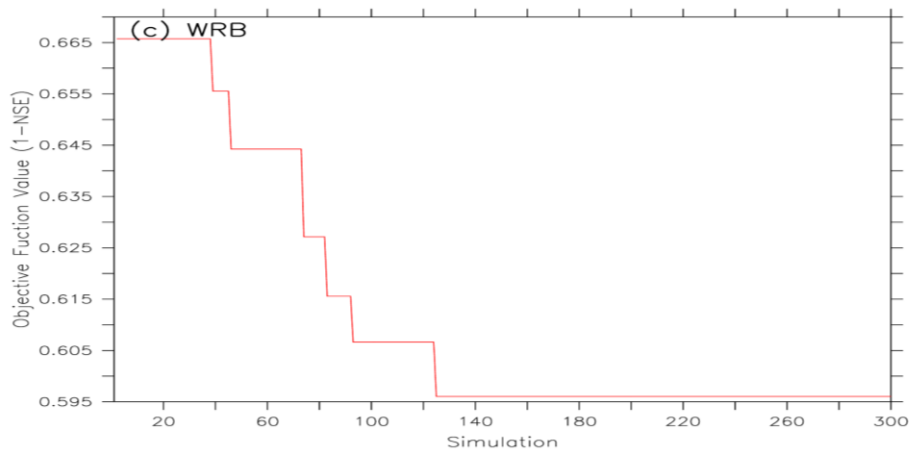


Figure 3.4: The convergence of SWAT+ simulations during the calibration over the river basins: (a) VRB, (b) LRB and (c) WRB.

3.3 Calibration and validation over the Vaal River basin

Figure 3.5 presents the time series of the observed and simulated streamflows at four hydrological stations (i.e. C3H007, C5H016, C2H003, and C9H009) in the VRB during the calibration and evaluation periods (1971-1980 and 1981-2005, respectively). The model simulation captures the characteristics of the observed streamflow at the four hydrological stations during the calibration and validation periods (Figure 3.1). It reproduces the annual cycle of the observed streamflow, captures the timing and magnitude of most peak flows, and replicates the interannual variability of the observed peaks. In agreement with the observation, the simulation shows that most of the water in the Vaal River main channel comes from the north-east mountain range. This is because the streamflow at station C9H009 (in the main channel) has almost the same magnitude as the streamflow at station C2H003 (at the foot of the north-east mountain range), and the magnitude of the streamflow at stations C5H016 and C3H007 (i.e. in the east and west tributaries, respectively) is small compared to that of the streamflow at station C2H003 (Figure 3.5). However, the performance of the simulation in replicating the observed streamflow varies over the stations. During the calibration period, the model performance is good at C9H009 (NSE = 0.5; $R^2 = 0.7$; PBIAS = -6%) and C5H016 (NSE = 0.8; $R^2 = 0.9$; PBIAS = -12%) but moderate at C3H007 (NSE = 0.1; $R^2 = 0.5$; PBIAS = -73%) and C2H003 (NSE = 0.4; $R^2 = 0.7$; PBIAS = -21.6%). At most stations, the model performance in the validation period is not as good as in the calibration period. For instance, at C5H016, the NSE decreases from 0.8 (in the calibration period) to 0.7 (in the validation period), and at C9H009, it decreases from 0.5 to -1.1. Nevertheless, there are cases where the model performance in the validation period is as good as in the calibration (e.g. $R^2 = 0.7$ at C2H003 and C2H009), or even better (e.g. R^2 increases from 0.5 to 0.8 and PBIAS decreases from -73% to -49% at C3H007). In general, the simulation features the best performance at C5H016 and the worst at C3H007.

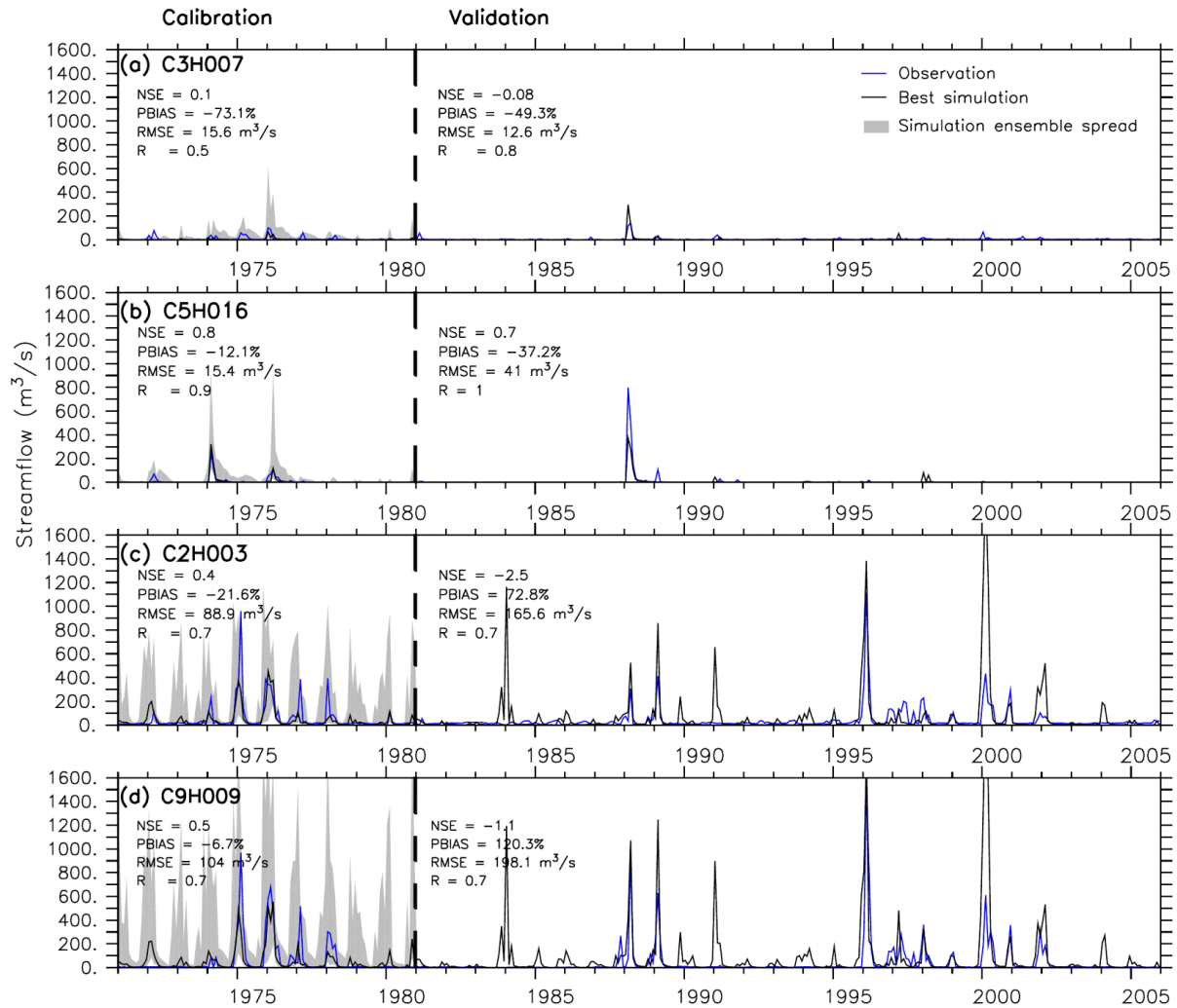


Figure 3.5: Evaluation of SWAT+ simulated streamflow at four hydrological stations (C3H007, C5H016, C2H003 and C9H009) in the Vaal River basin during the calibration and evaluation periods. The values of the statistical evaluation metrics (i.e. NSE, PBIAS, RMSE, and R) are indicated.

3.4 Calibration and validation over the Limpopo River basin

Figure 3.6 compares the simulated and observed streamflows at four hydrological stations (A2H059, A2H029, B3H017 and B7H015; Fig. 3.2) in the LRB calibration period (1988-1998) and validation period (1999-2009). The results show that the simulations capture the timing and magnitude of most peak flows, and replicate the interannual variability of the observed peaks. In most cases, the observed values are within the simulation spreads. However, there are some cases when all the simulations underestimate or overestimate the observed peaks. The performance of the simulation in replicating the observed streamflow varies over the stations. During calibration, model performance is good at station A2H059 (NSE = 0.6, PBIAS = -18.3%, RMSE = 14.5 m³ s⁻¹; R² = 0.7) and B7H015 (NSE = 0.8, PBIAS = -2.9%, RMSE = 39.8 m³ s⁻¹; R² = 0.9) (Figures 3.6(a) and (d)). Despite this, the model performs poorly at station A6H029 (NSE = -12.9, PBIAS = 236.4%, RMSE = 27 m³ s⁻¹, and R² = 0.6) and B3H017 (NSE

= 0.2, PBIAS = -80.3%, RMSE = 43.6 m³ s⁻¹, R² = 0.6) (Figures 3.6(b) and (c)). The performance of the model during the validation period is not as good as during the calibration period at most stations. For example, at B3H017, the NSE decreases from 0.2 (during calibration) to -0.2 (during validation), and at B7H015, it decreases from 0.8 to -3.4. Nonetheless, there are instances where the model output in the validation period is on par with (e.g. R² = 0.6 at A6H029) or better (e.g. PBIAS decreases from -236.4% to -14.1% and RMSE decreases from 27 m³ s⁻¹ to 11.4 m³ s⁻¹ at A6H029) than that in the calibration period. Overall, the simulation performs best at A2H059 and worst at B3H017 and B7H015.

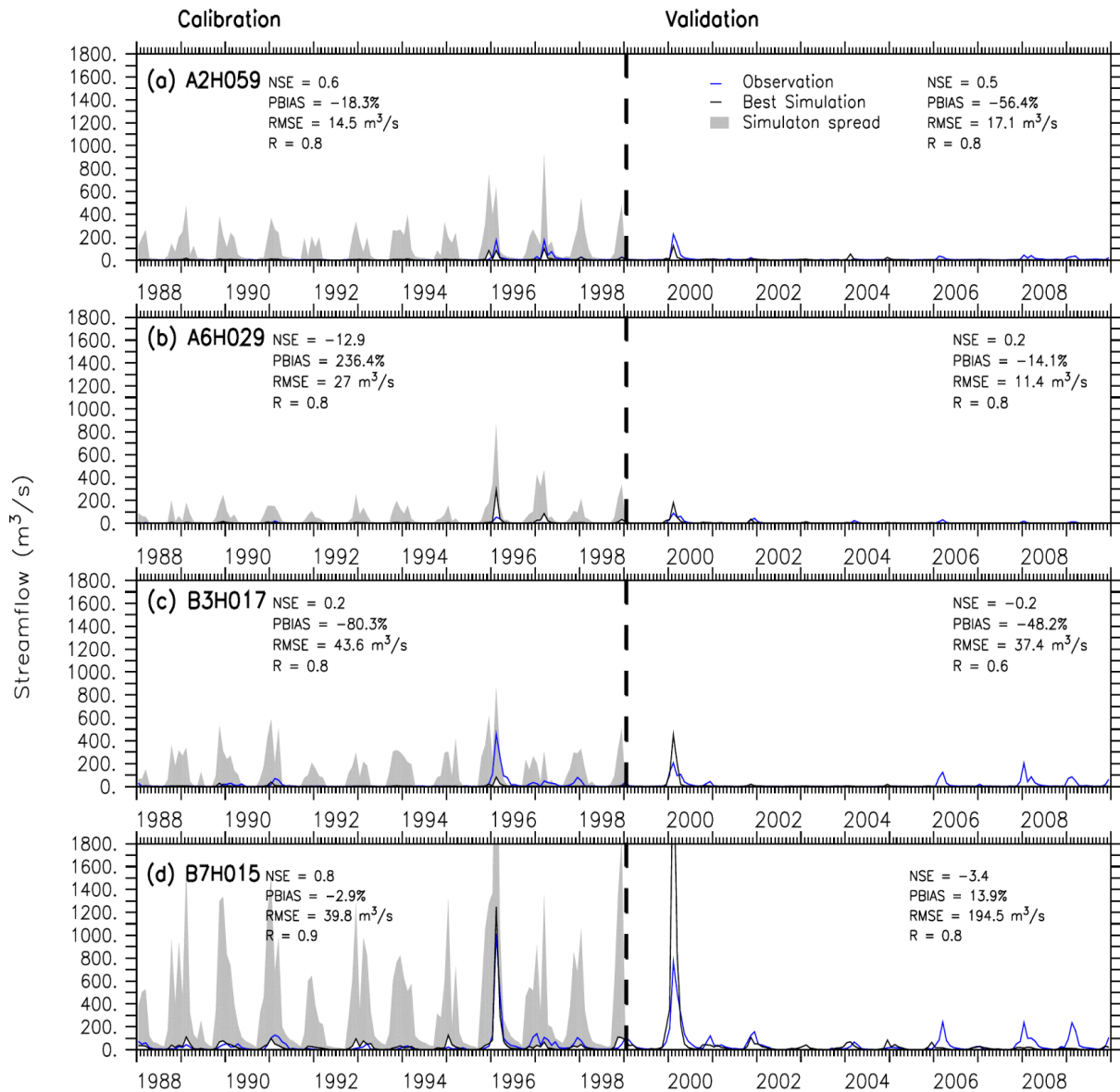


Figure 3.6: Evaluation of SWAT+ simulated streamflow at four hydrological stations (A2H059, A6H029, B3H017 and B7H015) in the Limpopo River basin during the calibration and evaluation periods. The values of the statistical evaluation metrics (i.e. NSE, PBIAS, RMSE, and R) are indicated.

3.5 Calibration and validation over the Western Cape River basins

Figure 3.7 shows a good agreement between the simulated and observed streamflows at the four hydrological stations (i.e. G1H013, H7H006, E2H003, and J1H019; Figure 3.3) in the WRB during the calibration period (1980-1990). The simulated streamflow values closely track the observed values in reproducing seasonal and annual variations of the streamflow. The model also captures the observed peaks and their inter-annual variability. In the calibration period (1980-1990), the simulation often envelops the observation, especially at stations H7H006 and E2H003. At some stations (i.e. G1H013, H7H006 and E2H003), the correlation between the simulated and observed flows is equal to or greater than 0.5 and the NSE is also more than 0.5. The simulation reproduces the differences in the magnitude of the streamflow across the stations. For instance, it agrees with the observation that, among the four stations, the streamflow is largest at H7H006 (i.e. Breede River) and G1H013 (i.e. Berg River) and lowest at J1H019 (i.e. Gouritz River). However, there are some notable model biases in the simulation. The model overestimates the magnitude of the peaks in some years and underestimates them in others. For instance, it overestimates the observed streamflow by more than $40 \text{ m}^3 \text{ s}^{-1}$ at H7H006 in 1986 and underestimates it by up to $120 \text{ m}^3 \text{ s}^{-1}$ at H7H006 in 1983. The model PBIAS ranges from -43.2% (at G1H013) to 72.8% (at J1H019). In most cases, the model performance is better (or the same) during the validation period (1991-2005) than in the calibration period (1980-1990) (Figure 3.7). For instance, at station G1H013, the model performance improves for NSE (from 0.4 to 0.5), PBIAS (-43.2% to -40.2%), and RMSE (from $17.5 \text{ m}^3 \text{ s}^{-1}$ to $17.2 \text{ m}^3 \text{ s}^{-1}$). Also, at station E2H003, it improves for PBIAS (from -30.8% to -31.2%), RMSE ($14.6 \text{ m}^3 \text{ s}^{-1}$ to $15.4 \text{ m}^3 \text{ s}^{-1}$), and for R^2 (from 0.5 to 0.7). However, the model improvement depends on the statistical metrics used in the performance evaluation. For example, at station H7H006, while the model performance remains constant for NSE (from 0.5 to 0.5), it improves for R (0.5 to 0.6), for PBIAS (-25.7% to -14.3%) and RMSE ($34.2 \text{ m}^3 \text{ s}^{-1}$ to $30.7 \text{ m}^3 \text{ s}^{-1}$). The difference in the model performance in the two periods may be due to differences in dominant processes or differences in the lengths of the observation data gaps in the periods, as evident in station J1H019, where the paucity of observation data makes the results unreliable.

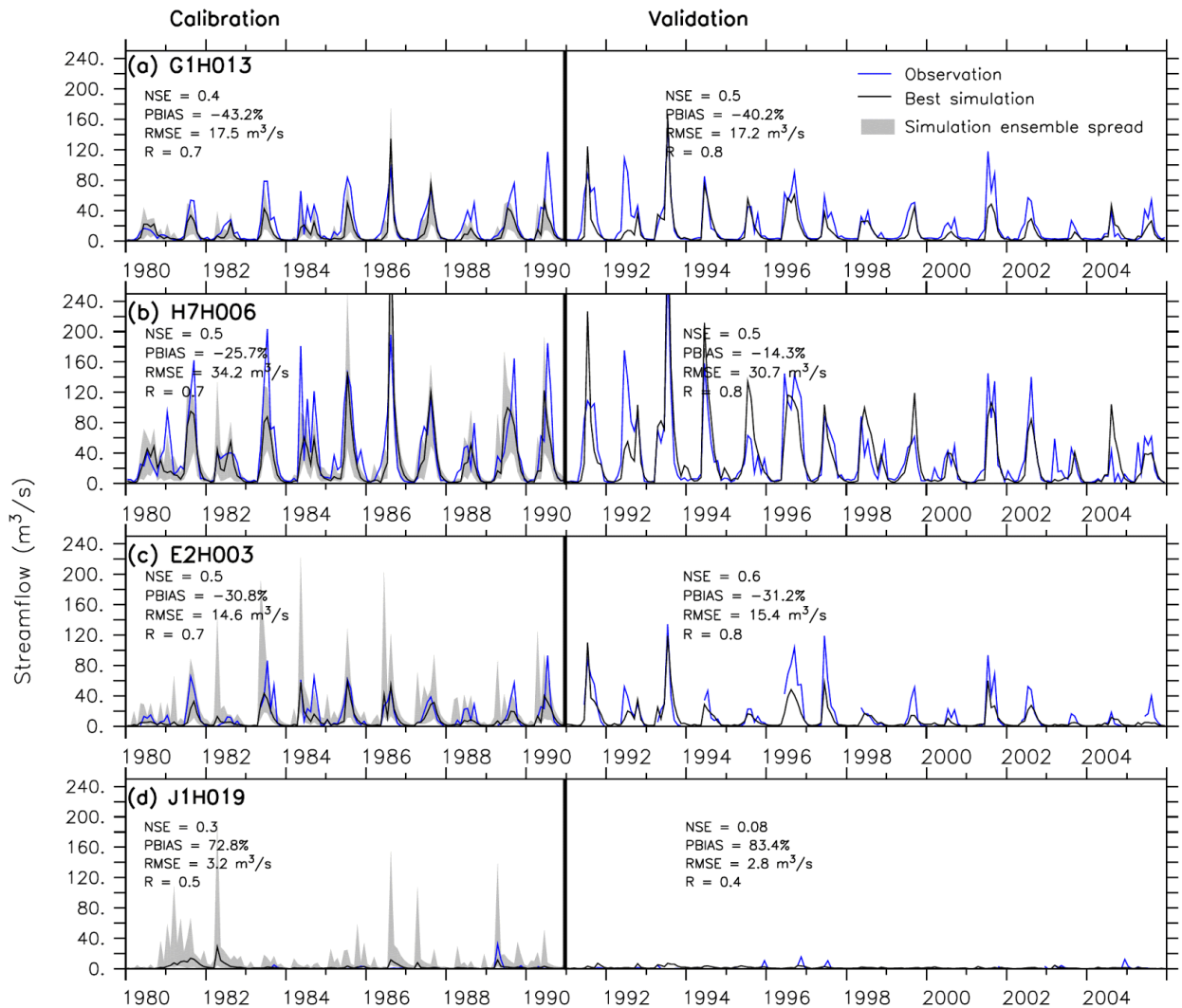


Figure 3.7: Evaluation of SWAT+ simulated streamflow at four hydrological stations (G1H013, H7H006, E2H003 and J1H019) in the Western Cape River catchments during the calibration and evaluation periods. The values of the statistical evaluation metrics (i.e. NSE, PBIAS, RMSE, and R) are indicated.

3.6 Summary

This chapter has calibrated and validated the SWAT+ model over three important river basins in South Africa. We used the GMFD dataset (described in Chapter 2) as the input climate data into the model and used streamflow observation data from four stations in each basin to calibrate and validate the model simulations over the basins. In general, SWAT+ gives credible simulations over all the basins. It reproduces the annual cycle of the observed streamflow at the hydrological stations in the VRB (i.e. C3H007, C5H016, C2H003, and C9H009), LRB (i.e. A2H059, A2H029, B3H017 and B7H015), (i.e. G1H013, H7H006, E2H003, and J1H019) during both calibration and validation periods. It also captures the timing and magnitude of most peak flows at the stations, in addition to replicating the interannual variability of the observed peaks. The coefficient of correlation (R) between the simulated and observed

streamflow is more than 0.6 over most of the stations. However, there are notable biases in the SWAT+ simulations. The biases may be attributed to several factors. They could be due to the shortcomings in the SWAT+ model or the model setup over each river basin. SWAT+ is still undergoing a series of testing and improvements. Lack of data to represent all the physical features (e.g. dams and reservoirs) and the operation rules (e.g. water abstractions and transfers) in the model setup may influence the simulation of hydrological processes. The biases could also be due to the deficiencies in the climate input dataset (i.e. GMFD reanalysis) in capturing the influence of complex topography on the rainfall pattern. However, the generally good performance of the SWAT+ in reproducing the peaks and the annual cycle of the streamflow is encouraging and shows that the model provides a reliable representation of hydrological processes over all the basins.

Chapter 4: Influence of bias correction of CORDEX datasets on hydrological simulations over the river basins

4.1 Introduction

Climate simulation datasets often have systemic biases that need to be corrected before the datasets can be used as input into hydrological models. This chapter reports on how the bias correction of the CORDEX climate datasets influences our hydrological simulations in the three selected basins. We employed the Quantile Delta Mapping (QDM) technique, which is one of the most popular bias-correction methods, to correct the bias in the CORDEX climate simulation dataset, using the GMFD climate dataset as the observed dataset. Details of the CORDEX and GMFD datasets, as well as the QDM techniques, are presented in Chapter 2.

4.2 Bias-correction experiments

Three experiments (GMFD, CORDEX_ORG, and CORDEX_QDM) were performed with the SWAT+ model. The simulation setups for the experiments are the same, except that the SWAT+ model was forced with the GMFD dataset in the GMFD experiment, with the original CORDEX dataset in the CORDEX_ORG experiment, and with the bias-corrected CORDEX dataset in the CORDEX_QDM experiment. Based on the CORDEX seven-member ensemble, the CORDEX_ORG and CORDEX_QDM experiment consist of seven simulations each, while the GMFD experiment consists of a single simulation. However, all the simulations cover a period of 30 years (1971-2000, starting after the 5-year model spin-up), and use the river basin domains described in Chapter 3 for the VRB (Figure 3.1), the LRB (Figure 3.2), and the WRB (Figure 3.3).

4.3 Influence of bias correction in the Vaal River basin

The results of the experiments over the VRB are presented in Figures 4.1 and 4.2. The SWAT+ simulations with CORDEX datasets (CORDEX_ORG and CORDEX_QDM) capture the spatial distribution of hydroclimatic variables over the basin as they do with the GMFD dataset, but the simulations with CORDEX_QDM simulation give better results than with CORDEX_ORG (Figures. 4.1 and 4.2). For instance, while both simulations capture the east-west gradient in the temperature (TMP) and the potential evapotranspiration (PET) fields and the west-east gradient in the precipitation (PRE) and the evaporation over land (ET) fields, the spatial correlation (R) between CORDEX and GMFD simulations results is higher with CORDEX_QDM ($R \geq 0.99$) than with CORDEX_ORG ($R > 0.82$), and the biases are much lower with CORDEX_QDM (Figure 4.1). The GMFD and CORDEX_QDM results agree that the north-eastern mountain range receives the highest rainfall (possibly due to orographic rainfall). It is also the coolest part of the basin, while the western part that receives the lowest rainfall is the warmest (Figs. 4.1(a) and (c)). The datasets also agree that the spatial distribution of PET (Figures 4.1(k) and (m)) follows that of TMP (Figures 4.1(a) and (e)), while the spatial

distribution of ET (Figures 4.1(p) and (r)) follows that of PRE (Figures 4.1(f) and (h)), suggesting that the ET distribution over the basin is more driven by precipitation than by atmospheric water demand (i.e. PET). Both datasets (GMFD and CORDEX_QDM) also show that the ability of the basin to meet the atmospheric water demand (i.e. ET/PET) varies over the basin (Figures 4.1(u) and (w)). While the basin meets more than 50% of the atmospheric water demand over the north-east mountain range (where PET is lowest and PRE is highest), it meets less than 10% of the demand on the south-west plain (where PET is highest, and PRE is lowest).

The agreement between GMFD and CORDEX results is better for climate variables (Figure 4.1) than for hydrological variables (Figure 4.2). For instance, while the spatial correlation between the two systems for climate variables ranges from 0.99 to 1.00 (0.79 to 0.99) with CORDEX_QDM (CORDEX_ORG), the spatial correlation between the systems for hydrological variables only ranges from 0.89 to 0.92 (0.50 to 0.70) with CORDEX_QDM (CORDEX_ORG). Also, for climate variables, the percentage bias (PBIAS) is less than 10% (45%) with CORDEX_QDM (CORDEX_ORG) but more than 50% (100%) with CORDEX_QDM (CORDEX_ORG). The reason for the poorer performance of the CORDEX_SWAT+ hydroclimatic system in reproducing hydrological variables than reproducing climate variables is because any uncertainty or error in the input climate data is usually amplified in the hydrological simulation. This is consistent with previous studies that have reported the amplification of climate input error in hydrological modelling (e.g. Teutschbein et al., 2011). However, the CORDEX_ORG and CORDEX_QDM simulations still capture the spatial distribution of the hydrological variables as happens in the GMFD results, and the CORDEX_QDM results are still better than the CORDEX_ORG results. In both the GMFD and the CORDEX_QDM results, the spatial distributions of soil water (Figures 5(a) and (c)) and runoff (Figures 4.2(k) and (m)) are consistent with those of PRE and ET, in that soil water and runoff feature their highest values over the north-east mountain range, where PRE and ET are highest. This is because, the higher the PRE, the higher the soil water and runoff. Also, the higher the soil water, the higher the ET (provided that $ET < PET$ and that the soil water is above the wilting point). However, the spatial distribution of percolation differs from that of other fields. The percolation does not feature the maximum values over the mountains, possibly because the steep topography over the range may not encourage the percolation of rainwater.

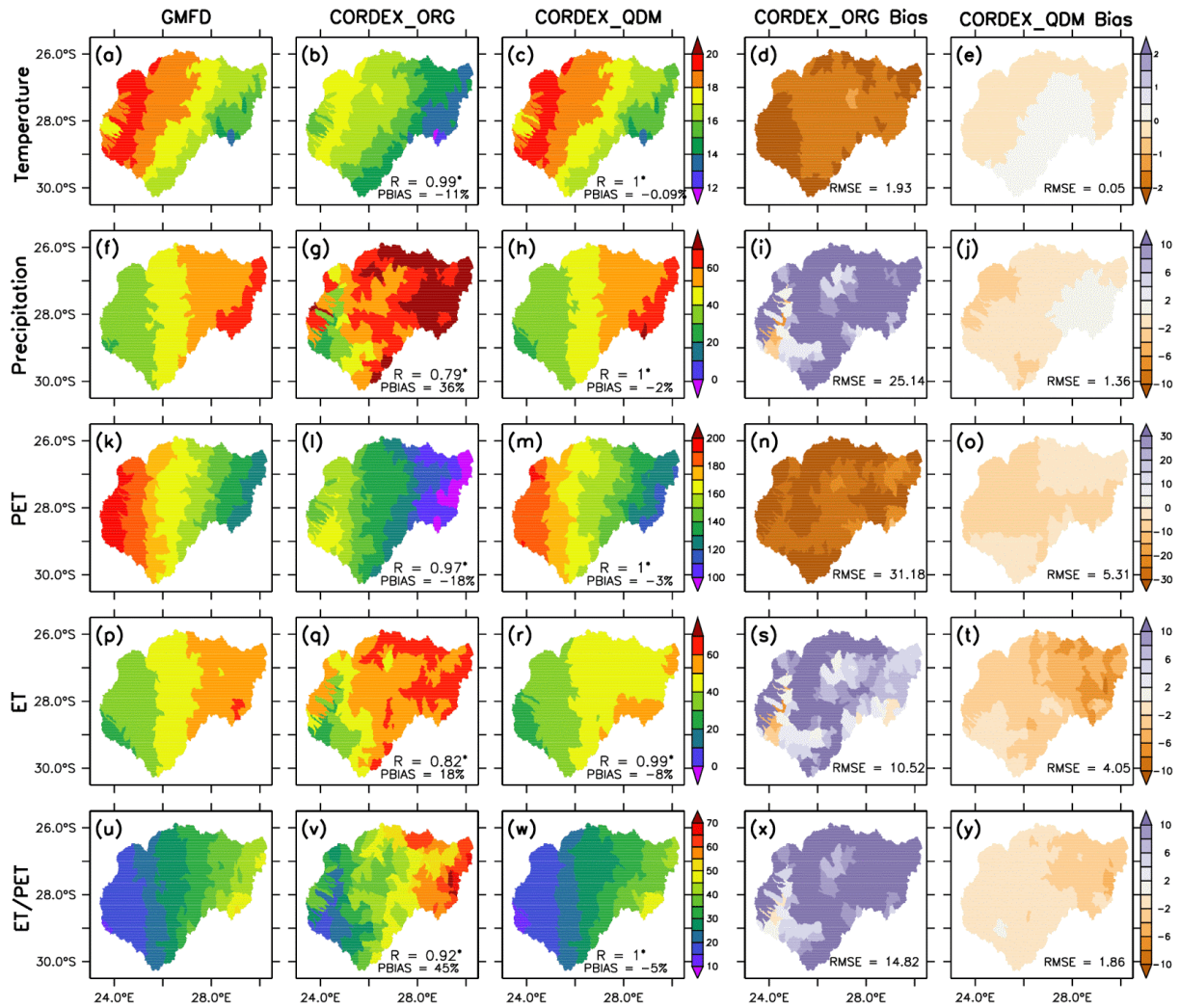


Figure 4.1: The spatial distribution of the climate variables over the Vaal River basin, as depicted by GMFD, original CORDEX (CORDEX_ORG) and QDM bias-corrected CORDEX (CORDEX_QDM) datasets, and the biases of the CORDEX datasets (with reference to GMFD). The associated correlation (R), percentage bias (PBIAS) and root mean square error (RMSE) are indicated.

The spatial distribution of the streamflow patterns is identical in the SWAT+ simulation with GMFD and CORDEX_QDM climate forcing, except that the magnitude of the flow is higher in the latter (Figure 4.2). While the magnitude of the river flow is less than $3000 \text{ m}^3 \text{ s}^{-1}$ with GMFD, it is up to $7000 \text{ m}^3 \text{ s}^{-1}$ with CORDEX_QDM. This bias may be attributed to the accumulation of errors in all the simulated hydroclimatic variables that contribute to the calculation of streamflow in the SWAT+ model. However, the two simulations agree that the runoff from the north-eastern mountain range is the main source of water in the VRB. Both datasets also agree on the magnitude and pattern of stream evaporation (ETS). The maximum ETS occurs in the south-west plain, where the lowest soil water and lowest ETS occur. The maximum ETS in this area can be attributed to the maximum PET and the largest river water

volume in the area. Unlike ETS, the capability of ETS to meet the atmospheric demand in the area is high because of the availability of open water in the channel.

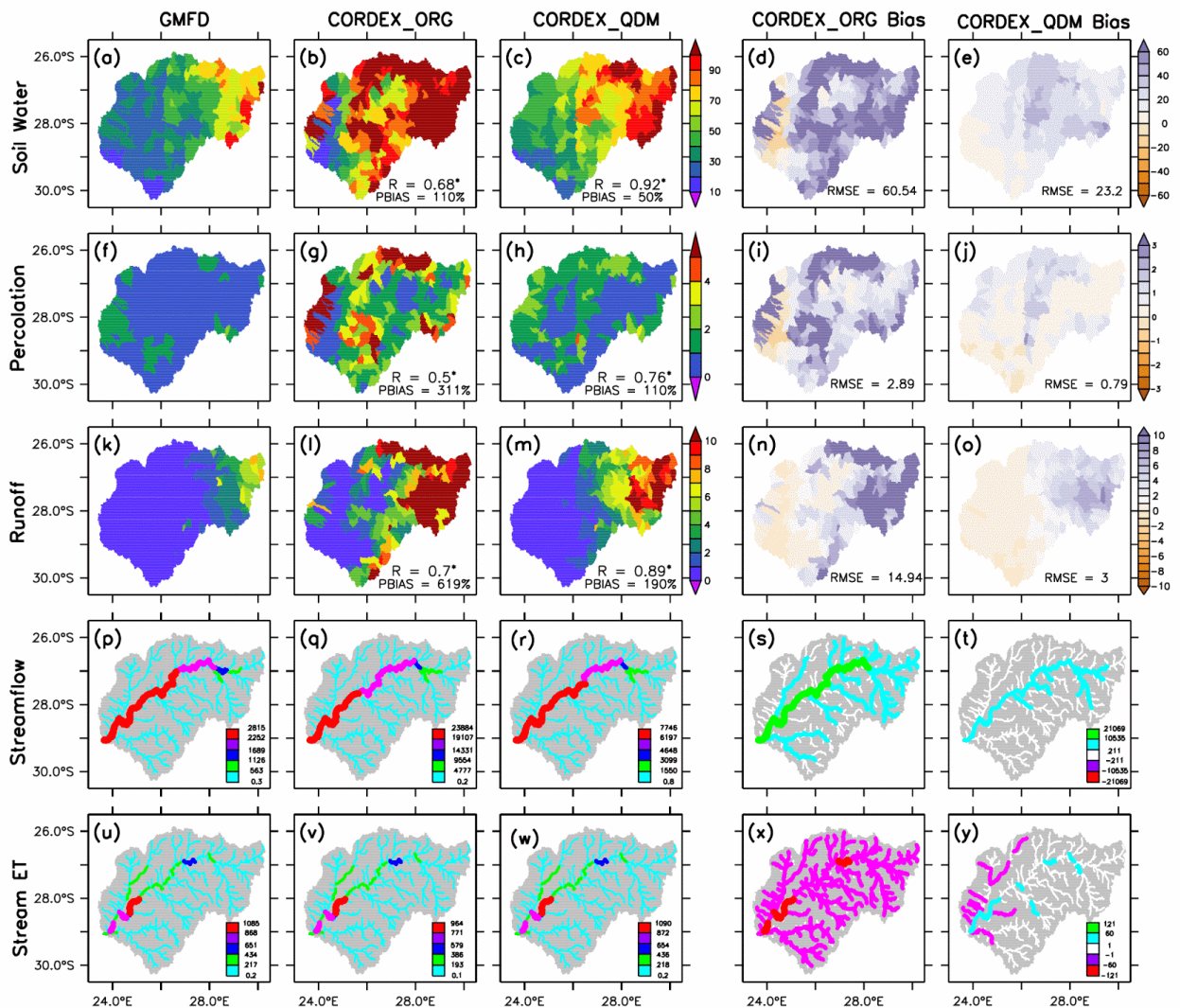


Figure 4.2: Same as Figure 4.1, except for hydrological variables.

In general, the CORDEX simulations give a credible simulation of all the important hydroclimatic variables over the basins and reproduce all the essential hydroclimatic processes in the basin. The QDM bias correction of the CORDEX datasets moreover improves the quality of the dataset. Given the added values of QDM bias correction in the CORDEX_QDM historical simulations, only the results of the CORDEX_QDM simulations for climate change projection and land-use change experiments will be discussed in the remaining parts of the paper. The CORDEX_QDM historical simulation will serve as a reference for the projection.

4.4 Influence of bias correction in the Limpopo River basin

The influence of bias correction of the CORDEX datasets over the LRB is summarised in Figures 4.3 and 4.4. The CORDEX_ORG simulation adequately simulates the spatial distribution of the climate variables over the basin (Figures 4.3 to 4.5). The CORDEX_QDM models capture the spatial pattern of temperature, which varies across the basin owing to the topography and the basin's proximity to the Indian Ocean. They feature the temperature maxima ($>22^{\circ}\text{C}$) over Mozambique and Zimbabwe (Figures 4.3(b) and (c)). The models reproduce a PET maximum (ranging from 130 to 150 mm month^{-1}) over the north-eastern half of the basin. They also reproduce the temperature minima (14°C) in areas of higher altitude along the escarpment in South Africa, over the Waterberg, Steelpoort mountains and the northern portion of the Drakensberg Mountain range. In agreement with the observations, the models simulate the precipitation maxima ($>60 \text{ mm month}^{-1}$) and ET maxima ($>60 \text{ mm month}^{-1}$) over the high elevation areas and over the north-eastern parts of Zimbabwe. The models replicate the precipitation and ET minima ($<20 \text{ mm month}^{-1}$) over the westernmost part of the basin in Botswana and over the southernmost part of South Africa. The low precipitation over these regions is attributable to its distance from the rain-bearing ITCZ and the southwest Indian Ocean tropical cyclones, which bring a substantial amount of precipitation over the northern and eastern parts of the basin. Furthermore, the low precipitation west of the basin is aggravated by the presence of a seasonal subtropical anticyclone, which develops at about 700 hPa during summer, known as the Botswana Upper High Influence (BUHI) (Reason and Smart, 2015). The BUHI creates unfavourable conditions for precipitation by rerouting the migration of the ITCZ away from the region. In addition, they simulate the observed zonal gradient in PRE and in the hydroclimatic variables (SW, PERC, Runoff and WYLD), with the maxima ($>30 \text{ mm month}^{-1}$, $>0.6 \text{ mm month}^{-1}$, $>4 \text{ m}^3 \text{ s}^{-1}$ and $>10 \text{ mm month}^{-1}$, respectively) over the high-altitude areas and the minima ($<0 \text{ mm month}^{-1}$, $<0.2 \text{ mm month}^{-1}$, $<2 \text{ m}^3 \text{ s}^{-1}$ and $<2 \text{ mm month}^{-1}$) over the western parts of the basin. The east to west decrease in precipitation has been reported by Mosase et al. (2019). The models also reproduce the stream ET maxima (2193.8 mm month^{-1}) over the Lower Limpopo found east of the LRB and the stream ET minima (0.4 mm month^{-1}) further west of the basin (Figures 4.5(c) and (h)). The models also simulate streamflow (up to 17573.2 $\text{m}^3 \text{ s}^{-1}$) across the basin (Figure 4.5(o)).

Nevertheless, there are notable biases in the CORDEX_ORG ensemble mean climate variables (Figures 4.4(d), (f), (n), and (s)). The cold and wet bias identified in Figure 4.1 is evident across various regions of the basin (Figures 4.4(d) and (f)). The cold bias featured in the ensemble mean is noticeably weaker ($0\text{-}1^{\circ}\text{C}$) over the northern half of the basin and stronger ($1.5\text{-}2^{\circ}\text{C}$) over the southern half, more especially over the high-altitude areas along the escarpment (Figure 4.3(d)). The cold bias contributes to the underestimation of PET (about 20 mm month^{-1}) across the basin (Figure 4.3(n)). The PET bias is particularly strong over the north-eastern part of the basin as well as along the escarpment. The wet bias simulated by the CORDEX_ORG models is substantial over Zimbabwe and northern South Africa, which suggests that the models simulate stronger ITCZ convergence. Additionally, the models also simulate patches of a dry bias (about 12 mm month^{-1}) over the high-altitude regions. This suggests that the resolution of the models may be too low for capturing the influence of the

orographic effect on temperature and precipitation over Limpopo (Kalognomou et al., 2013). Furthermore, the dry bias influences the underestimation of ET (up to 12 mm month^{-1}) over the high-altitude region (Figure 4.3(s)). The errors in the precipitation and ET fields produce a bias in the distribution of the hydroclimatic variables ranging from soil water ($-10 \text{ mm month}^{-1}$), PERC ($-0.4 \text{ mm month}^{-1}$), Runoff ($-2 \text{ m}^3 \text{ s}^{-1}$) and WYLD (-2 mm month^{-1}) over northern South Africa to soil water (80 mm month^{-1}), PERC (2 mm month^{-1}), Runoff ($10 \text{ m}^3 \text{ s}^{-1}$) and WYLD (10 mm month^{-1}) over the high elevation regions in the basin (Figures 4.4(d), (f), (n) and (s)). The negative bias in the hydroclimatic variables is due to the underestimation of precipitation, while the positive bias in SW, PERC, runoff, and water yield is caused by the underestimation of PET. Following a similar spatial pattern to the PRE distribution, the models simulate a wet bias ($578.8 \text{ mm month}^{-1}$) over the channels, predominantly over the Lower Limpopo in Mozambique and northern South Africa (Figure 4.4(d)). The ET is underestimated across the entire basin (up to $-299.6 \text{ mm month}^{-1}$); however, the negative ET bias is stronger over the areas with a wet bias, as more water is available for evaporation in those channels (Figure 4.4(i)). The streamflow is mostly influenced by precipitation and ET. Consequently, there is a positive streamflow bias (about $14049.2 \text{ m}^3 \text{ s}^{-1}$) over the eastern half of the basin, which is strongest over the Lower Limpopo (Figure 4.4(n)).

The bias-correction method QDM nearly eliminates the above-mentioned biases (Figures 4.3 and 4.4). All the climate features are better represented in the bias-corrected datasets than in the CORDEX_ORG. The bias-corrected CORDEX_QDM models improve the cold and wet bias across the basin by $>1.5^\circ\text{C}$ and $>10 \text{ mm month}^{-1}$ and the dry bias over the high elevation areas by $>10 \text{ mm month}^{-1}$ as well (Figures 4.3(e) and (j)). A reduction of the cold bias error led to the correction of the negative PET bias by $>18 \text{ mm month}^{-1}$ across the basin (Figure 4.3(o)). The negative bias in ET over the regions with high topography is reduced by about 12 mm month^{-1} , while the positive ET bias across the basin is reduced by $>12 \text{ mm month}^{-1}$ (Figure 4.3(t)). The correction of the precipitation and ET biases correct the negative (positive) bias of soil water by 20 mm month^{-1} ($>70 \text{ mm month}^{-1}$), PERC by $0.2 \text{ mm month}^{-1}$ ($>1.8 \text{ mm month}^{-1}$), and both Runoff and WYLD by $2 \text{ m}^3 \text{ s}^{-1}$ (8 mm month^{-1}) (Figures 4.4(e), (j), (o) and (t)). The negative ET bias is reduced by $150 \text{ mm month}^{-1}$ over the lower Limpopo (Figures 4.4(e) and (j)). This results in a better representation of streamflow over the region, as the positive bias improves by $>7024.6 \text{ m}^3 \text{ s}^{-1}$ (Figure 4.4(o)).

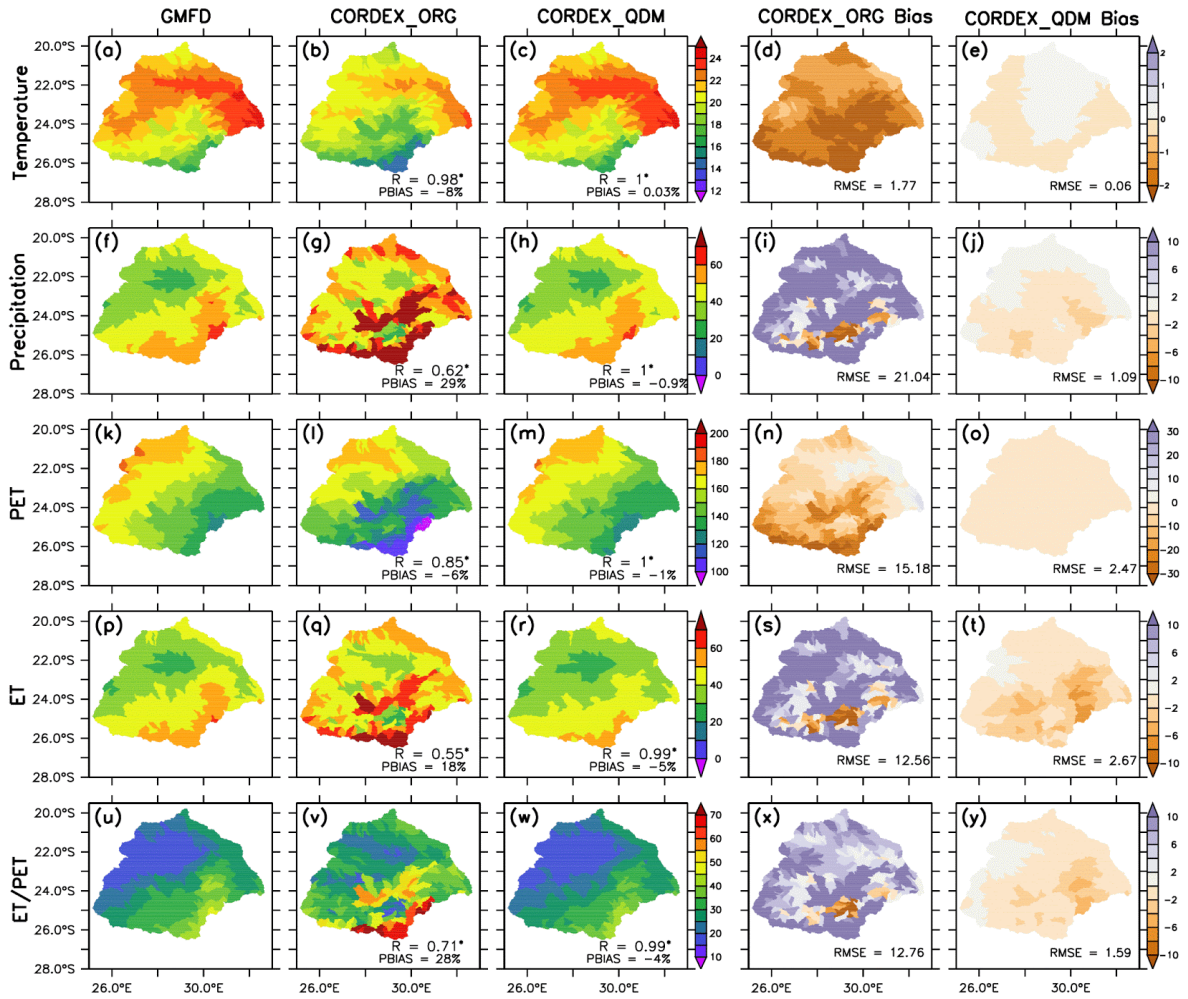


Figure 4.3: The spatial distribution of the climate variables over the Limpopo River basin, as depicted by GMFD, original CORDEX (CORDEX_ORG) and QDM bias-corrected CORDEX (CORDEX_QDM) datasets, and the biases of the CORDEX datasets (with reference to GMFD). The associated correlation (R), percentage bias (PBIAS) and root mean square error (RMSE) are indicated.

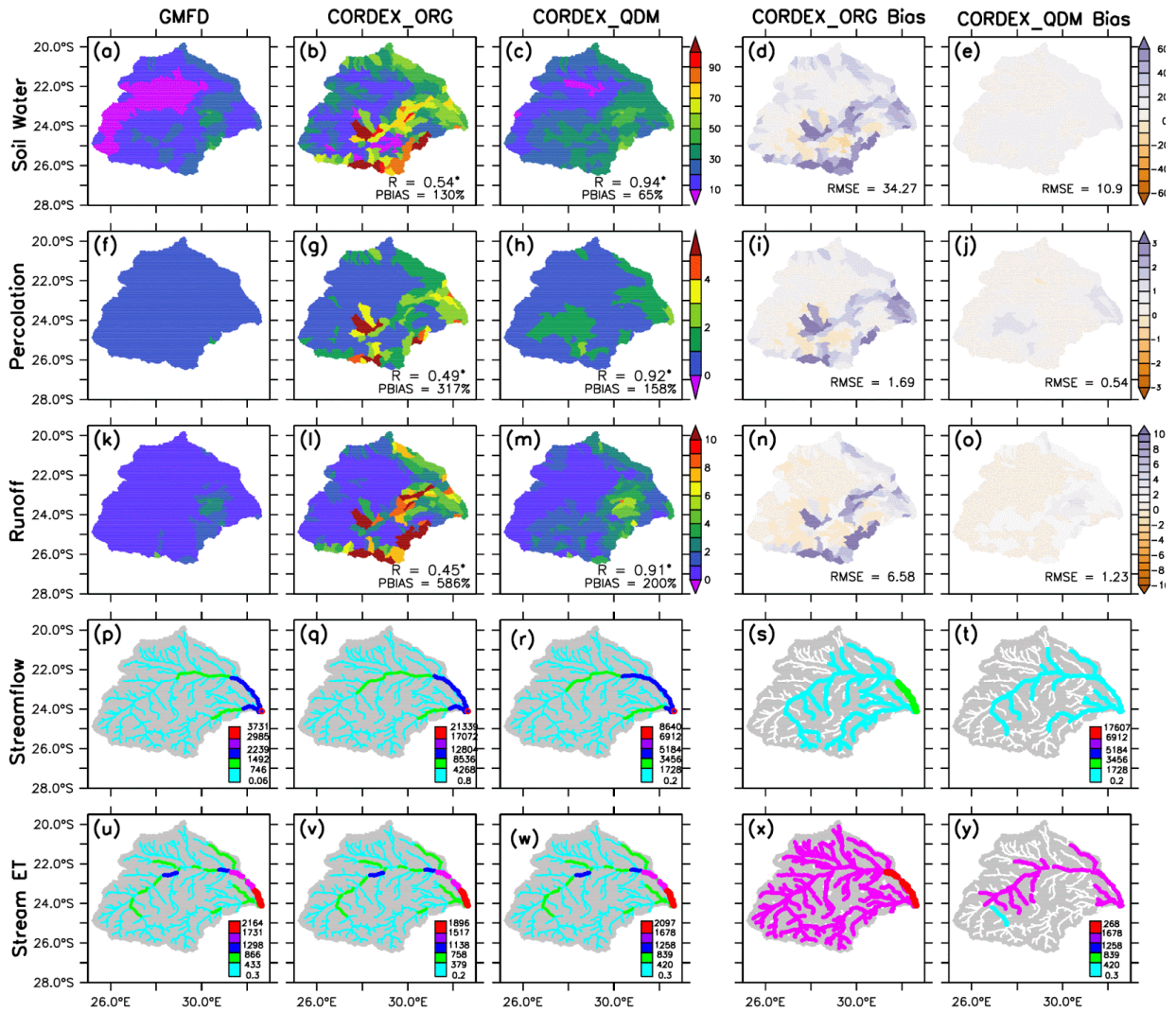


Figure 4.4: Same as Figure 4.3, except for hydrological variables.

4.5 Influence of bias correction in the Western Cape River basins

Figures 4.5 and 4.6 show the influence of the bias correction over the WRB. The CORDEX_ORG simulation captures the spatial distribution of climate variables across the Western Cape, but with some notable biases. The QDM bias correction reduces the biases (PBIAS) and improves the correlation (R) between the CORDEX_ORG and GMFD results. For example, the bias correction reduces PBIAS TMP from -13% to -0.6% and increases the R from 0.87 to 1.0. Although it does not improve the PRE PBIAS, it increases the R from 0.75 to 1.0. However, the corrected dataset (i.e. CORDEX_QDM) generally improves on the original dataset (CORDEX_ORG) and reproduces the spatial distribution of climate variables better. In agreement with GMFD, CORDEX_QDM simulates the highest TMP over the north-western part of the basin and the lowest temperature over the mountain range at the centre of the study domain. It also captures the location of the maximum precipitation on the south-western side of the mountain. Both datasets (GMFD and CORDEX_QDM) agree on the difference in the spatial distribution of PET and ET over the region. While PET increases from south to north,

ET increases from north to south, suggesting the spatial distribution of evaporation of the basin is more driven by water availability (through precipitation) rather than by atmospheric demand (PET). However, in both datasets, the capability of the Western Cape catchments in meeting the atmospheric demand (i.e. ET/PET) decreases from south-west to north-east in accordance with PRE distribution. Generally, the capability of catchments to meet the atmospheric water demand is higher over the Berg and Breede than over the Olifants and Gouritz rivers.

The bias correction of the CORDEX dataset also improves the hydrological simulations over the catchments, but the performance of CORDEX_QDM is lower for hydrological variables (i.e. $29\% \leq \text{PBIAS} \leq 116\%$) than for climate variables ($-6\% \leq \text{PBIAS} \leq -0.6\%$) (Figure 4.6). However, with reference to the GMFD results, the CORDEX_QDM still captures the spatial distribution of hydrological variables across Western Cape well. For instance, in both datasets, the spatial distributions of soil water, PERC, and runoff follow that of PRE. In contrast to CORDEX_ORG, CORDEX_QDM agrees with GMFD that the Breede catchment features the highest streamflow, while the Gouritz River has the lowest. Nevertheless, in both datasets, the ET is higher over the Gouritz than over the Breede. This is because PET is higher over the former than the latter and, as long as there is water in a river, the ET over the river is not limited by a lack of precipitation or by low soil water.

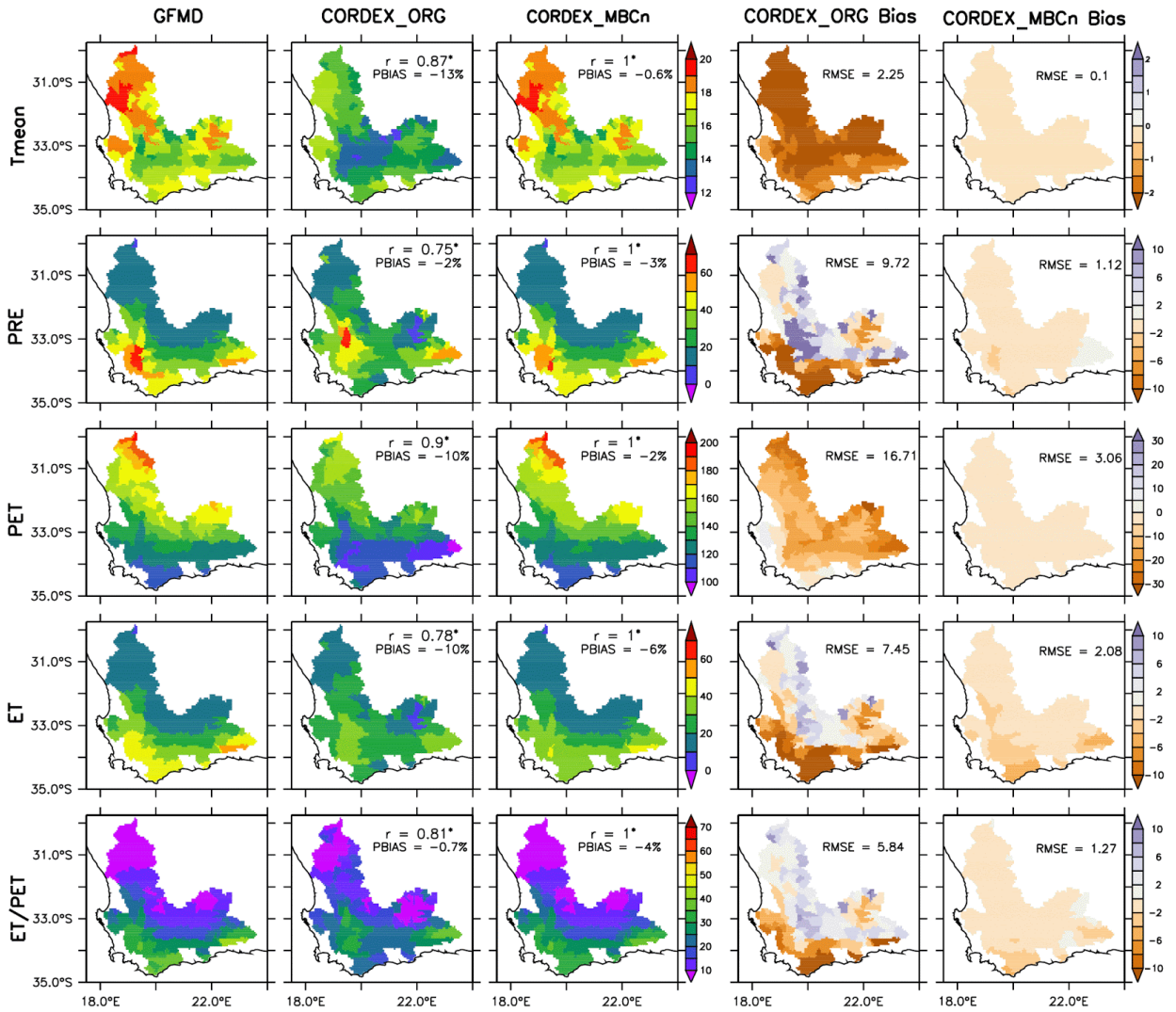


Figure 4.5: The spatial distribution of the climate variables over the Western Cape River basins, as depicted by GMFD, original CORDEX (CORDEX_ORG) and QDM bias-corrected CORDEX (CORDEX_QDM) datasets, and the biases of the CORDEX datasets (with reference to GMFD). The associated correlation (R), percentage bias (PBIAS) and root mean square error (RMSE) are indicated.

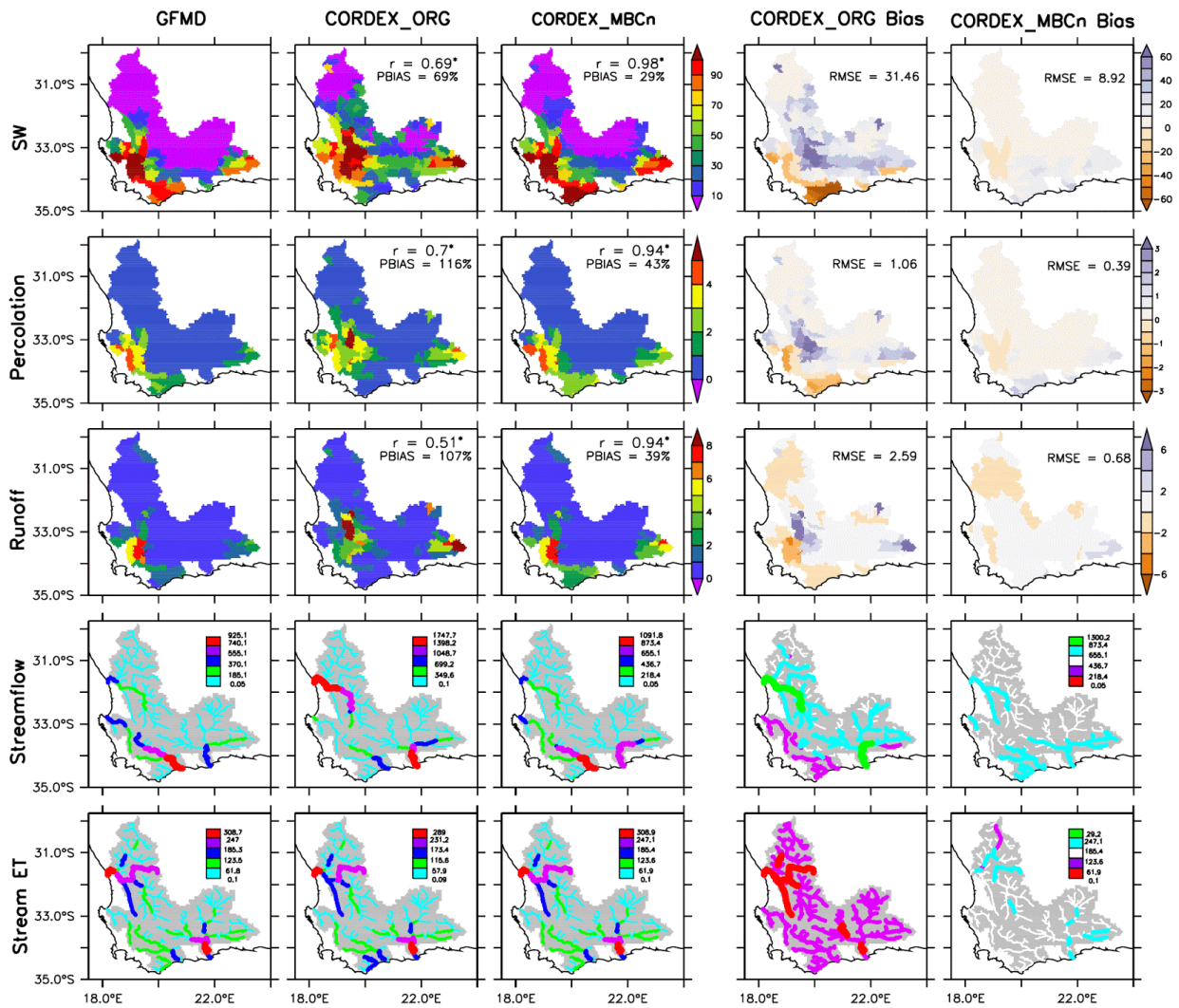


Figure 4.6: Same as Figure 4.5, except for hydrological variables.

4.6 Summary

This chapter has investigated how the bias correction of the climate dataset used in SWAT+ hydrological modelling can influence the quality of the hydrological modelling over the selected river basin. For the investigation, we coupled the calibrated SWAT+ model to the GMFD, original CORDEX and bias-corrected CORDEX datasets in simulating the hydrological variables over the three river basins. The results of the SWAT+ simulation with the GMFD dataset were used to evaluate the results of the simulations with the CORDEX datasets (both original and bias-corrected). The hydrological simulations with the original datasets give credible simulations over all the basins, but there were notable biases in all the hydrological variables. Simulations with bias correction reduced the magnitude of these biases (by more than 50%) and improved the correlation between the GMFD and CORDEX simulations. This result stresses the importance of performing bias correction of climate datasets before using them as input into SWAT+ hydrological modelling. Nevertheless, before doing a bias correction of any climate dataset over a basin, it is essential to ensure that the

dataset gives realistic simulations of climate variables over the basin and that it captures all the important climate processes over the basin. It is important to emphasise that bias correction cannot compensate for the inability of a climate dataset to capture all the essential large-scale atmospheric processes over a basin.

Chapter 5: Using land-use change to mitigate future impacts of climate change on hydrological droughts in the Vaal River basin

5.1 Introduction

Although the VRB is the heartbeat of many socio-economic activities in South Africa, the streamflow in the basin is highly erratic due to high rainfall variability and excessive evaporation, which often induce hydrological droughts in this basin. So, while the Vaal River is the most developed and most regulated river in South Africa, hydrological drought poses a big challenge to water resource management in the basin. Previous studies have shown how climate change could enhance the severity of hydrological droughts in the future (Abiodun et al., 2019; Akanbi et al., 2021; Jury, 2016; Otieno et al., 2009). For example, Akanbi et al. (2021) projected a temperature increase of about 5°C, a precipitation decrease of 30%, and a streamflow reduction of 10% over the basin in the periods 2011-2040, 2014-2070, and 2071-2100 under the Representative Concentration Pathway 8.5 (RCP8.5) future climate scenario. Several studies have documented how LULC changes can influence the hydrological cycles and water yield in a basin, but there is a dearth of information on the extent to which LULC changes can influence climate change impacts on hydrological droughts in the VRB. Such information will thus be valuable in formulating appropriate LULC policies towards mitigating the impacts of climate change on hydrological droughts in the future. This chapter thus reports on our study in this regard.

5.2 Land-use change experiments

Five experiments (CtrlLand, GrLand, CrLand, CrGrLand and BrLand) were performed with SWAT+ to investigate the impacts of climate change and idealised LULC in the VRB (Table 5.1). The model setup in all the experiments is as presented in Chapter 3 (Figure 3.1), except for the LULC pattern. While the model used the present-day LULC pattern (Figure 5.1(a)) in the Control experiment, it used the idealised LULC pattern in the other four experiments. In the idealised LULC pattern, the targeted LULC type was used to replace the default LULC type in some areas (Table 5.1 and Figure 5.1). In all the experiments, the SWAT+ model was forced with the bias-corrected CORDEX datasets (CORDEX_QDM) to simulate the hydrological condition in the basin for the period 1971-2090, after a five-year model spin-up. Each experiment consisted of simulations based on the CORDEX_QDM seven-member ensemble. To obtain the impacts of climate change at a given GWL in the Control experiments, the simulations of the present-day climate period (1971-2000) are subtracted from those of the GWL climate period. The GWL periods of the simulations are the same as the GWL periods of the CORDEX dataset (described in Table 3.1) used in generating the simulation. To obtain the impacts of LULC change in an experiment, the simulations of the experiment are subtracted from the corresponding simulations in the Control experiment at the same GWL.

Table 5.1: Summary of LULC change experiments in the Vaal River basin.

Experiments	Description	LULC pattern
CtrlLand	<ul style="list-style-type: none"> ● Control LULC, which is SWAT+ default land use. 	Figure 5.1(a)
GrLand	<ul style="list-style-type: none"> ● Expansion of grassland expansion (i.e. grass invasion). ● GRAS replaces CRDY, CRWO, and CRGR. ● GRAS occupies 92.3% of the basin. 	Figure 5.1(b)
CrLand	<ul style="list-style-type: none"> ● Extensive cropping. ● CRDY replaces CRWO, GRAS, and CRGR ● CRDY covers 92.3% of the basin. 	Figure 5.1(c)
CrGrLand	<ul style="list-style-type: none"> ● Cropland/grassland expansion. ● CRGR replaces CRDY, CRWO, and GRAS. ● CRGR covers 92.3% of the basin. 	Figure 5.1(d)
BrLand	<ul style="list-style-type: none"> ● Extensive vegetation removal. ● BSVG replaces GRAS, CRDY, CRWO and CRGR ● BSVG covers 92.6% of the basin. 	Figure 5.1(e)

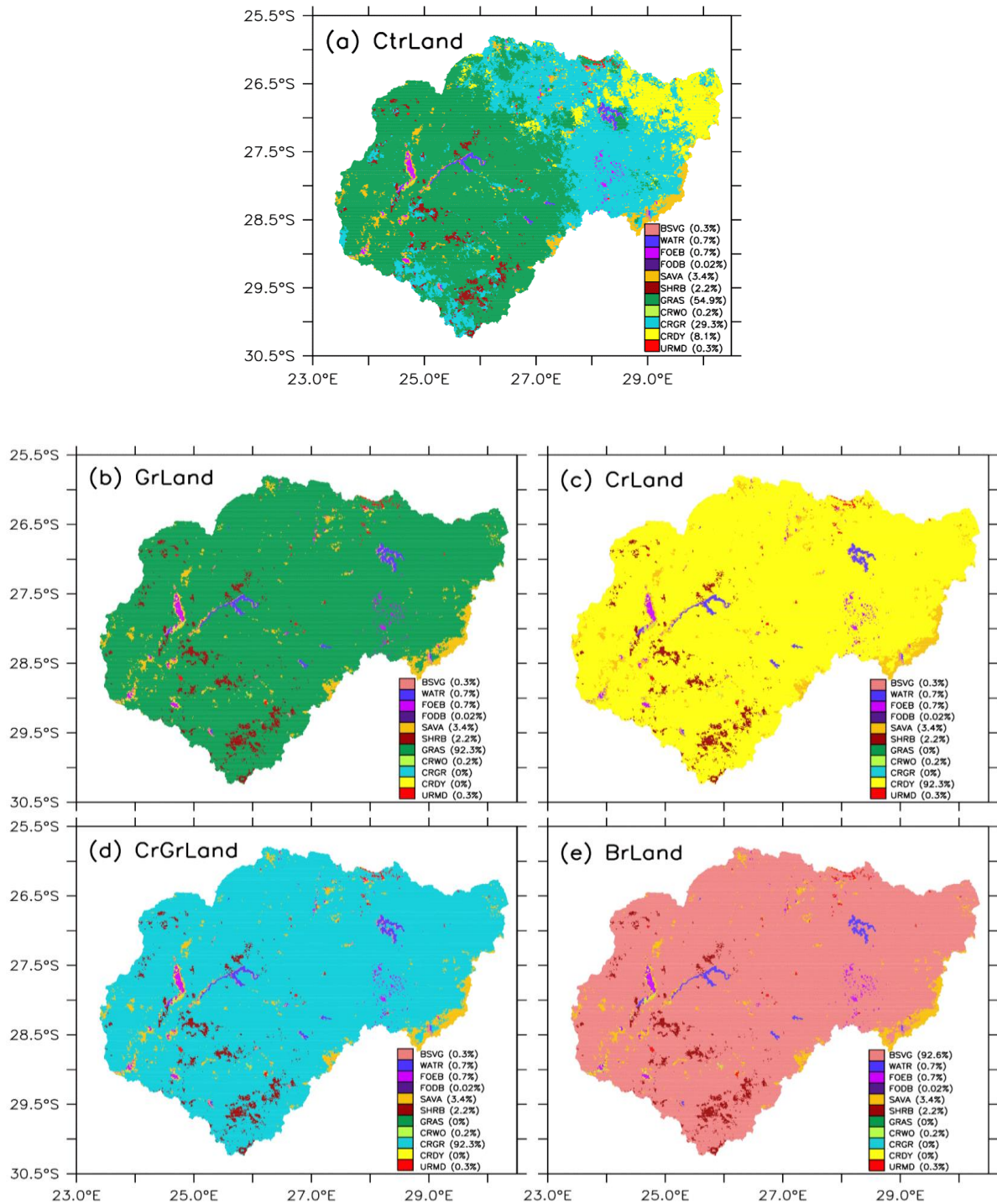


Figure 5.1: The LULC patterns used in the LULC change experiments for the Vaal River basin: (a) CtrLand, (b) GrLand, (c) CrLand, (d) CrGrLand and (e) BrLand. The experiments are described in Table 5.1. The LULC types are: Bare ground/sparse vegetation (BSVG), Water (WATR), Evergreen broadleaf forest (FOEB), Deciduous broadleaf forest (FODB), Savanna (SAVA), Shrubland (SHRB), Grassland (GRAS), Cropland/woodland mosaic (CRWO), Cropland/grassland mosaic (CRGR), Dry cropland and pasture (CRDY), Urban residential medium density (URMD). The percentage of each LULC type is indicated in brackets.

5.3 Impacts of climate change

The temporal variations of temperature and precipitation projections over the VRB differ (Figures 5.2(a) and (b)). A temperature increase (about 6.0°C by 2099) is projected over the basin, but there is no discernible trend in the precipitation projection. The PET and ET projections respond differently to warming. The positive trend in the PET projection (about 40 mm month⁻¹ by 2099) is consistent with that of the temperature projection, while the variation of the AET projection is consistent with that of the precipitation projection. This indicates that, while PET is solely driven by temperature, ET (which depends on various atmospheric and land variables) is more driven by PRE than by PET. Owing to the lack of trends in the PRE and ET projections, no substantial trend is projected for the surface water balance (PRE - ET) in the basin (Figure 5.2(f)), but the capability of the basin to meet the atmospheric water demand (ET/PET) decreases because of higher moisture demand from the atmosphere (increased PET). However, the similarity between the temporal variability of soil water and ET/PET suggests that, despite the lack of discernible trends in the ET projection over the basin, the increase in PET may deplete the soil water and drive it to the wilting point. This could stress the vegetation and reduce crop production in the basin. It could also expose the soil to wind erosion and degrade the soil. However, in agreement with the precipitation projection, no discernible trend is projected for other hydrological variables (i.e. runoff, percolation, and river discharge). Hence, while the impacts of climate change produce a trend in soil water projection in the basin, they produce no discernible trends in other hydrological variables because of the lack of a trend in the precipitation projections.

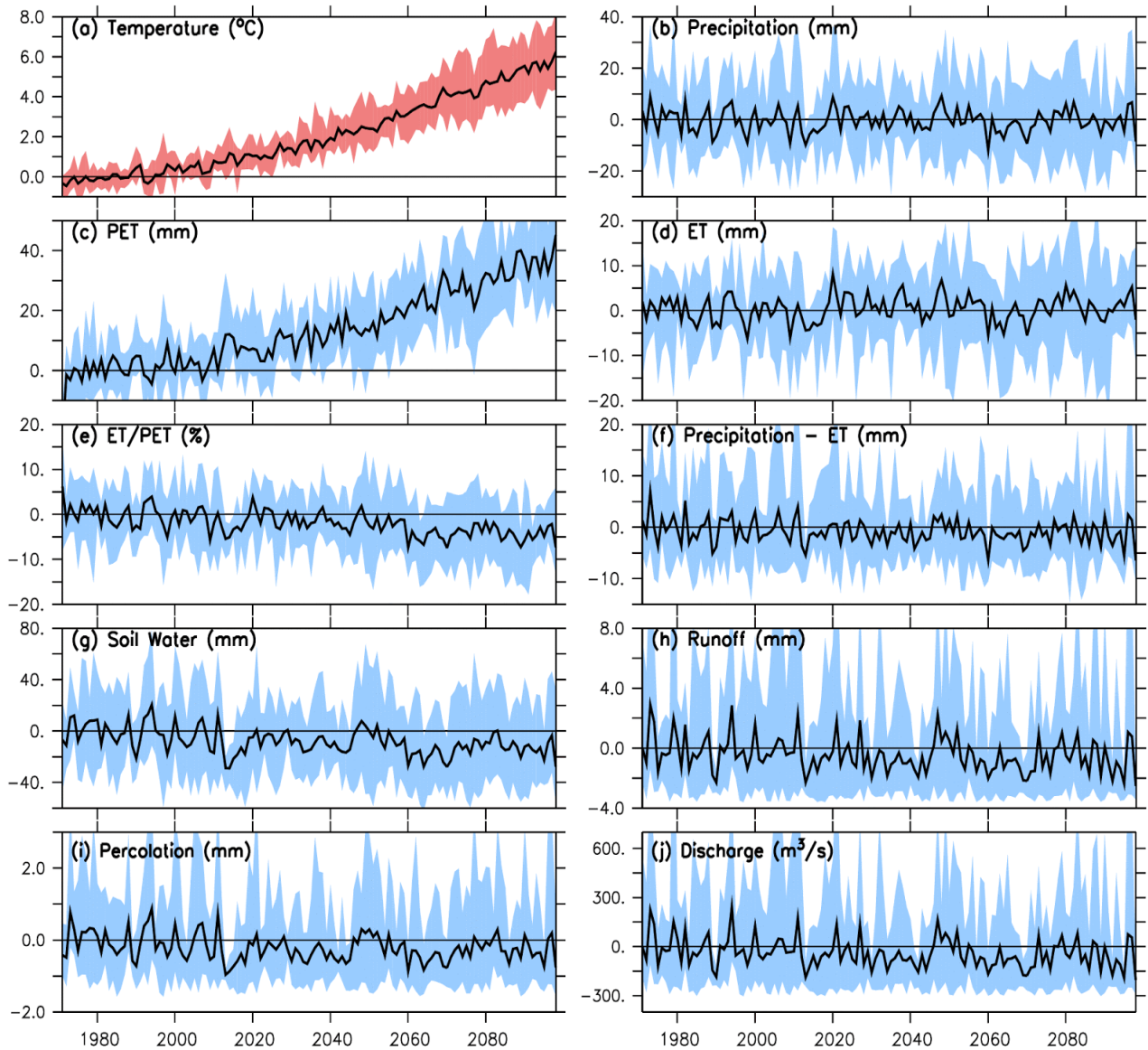


Figure 5.2: Temporal variations of the changes in hydroclimatic variables over the Vaal River basin in the period 1971-2099 under the RCP8.5 climate scenario. The changes are calculated with reference to the present-day climate (1971-2000). The solid lines represent the multi-model ensemble mean of selected climate models, and the spreads represent the range of selected climate models.

The spatial distribution of the projection at various GWLs (i.e. GWL1.5, GWL2.0, GWL2.5, and GWL3.0) is presented in Figures 5.3 to 5.6. At each GWL, the spatial distribution of precipitation and temperature changes over the basin also differ (Figure 5.3). While the projected temperature increase is uniform over the basin, the precipitation changes vary in sign and magnitude. The precipitation pattern also varies across the GWLs. For example, at GWL1.5, an increase in precipitation ($>2 \text{ mm month}^{-1}$) is projected over the north-eastern mountain range, but at GWL3.0, the increase is replaced with a decrease (-3 mm month^{-1}).

Also, the projected precipitation decrease ($< -2 \text{ mm month}^{-1}$) over the north-western part at GWL1.5 is replaced with a precipitation increase ($> 2 \text{ mm month}^{-1}$) at GWL3.0. However, a decreased precipitation is indicated over the south-eastern mountain range at all the GWLs (Figures 7(e)-(h)). Unlike in the temporal variation, the spatial distribution of PET changes differs from that of temperature, and the spatial variation of ET changes also differs from that of precipitation. While an increase in PET is projected over the whole basin (Figures 5.3(i)-(l)), the magnitude of the increase is higher over the western half of the basin. At all GWLs, an increase in ET is projected over the north-eastern mountain range, while a decrease is indicated over the south-eastern mountain range and at the centre of the basin. The decrease in ET over the south-east can be attributed to the decrease in precipitation over the area. Nevertheless, despite the projected decrease in precipitation over the north-eastern mountain range, an increase in ET is projected over the north-eastern mountain range at the expense of soil water (Figures 5.3 and 5.4). While ET/PET decreases across the entire basin, the largest decrease is projected over the northern part of the basin and along the south-eastern mountain range, where a decreased ET is projected (Figure 5.3). At GWL3.0, runoff and soil water are also projected to decrease over most parts of the basin, but with the maximum decrease occurring over the north-eastern mountain range, where the largest decrease in PRE and the highest increase in ET are simulated. Hence, at GWL3.0, the hydrological impacts of climate change (i.e. on soil moisture, and runoff) are projected to be most severe over the north-eastern part of the basin, where the maximum decrease in PRE and the maximum increase in ET are indicated.

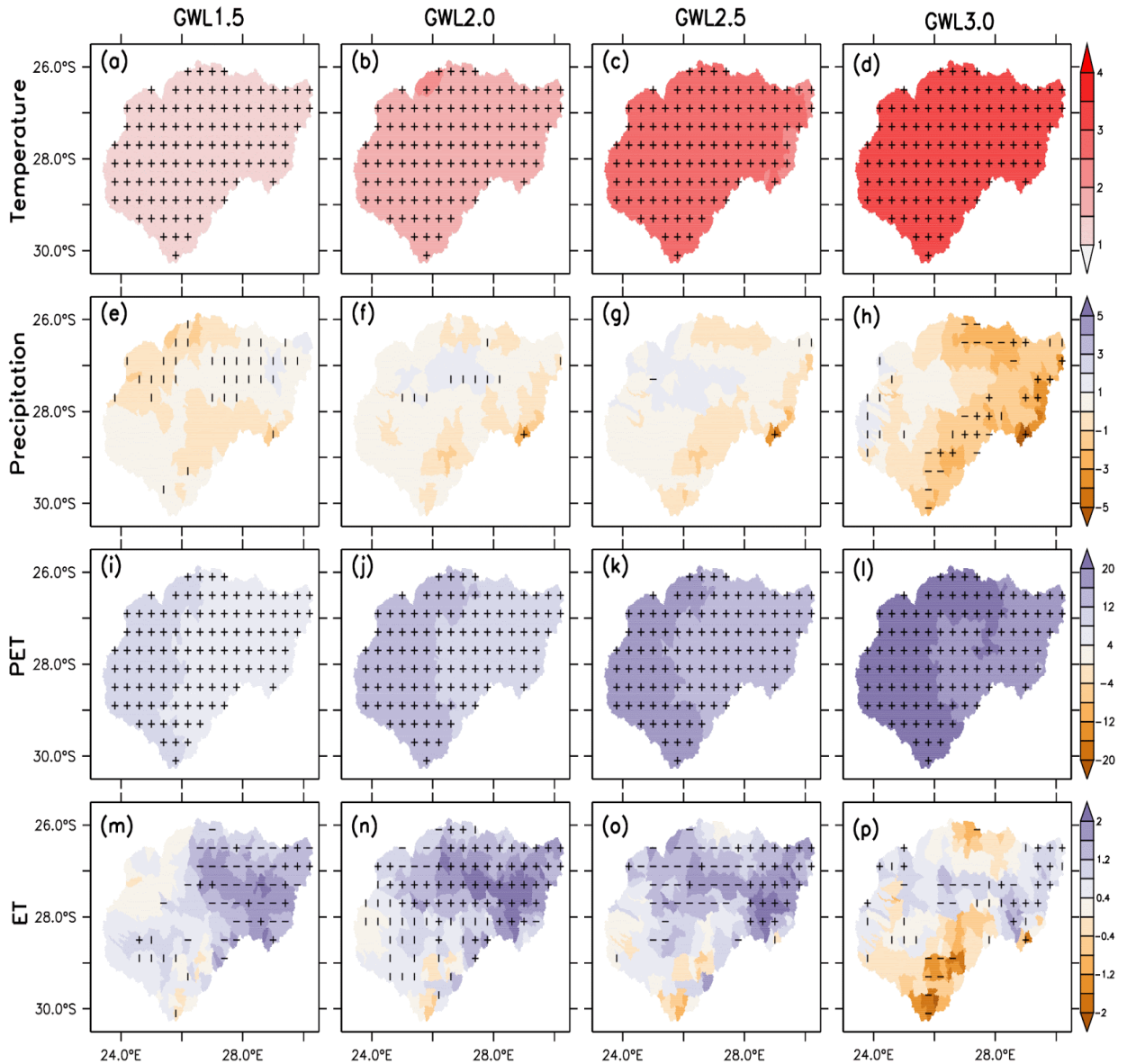


Figure 5.3: Spatial distribution of the projected changes in temperature ($^{\circ}\text{C}$), precipitation (mm month^{-1}), potential evapotranspiration (PET, mm month^{-1}) and evapotranspiration (ET, mm month^{-1}) over the Vaal River basin at different global warming levels (GWL1.5, GWL2.0, GWL2.5, and GWL3.0). The vertical strip (|) indicates where at least 80% of the simulations agree on the sign of the changes, while the horizontal strip (–) indicates where at least 80% of the simulations agree that the projected change is statistically significant (at 99% confidence level). The cross (+) shows where both conditions are satisfied, hence the change is robust.

In contrast to the ET projection, an increase in stream evaporation (ETS) is projected over all the river channels, but with the maximum increase ($>65 \text{ m}^3 \text{ s}^{-1}$) occurring along the main river channel (Figure 5.5). The difference between the ET and ETS projections can be attributed to the availability of more water for evaporation in the channels than in the soil. As both variables

increase in response to the enhanced atmospheric water demand (PET) over the basin, the increase in ET stops, when the soil reaches its wilting point (due to decreased precipitation), while the increase in stream ETS continues (due to availability of water in the river channels). However, the increase in ETS occurs at the expense of streamflow. Figures 5.5(i) to 5.5(l) show that, despite the increase in precipitation over some parts of the basin, a decrease in streamflow (up to $85 \text{ m}^3 \text{ s}^{-1}$) is projected over the main channels. This decrease can be attributed to two things: Firstly, the substantial decrease in runoff over the north-eastern mountain range (following the decreased precipitation and increased ET over the mountain range) will decrease the streamflow in the main channel because the north-eastern mountain range is the major source of the water in the main channel. Secondly, the increase in ETS (following the increase in PET over the entire basin) would also reduce the water availability in the basin. However, the decrease in streamflow in the river channels has a huge implication for water availability in the Vaal dam and for various socio-economic activities that depend on water from the VRB.

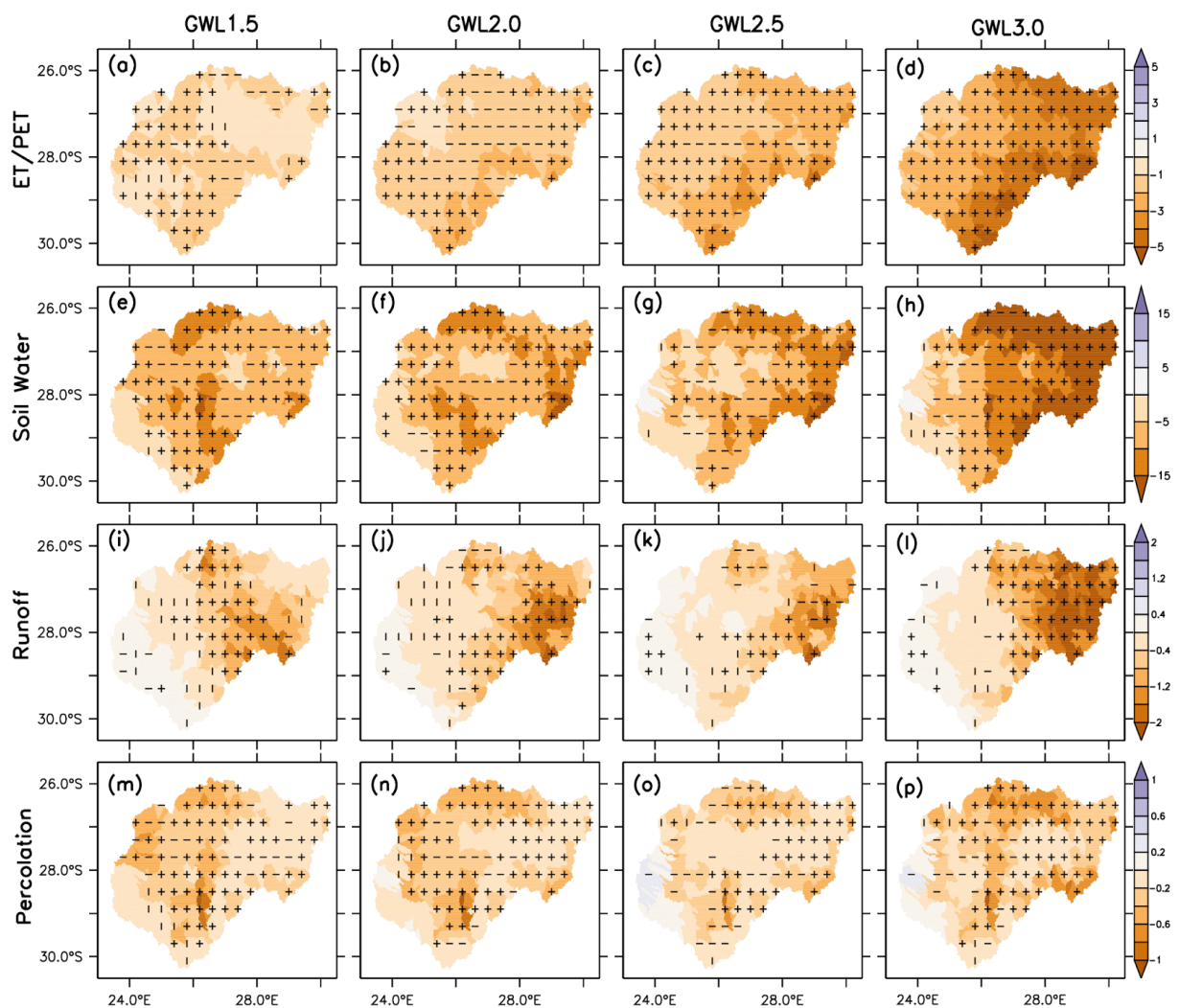


Figure 5.4: Same as Figure 5.3, except for ET/PET (%), soil water (mm month^{-1}), surface runoff (Runoff, $\text{m}^3 \text{ s}^{-1}$) and percolation (mm month^{-1}).

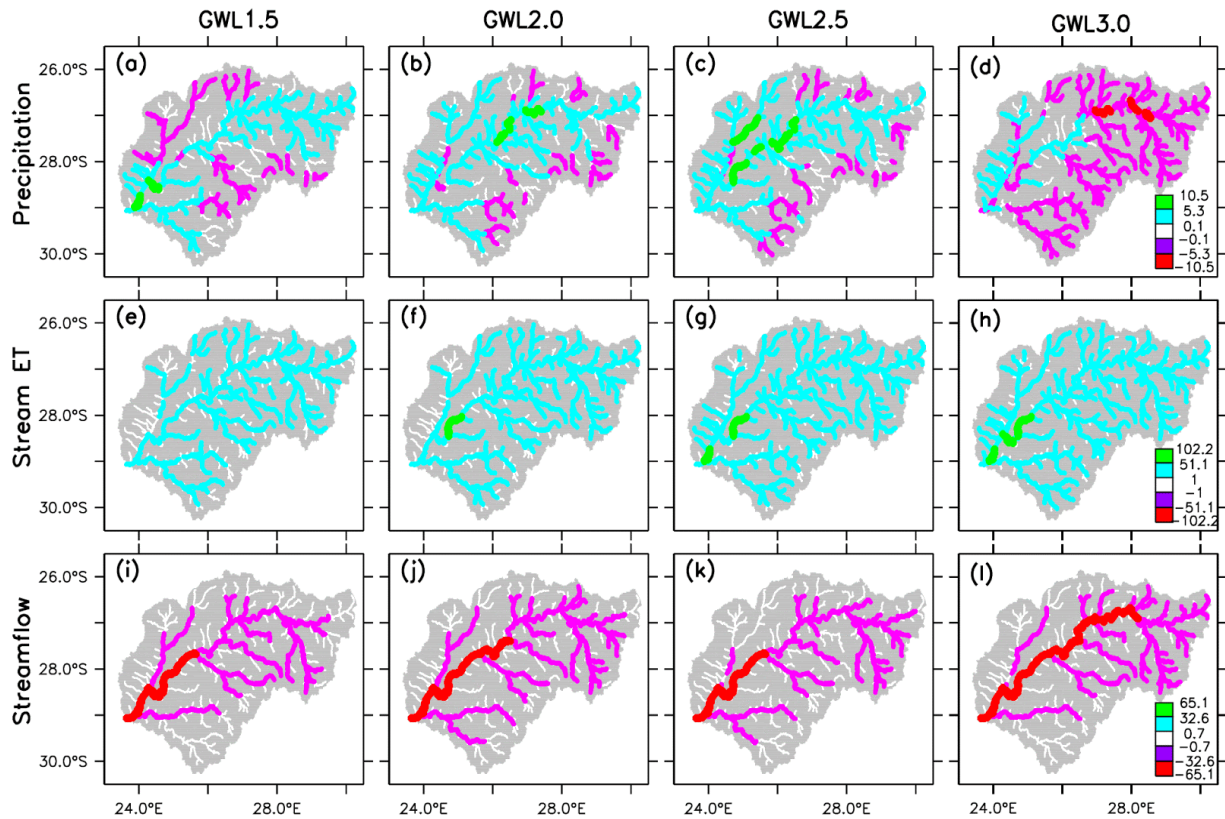


Figure 5.5: Same as Figure 5.3, but for channel variables: precipitation (mm month^{-1}), stream ET (mm month^{-1}), and streamflow ($\text{m}^3 \text{s}^{-1}$).

5.4 Impacts of LULC changes

The impacts of the LULC changes (i.e. GrLand, CrLand, CrGrLand, and BrLand) on the hydrological projections can be explained through the influence of the LULC changes on the curve number (CN) (Figure 5.6). With GrLand, CN decreases over the north-eastern part of the basin (Figure 5.6 (a)), where GRAS replaces CRWO and CRDY (Figure 5.1). With the increase in CN, more rainwater is retained in the soil but at the expense of runoff that feeds the Vaal River. The increase in soil water makes more water available for evaporation over the area. Hence, with GrLand, both soil water and ET increase (by up to 2 mm month^{-1} and $0.5 \text{ mm month}^{-1}$, respectively) over the north-eastern mountain range, while runoff decreases (by up to $0.5 \text{ mm month}^{-1}$). The decrease in runoff in turn decreases streamflow (by up to $434 \text{ m}^3 \text{ s}^{-1}$) in the main river channel. With other LULC changes (i.e. CrGrLand and BrLand), CN increases over the south-western half of the basin, but the highest increase (>10) occurs with BrLand, while the lowest increase (<8) occurs with CrGrLand. The increase in CN converts more of the rainwater to runoff and retains less in the soil. So, with these LULC changes, the soil water decreases by more than 2 mm month^{-1} . The decrease occupies the largest area in the BrLand experiment and the smallest area in the CrGrLand experiment. The decrease in soil water results in a decrease in ET (by up to $0.1 \text{ mm month}^{-1}$ in CrGrLand and $0.8 \text{ mm month}^{-1}$ in BrLand). In

contrast to soil water, the runoff increases (by up to $0.5 \text{ mm month}^{-1}$) over most parts of the basin, leading to an increase in the streamflow along the main river channel. However, while the increase in the streamflow at the river discharge is less than $9 \text{ m}^3 \text{ s}^{-1}$ in the CrGrLand experiment, it is more than $860 \text{ m}^3 \text{ s}^{-1}$ in the BrLand experiment. These results are consistent with previous studies, which showed that an increase in vegetation cover (GrLand) lowers water yield due to a higher rate of evapotranspiration and water infiltration, while a decrease in vegetation (BrLand) enhances water yield because of the hard impermeable surface of barren land (Koneti et al., 2018; Li et al., 2018; Setyorini et al., 2017).

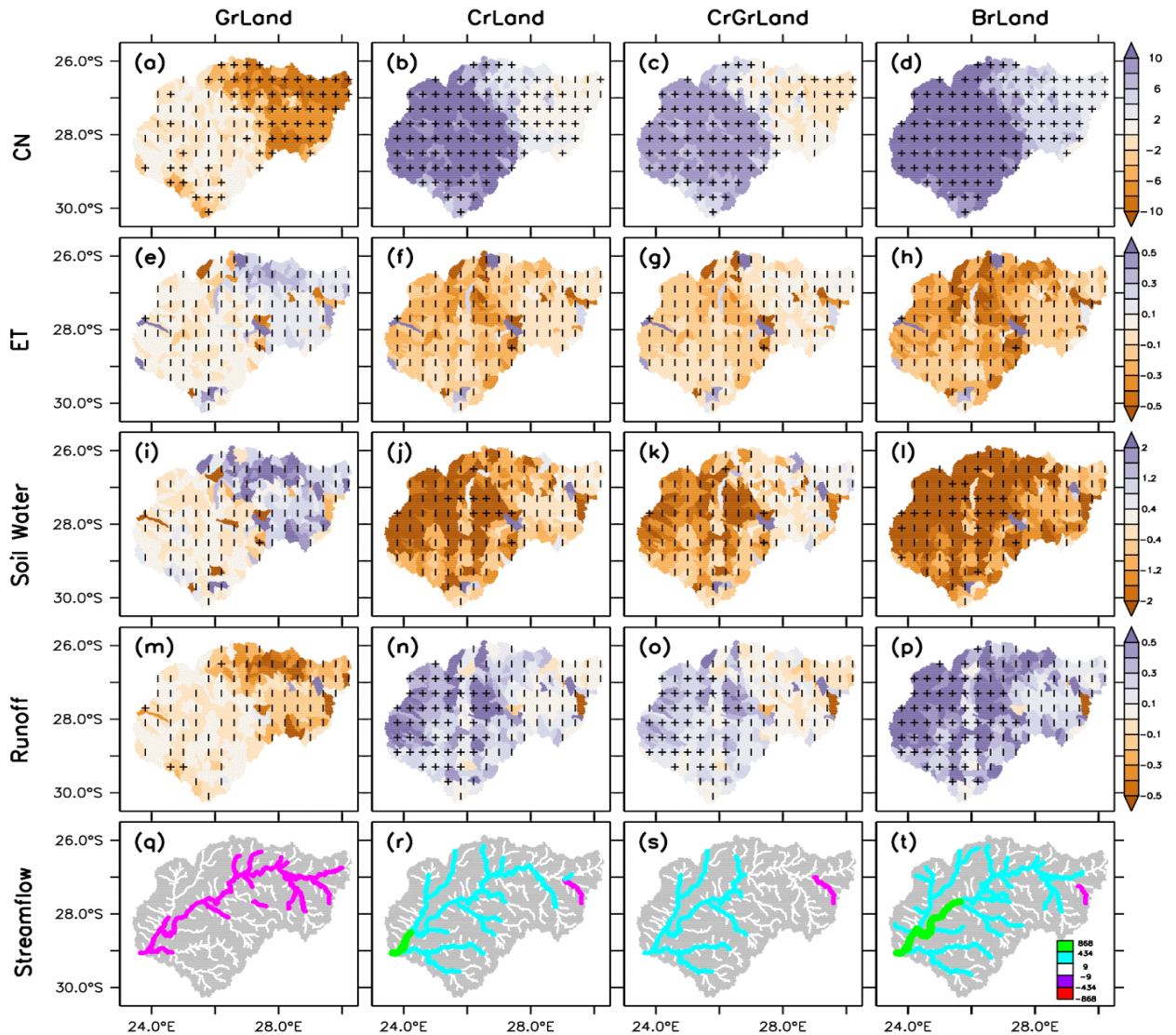


Figure 5.6: Impacts of LULC changes on hydrological variables over the Vaal River basin: CN (unitless), soil water (mm month^{-1}), surface runoff (Runoff, $\text{m}^3 \text{ s}^{-1}$) and streamflow ($\text{m}^3 \text{ s}^{-1}$). The vertical strip (|) indicates where at least 80% of the simulations agree on the sign of the changes, while the horizontal strip (-) indicates where at least 80% of the simulations agree that the projected change is statistically significant (at 99% confidence level). The cross (+) shows where both conditions are satisfied, hence the change is robust.

5.5 A comparison of impacts of climate and LULC changes

Since the main goal of the study is to investigate the extent to which the LULC changes can be used to mitigate climate change impacts in the VRB, this section compares the direction and magnitude of LULC change impacts with those of climate change, by focusing on the mean hydrological variables and drought characteristics (i.e. intensity and frequency) (Figure 5.7 and 5.8). In general, the uncertainty in the simulated impacts (i.e. simulation ensemble spread) is larger for climate change than for LULC changes (Figure 5.7 and 5.8), so the median of the simulation ensemble will be used for the comparison.

The comparison shows that, in some cases, the LULC changes reduce the climate change impacts, but in other cases, they enhance the impacts (Figure 5.7). However, for some variables, the LULC change impacts are negligible (i.e. the magnitude is very small compared to that of climate change impacts), while for some variables, they are substantial (i.e. the magnitude is comparable to that of climate change impacts). For example, at GWL3.0 (Figure 5.7 (d)), the impacts of all LULC changes (i.e. GrLand, CrLand, CrGrLand, and BrLand) on ET and ET/PET are negligible (i.e. <1%). Although GrLand increases the soil water by about 1%, while other LULC changes decrease it by up to 2%, these changes are small, compared to a decrease of 12% from climate change. In short, for all the variables, the impact of GrLand is less than 10% of the climate change. The reason for the small impacts of GrLand on hydrological variables in the VRB may be due to the small areas over which the grass replaces other land-use types in GrLand. The VRB is already dominated by grassland (which already occupies about 55% of the basin) and in GrLand, only about 30% of the basin (occupied by CRDY and CRGR) changes to grass. Another reason could be that GrLand keeps the water in the soil, where evapotranspiration can still deplete the soil water. However, these results indicate that GrLand may not be efficient in mitigating the hydrological impacts of climate change in the basin.

Other LULC changes produce substantial impacts on hydrological variables (i.e. runoff, percolation, water yield, and streamflow). However, while they reduce climate change impacts on runoff, water yield, and streamflow, they enhance climate change impacts on percolation. For example, at GWL3.0 (Figure 5.7(d)), CrLand and BrLand produce about a 15% increase in runoff, water yield, and streamflow that could completely offset the less than 15% decrease in these variables due to climate change. Nevertheless, these LULC changes would decrease percolation by about 15%, in addition to the 13% decrease produced by climate change, making a net decrease of 28% in percolation in the future at GWL3.0. This may have a huge implication for underground water storage in the basin. Also, the BrLand change overcompensates for climate change impacts on runoff by more than 2%. This can enhance peak flow, soil erosion, and land degradation in the basin.

In agreement with Abiodun et al. (2019), Figure 5.7 shows that the impacts of climate change on the frequency of meteorological droughts are higher for SPEI drought than for SPI droughts. As anticipated, the projected changes in the hydrological droughts (SWI, PERCI, RFI, WYLDI, and DI) fall within that of SPI and SPEI. This implies that the projected increase in the

frequency of hydrological droughts is more than that of SPI drought but less than that of SPEI drought. However, at GWL3.0, the projected hydroclimatic impacts of climate change are most severe on soil drought frequency (with an increase of more than 38 months decade⁻¹) and least pronounced with regard to percolation drought frequency (where an increase of less than 30 months decade⁻¹ is indicated). GrLand only reduces the frequency of soil and percolation droughts by 1 month decade⁻¹ but increases the frequency of runoff, water yield, and streamflow droughts by up to 5 months decade⁻¹. Compared to climate change impacts (an increase of 30-38 months decade⁻¹), while a decrease of 1 month decade⁻¹ (<3%) is negligible, the increase of 5 months decade⁻¹ (>13%) is substantial. Other LULC changes (CrGrLand, CrLand and BrLand) increase the frequency of soil and percolation droughts by 1 month decade⁻¹ but reduce that of runoff, water yield, and streamflow droughts by 5-60 months decade⁻¹. Among the three LULC changes, BrLand features the lowest impacts on the drought frequency, while CrGrLand shows the largest impacts.

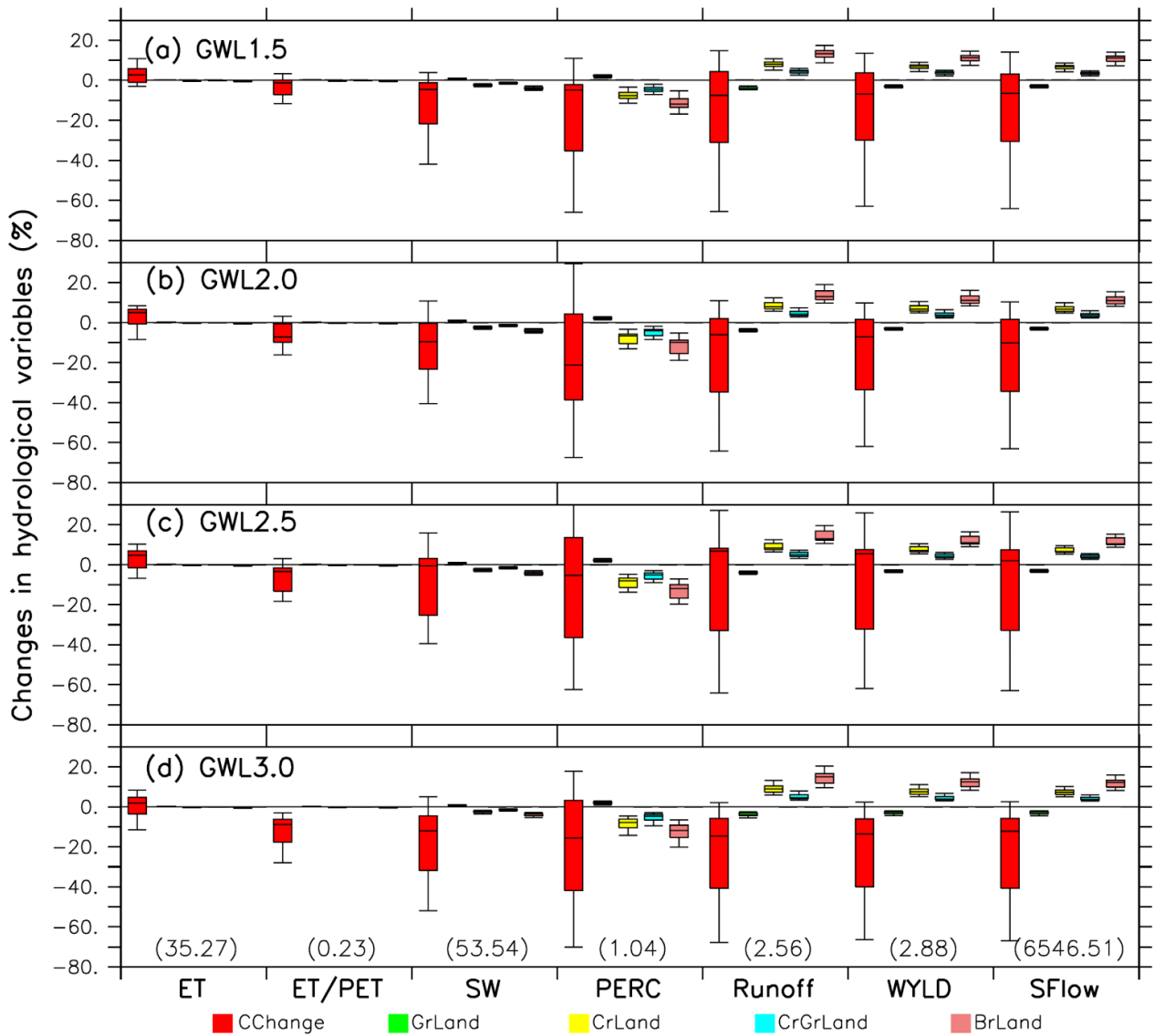


Figure 5.7: A comparison of the impacts of climate change (CChange) and LULC change (FrLand, GrLand, CrLand, and CrGrLand) on hydrological variables: ET, ET/PET, soil water (SW), percolation (PERC), Runoff, water yield (WYLD), and streamflow (SFlow) over the Vaal River basin at different global warming levels (GWL1.5, GWL2.0, GWL2.5 and GWL3.0). The present-day climatological value for each variable is indicated in brackets.

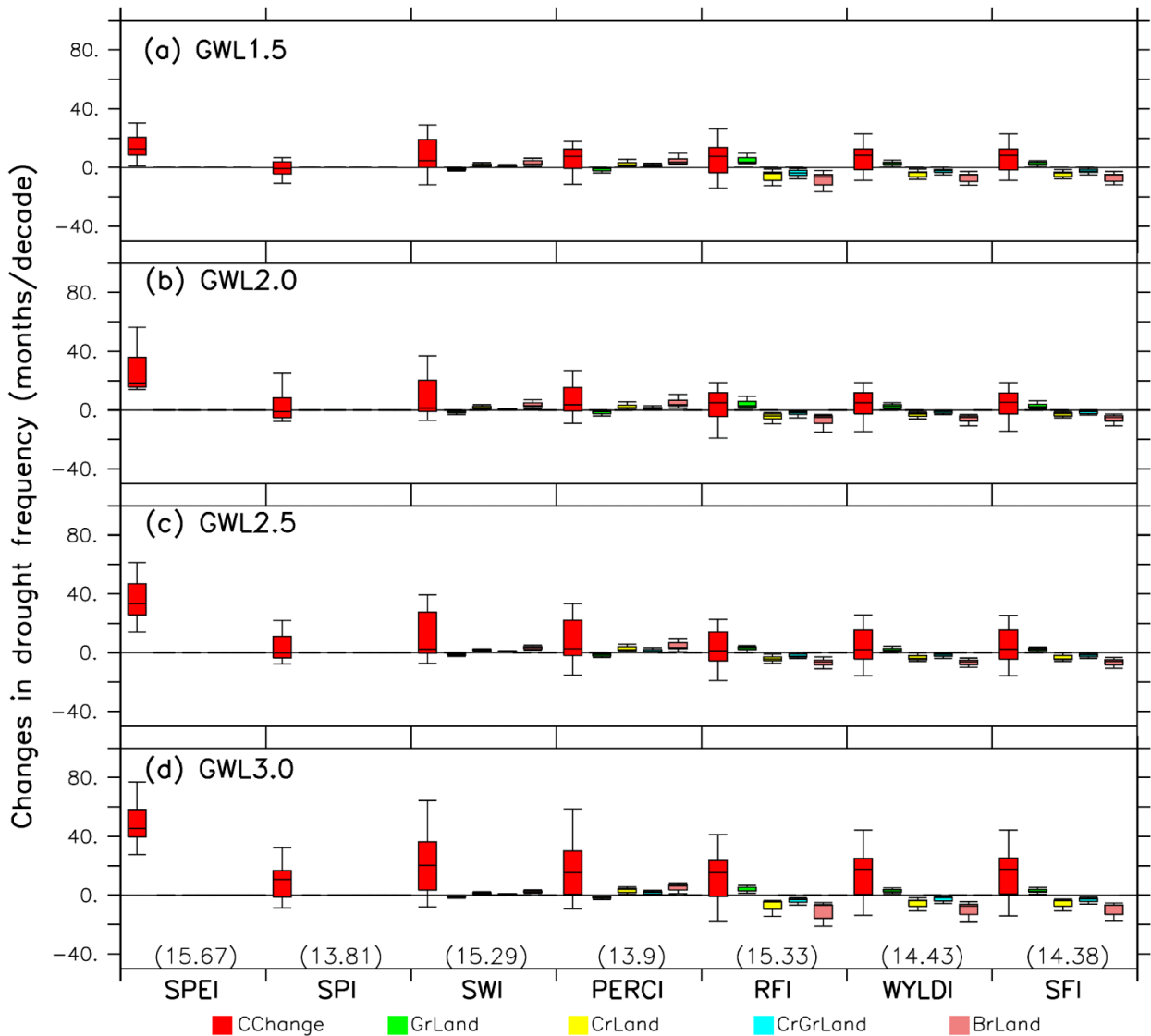


Figure 5.8: A comparison of the impacts of climate change (CChange) and LULC change (FrLand, GrLand, CrLand, and CrGrLand) on the frequency of droughts (SPEI, SPI, SWI, PERCI, RFI, WYLDI and SFI) over the Vaal River basin at different global warming levels (GWL1.5, GWL2.0, GWL2.5 and GWL3.0). The present-day climatological value for each variable is indicated in brackets.

5.6 Summary

This chapter has examined the extent to which LULC changes can be applied in reducing climate change impacts on the VRB (South Africa) with a focus on hydrological droughts. For the study, the SWAT+ model calibrated in Chapter 3 was coupled with the bias-corrected CORDEX datasets to conduct a series of hydrological simulations over the basin. The climate change impacts on the hydroclimatic variables and the drought frequency are projected at four GWLs, and the extent to which four land cover scenarios (i.e. expansion of grassland, cropland, cropland/grassland mosaic, and barren land) can influence the projections are quantified. The future climate projections over the basin show an increasing trend in temperature and potential

evaporation, with no trend in precipitation and hydrological variables. However, the spatial distribution of the projections shows a uniform increase in temperature across the basin, with a decrease in precipitation, soil water, percolation, surface runoff and streamflow over most parts of the basin. The model simulations reveal that the expansion of grassland reduces the climate change impacts on soil water, percolation, and the associated drought frequency, but the magnitude of the reduction is negligible compared to the climate change impacts. Conversely, it enhances the climate change impacts on runoff, water yield, streamflow, and the associated drought frequency. In contrast, the expansion of other LULC changes mitigates the climate change impacts on runoff, water yield, streamflow, and the associated drought frequency, but it enhances the impacts of climate change on soil water, percolation, and the drought frequency both variables. The results of the study have application in the development of mitigation and adaptation strategies or policies to address the impacts of climate change in river basins, particularly in South Africa.

Chapter 6: Using land-use change to mitigate future impacts of climate change on hydrological droughts in the Limpopo River basin

6.1 Introduction

The LRB is one of the most economically important river basins in Southern Africa because it supports the socio-economic activities in the four neighbouring riparian countries (i.e. Botswana, Mozambique, South Africa, and Zimbabwe) and contributes to the economy of the entire SADC region by supporting a wide range of socio-economic activities. However, as hydrological drought poses a big threat to resources in the riparian countries of the LRB, there is a need to understand the future characteristics of hydrological droughts in the basin. This chapter thus projects the impacts of climate change on meteorological and hydrological droughts over the basin and examines how land-use changes could influence such hydrological drought projections.

6.2 Land-use change experiments

We performed five experiments (CtrLand, FrLand, GrLand, CrLand, and CrGrLand) to project the impact of climate change on basin hydrology, and to investigate how idealised LULC changes could influence these projections (Table 6.1). All the experiments used the same model setup as described in Chapter 3 (Figure 3.1) but with different LULC patterns. The Control experiment used the present-day LULC pattern (Figure 5.1(a)), while other experiments used the idealised LULC pattern described in Table 6.1 and shown in Figure 6.1. In FrLand, forest (FOEB) invades savanna (SAVA) areas, leading to a shift in tree-grass dynamics of vegetation. This scenario of land-use change is chosen after consideration of a general trend towards more tree-dominated ecosystems in the Limpopo Province, particularly in open grassland and savanna areas (Scheiter et al., 2018). In GrLand, grass replaces cropland areas (CRDY and CRGR), depicting a restoration of grassland scenario. In CrLand, which represents the expansion of agriculture scenario, crop (CRDY) replaces semi-natural vegetation (GRAS, CRGR and CRWO). This scenario is warranted, since the Limpopo province is one of South Africa's prime agricultural regions with respect to the production of livestock, fruits, vegetables, cereals, and tea. In CrGrLand, the mixture of cropland and grassland (CRGR) replaces semi-natural vegetation (GRAS, CRDY and CRWO), indicating a scenario where cropland and grassland exist in an equilibrium "mosaic" (Table 6.1).

However, in all the experiments, the SWAT+ simulations were forced with the bias-corrected CORDEX datasets (CORDEX_QDM) over the period 1971-2090, after a five-year model spin-up. Each experiment consists of simulations based on the CORDEX_QDM seven-member ensemble. To obtain the impacts of climate change at a given GWL in the Control experiments, the simulations of the present-day climate period (1971-2000) are subtracted from those of the GWL climate period. The GWL periods of the simulations are the same as the GWL periods of

the CORDEX dataset (described in Table 3.1), which were used in producing the simulation. To obtain the impacts of LULC change in an experiment, the simulations of the experiment are subtracted from the corresponding simulations in the Control experiment at the same GWL.

Table 6.1: Summary of LULC change experiments in the Limpopo River basin.

Experiments	Description	LULC pattern
CtrlLand	<ul style="list-style-type: none"> Control LULC, which is SWAT+ default land use. 	Figure 6.1(a)
FrLand	<ul style="list-style-type: none"> Increase in evergreen broadleaf forest (i.e. shift in the tree-grass dynamics of SAVA). FOEB occupies 46.35% of the basin. 	Figure 6.1(b)
GrLand	<ul style="list-style-type: none"> Expansion of grassland expansion (i.e. grass invasion). GRAS replaces CRDY, CRWO, and CRGR. GRAS occupies 81.27% of the basin. 	Figure 6.1(c)
CrLand	<ul style="list-style-type: none"> Extensive cropping. CRDY replaces CRWO, GRAS, and CRGR. CRDY covers 81.27% of the basin. 	Figure 6.1(d)
CrGrLand	<ul style="list-style-type: none"> Cropland/grassland expansion. CRGR replaces CRDY, CRWO, and GRAS. CRGR covers 81.27% of the basin. 	Figure 6.1(e)

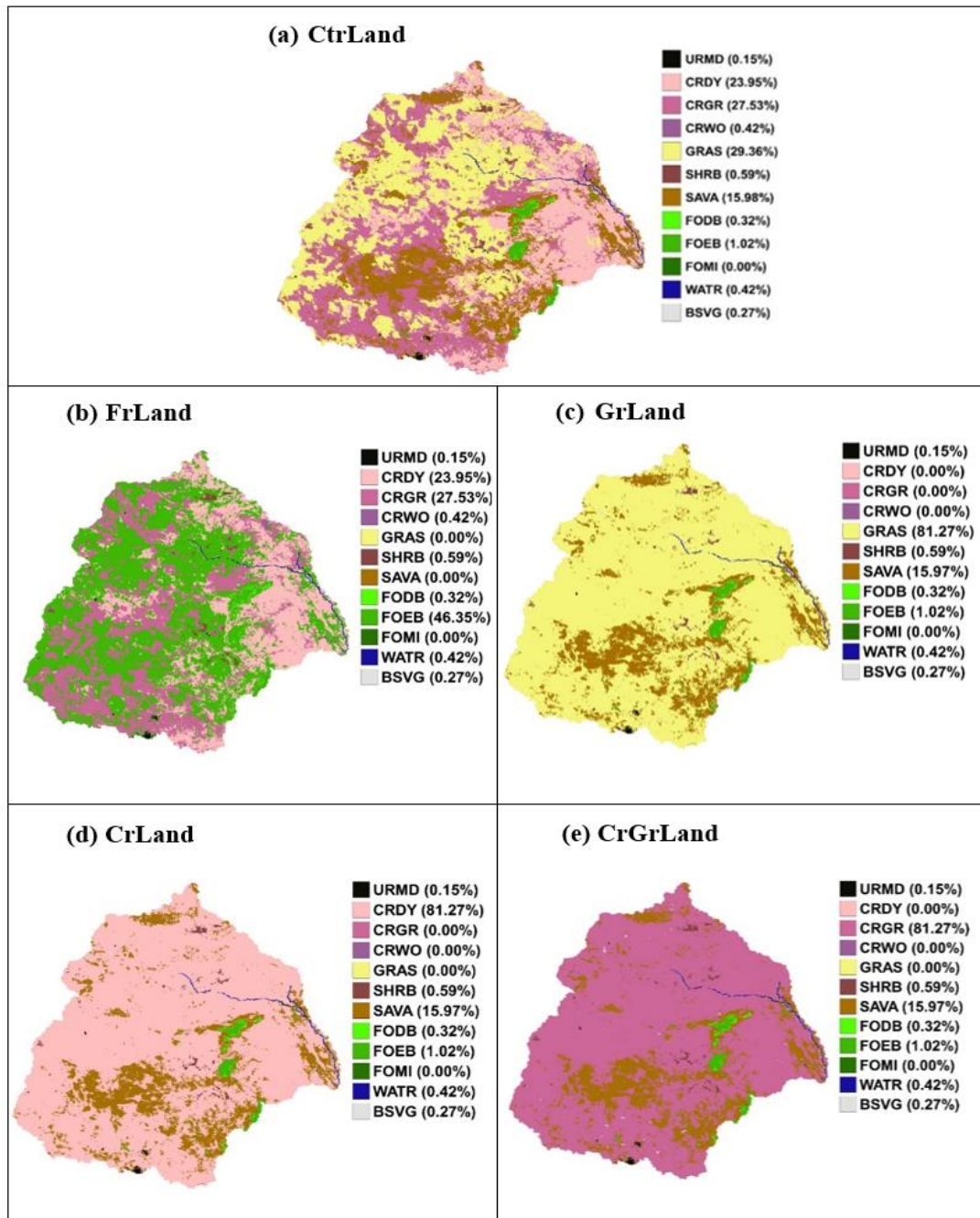


Figure 6.1: The LULC patterns used in the LULC change experiments for the Limpopo River basin: (a) CtrLand, (b) FrLand (c) GrLand (d) CrLand and (e) CrGrLand. The land-use types are urban residential medium density (URMD), cropland/dryland and pasture (CRDY), cropland/grassland mosaic (CRGR), cropland/woodland mosaic (CRWO), grassland (GRAS), shrubland (SHRB), savanna (SAVA), forest – deciduous broadleaf (FODB), forest – evergreen broadleaf (FOEB), forest – mixed (FOMI), water (WATR), and Bare ground/sparse vegetation (BSVG). The percentage of each LULC type is indicated in brackets.

6.3 Impacts of climate change

The time series of the projected changes in the hydroclimatic variables over the basin for the period 1951-2099 are presented in Figure 6.2. The models project an increase in temperature over the period, with the increase reaching about 5°C in 2099. This temperature increase is higher than global warming (about 4.2°C by 2100) at the same scenario (Intergovernmental Panel on Climate Change (IPCC), 2013), meaning that the warming rate over the LRB may be higher than the global average. The projected increase in temperature agrees with the results obtained by Aich et al. (2014), Engelbrecht et al. (2015), James and Washington (2013), and Maúre et al. (2018) over the basin. The spatial distribution of the temperature projection (Figure 6.2) shows that the warming is uniform over the basin, and that the magnitude of the warming increases with the increasing GWLs.

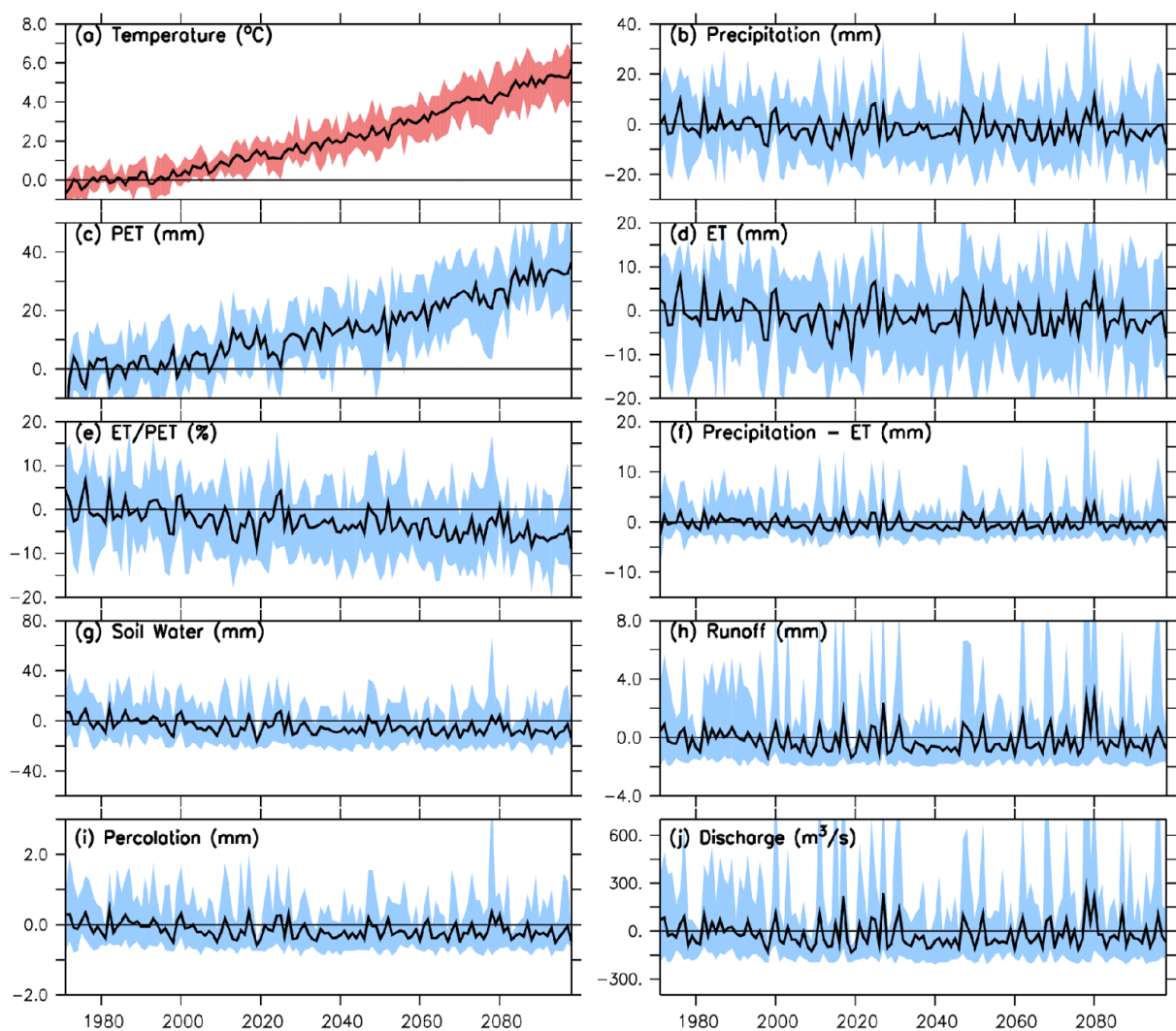


Figure 6.2: Temporal variation of the changes in hydroclimatic variables over the Limpopo River basin in the period 1971-2099 under the RCP8.5 climate scenario. The changes are calculated with reference to the present-day climate (1971-2000). The solid lines represent the multi-model ensemble mean of selected climate models, and the spreads represent the range of selected climate models.

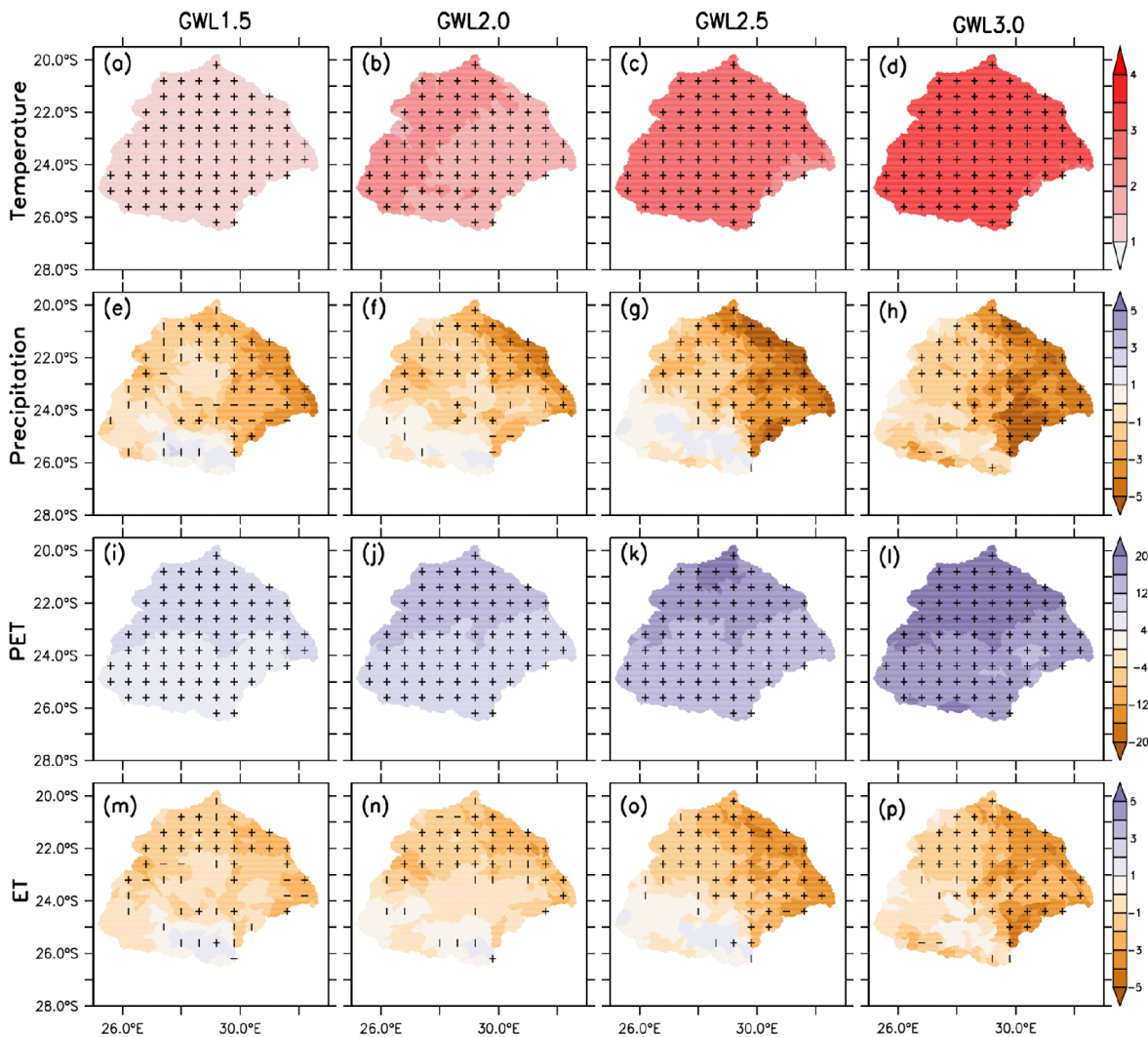


Figure 6.3: Spatial distribution of the projected changes in temperature ($^{\circ}\text{C}$), precipitation (mm month^{-1}), potential evapotranspiration (PET, mm month^{-1}) and evapotranspiration (ET, mm month^{-1}) over the Limpopo River basin at different global warming levels (GWL1.5, GWL2.0, GWL2.5, and GWL3.0). The vertical strip (|) indicates where at least 80% of the simulations agree on the sign of the changes, while the horizontal strip (–) indicates where at least 80% of the simulations agree that the projected change is statistically significant (at 99% confidence level). The cross (+) shows where both conditions are satisfied, hence the change is robust.

There is no discernible trend in the projection of precipitation over the LRB, as there is no indication of a future increase or decrease in the magnitude of rainfall variability over the basin (Figure 6.2). This suggests a long-term consistency in the amount of rainfall water in the basin. However, there is an indication of an incremental increase in the frequency of extreme wetness and dryness, as depicted by the model ensemble from 2030. Nonetheless, the spatial variation of the rainfall projection at GWL1.5 indicates that most parts of the basin (especially, the

eastern part) may experience a decrease in rainfall ($>6 \text{ mm month}^{-1}$), while the southern parts may experience an increase (up to 2 mm month^{-1}). Despite this, the area with decreasing rainfall expands with the increasing GWLs. Several studies found similar results (Aich et al., 2014; Maúre et al., 2018; Zhu and Ringler, 2012) of a decline in precipitation over the LRB. This is likely to have negative impacts on agriculture and water resources. This drying condition is not seen in the projections of Singh et al. (2014), which indicate a wetter future northeast of the basin. This discrepancy may be a result of the sensitivity to the variability of rainfall of the downscaling method used in their study.

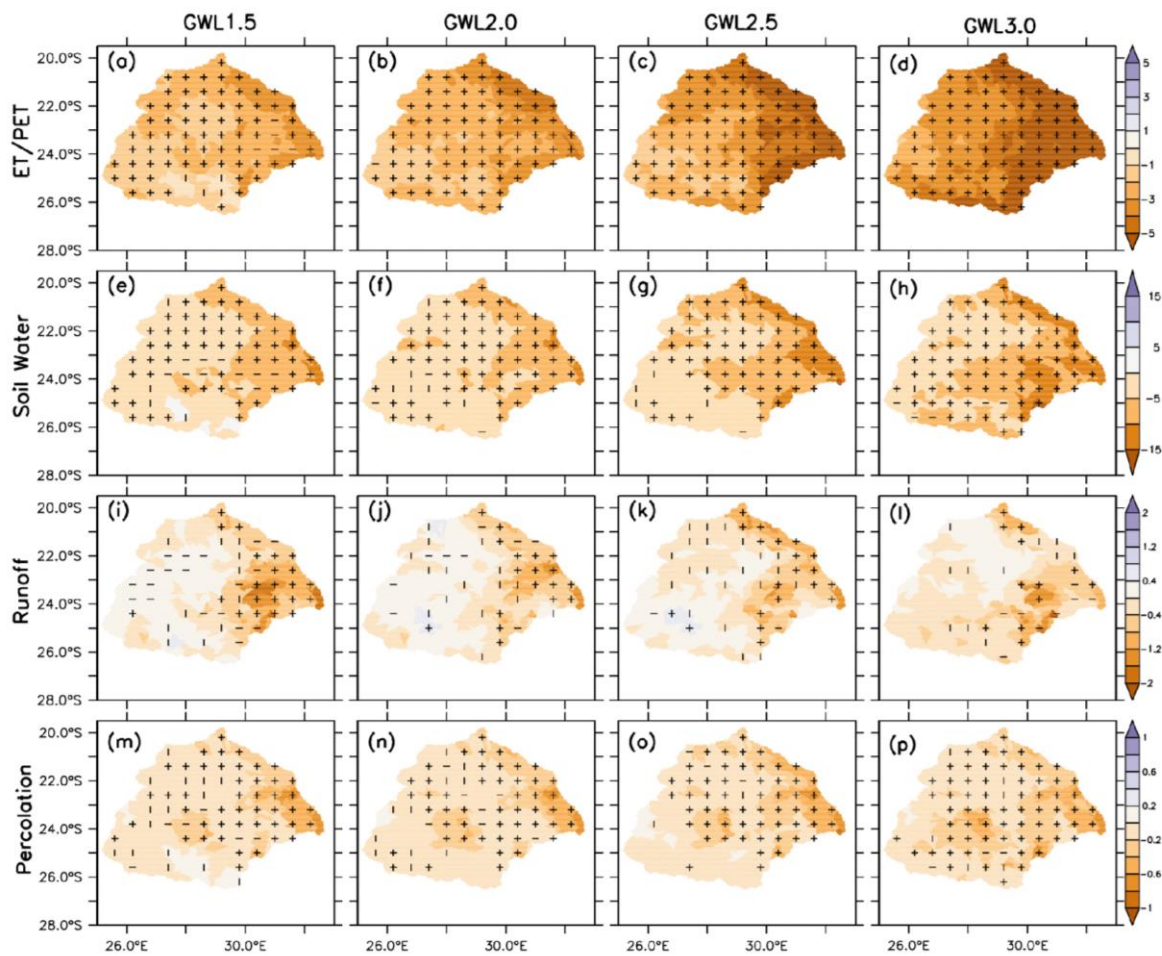


Figure 6.4: Same as Figure 6.2, except for ET/PET (%), soil water (mm month⁻¹), surface runoff (Runoff; m³ s⁻¹) and percolation (mm month⁻¹).

The SWAT+ projection shows a gradual increase in PET following the increasing temperature trend evident in Figure 6.1. The spatial distribution of the increase not only grows with increasing GWLs, but also shows that the magnitude of the increase is lower in the eastern part of the basin than in the rest of the entire basin. A similar pattern of increasing temperature, and consequently PET was found by Singh et al. (2014) over the Olifants River basin using

downscaled GCMs. The ET projection follows that of rainfall, showing no discernible trend. Even so, the spatial variation of the projection reveals an increase in ET further south of the basin and a decrease (about 6 mm month^{-1}) over the rest of the basin. From Figure 6.2, it is evident that there is better agreement between ET and rainfall projections than between ET and PET projections. This may be because, over land, ET depends on the availability of moisture, which relies heavily on the amount of rainfall. Once the soil moisture (which is limited by rainfall amount) is depleted, ET stops, irrespective of the evaporative demand by the atmosphere (i.e. PET). Hence, over land, changes in ET depend more on changes in rainfall than on changes in PET. Additionally, the evaporative demand of the atmosphere is higher than the actual ET, indicating that rainfall, which falls over the LRB, cannot meet the ET demand and all precipitation (except run-off) transforms into ET. This may result in increased aridity over the already arid to semi-arid LRB. The projected changes in temperature, PET and precipitation are in line with those found by Li et al. (2015) using a high-resolution Regional Climate Model (RCM) over Southern Africa. Furthermore, Abiodun et al. (2019) found that the projected decrease in precipitation and ET, along with a maximum increase in temperature and PET over the water-stressed LRB, are consistent with the increased occurrence of severe drought.

Consistent with the precipitation and ET projections, the impact of global warming on the hydrological variables (SW, PERC, Runoff and WYLD) shows no discernible trend, as the projection of the hydrological variables shows no significant change (Figure 6.3). Nevertheless, the spatial distribution of the SW projection shows a future decrease in SW, with the higher decrease (up to 10 mm month^{-1}) over the eastern half of the basin and the lower decrease (about 5 mm month^{-1}) over the west (Figure 6.4). In contrast, the spatial distributions of the other hydrological variables (PERC, Runoff and WYLD) project an increase ($>0.1 \text{ mm month}^{-1}$ and $>1 \text{ mm month}^{-1}$) over the western half of the basin, as well as a decrease ($<0.5 \text{ mm month}^{-1}$ and $<1 \text{ mm month}^{-1}$) over the eastern half at all the GWLs. This projected decrease may offset the increase and may be the reason behind the indiscernible trend among these variables. The decrease in Runoff and WYLD may be attributed to the projected decrease in precipitation and ET, along with the projected increase in temperature and PET. These projections are comparable with those of previous studies (Arnell et al., 2003; Li et al., 2014), which found a decrease in runoff over Southern Africa. Using downscaled GCMs as input for a hydrological model, Zhu and Ringler (2012) projected a decrease of up to 35% in runoff over the LRB.

The projected changes of the hydroclimatic variables over the river channels are shown in Figure 6.5. In contrast to the ET over land, SWAT+ projects a future increase of about 15 mm month^{-1} in 2099 in ET over the channels (i.e. stream ET). This implies that the LRB may lose more water through evapotranspiration of the streamflow than over land. This is because, over land, ET is limited by the amount of soil moisture and precipitation that occurs over the land; once the SW is depleted, ET stops. Conversely, evaporation is continuous over the channel due to the availability of the streamflow. Hence, changes in ET may be more driven by PET than by rainfall. Even so, the time series of the future projection of streamflow over the basin has no distinguishable change. Yet the spatial distribution of streamflow projects an increase ($37 \text{ m}^3 \text{ s}^{-1}$) over the western and central channels and a decrease ($37 \text{ m}^3 \text{ s}^{-1}$) over the channels

located in the eastern half of the basin. These results are in line with those of McCluskey and Strzepek (2007), who projected a significant reduction in streamflow over the majority of Southern Africa using GCMs over Africa. Aich et al. (2014) projected an increase in the mean annual streamflow over the LRB using inputs from the CMIP5 model ensemble as input in SWAT at RCP 2.6 and 8.5.

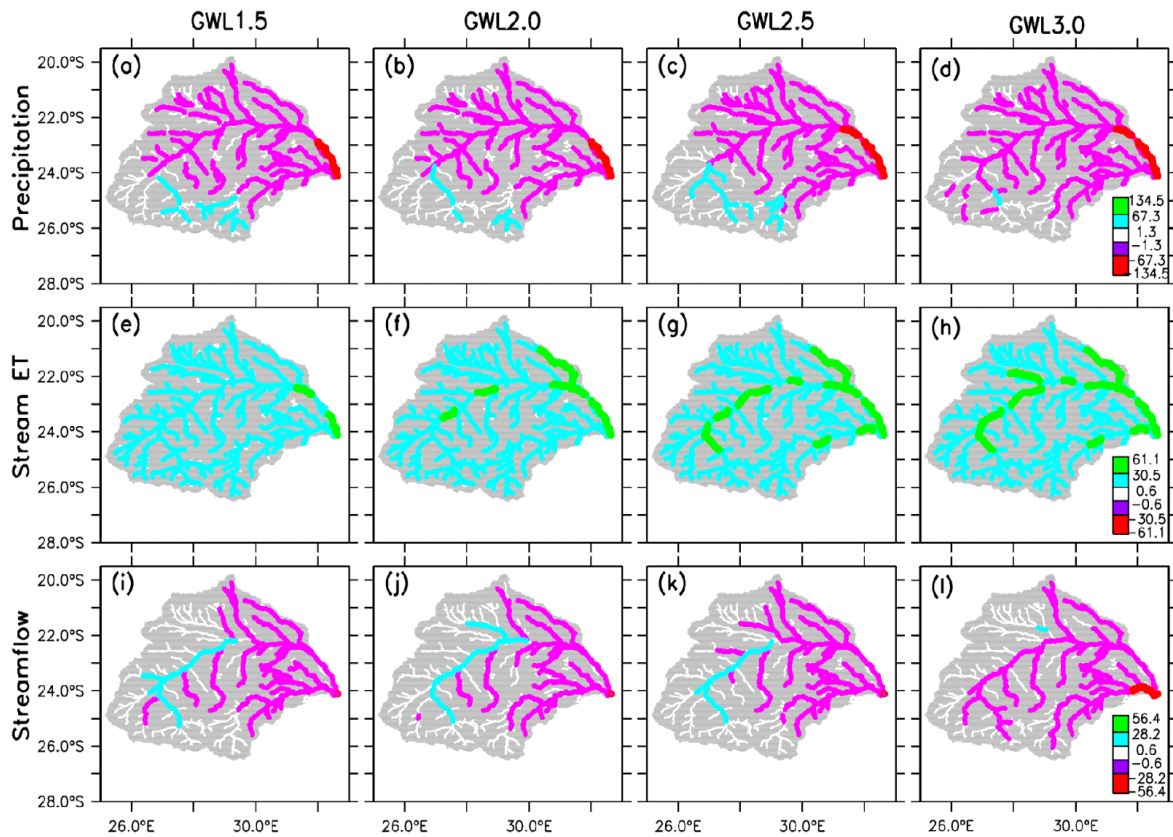


Figure 6.5: Same as Figure 6.3, but for channel variables: precipitation (mm month^{-1}), stream ET (mm month^{-1}), and streamflow ($\text{m}^3 \text{s}^{-1}$).

6.4 Impacts of LULC changes

The LULC change scenarios produce different impacts over the basin. However, their influences on CN can be grouped into two categories. While FrLand and GrLand (i.e. the expansion of FOEB and GRAS, respectively) decrease CN, CrLand and CrGrLand (the expansion of CRDY and CRGR, respectively) increase it over most parts of the basin. The influence of FrLand and GrLand on ET and soil moisture are quite patchy, and the direction of the influence is not the same across the basin. However, in accordance with the decreased CN, both LULC change scenarios decrease runoff (up to $0.5 \text{ mm month}^{-1}$ in FrLand) and streamflow (up to $305 \text{ m}^3 \text{ s}^{-1}$ in GrLand). Although the influence of CrLand and CrGrLand on ET and soil water are also patchy, both LULC change scenarios decrease ET and soil water over most parts of the basin. A comparison of the changes in GrLand, CrLand and CrGrLand results show that, in the case of CrGrLand, the impacts of cropland on ET and soil water are more than that of grassland. Nevertheless, consistent with the decrease in CN, both CrLand and CrGrLand

increase runoff and streamflow over most parts of the basin, except that the magnitude of the increase is higher in the case of CrLand.

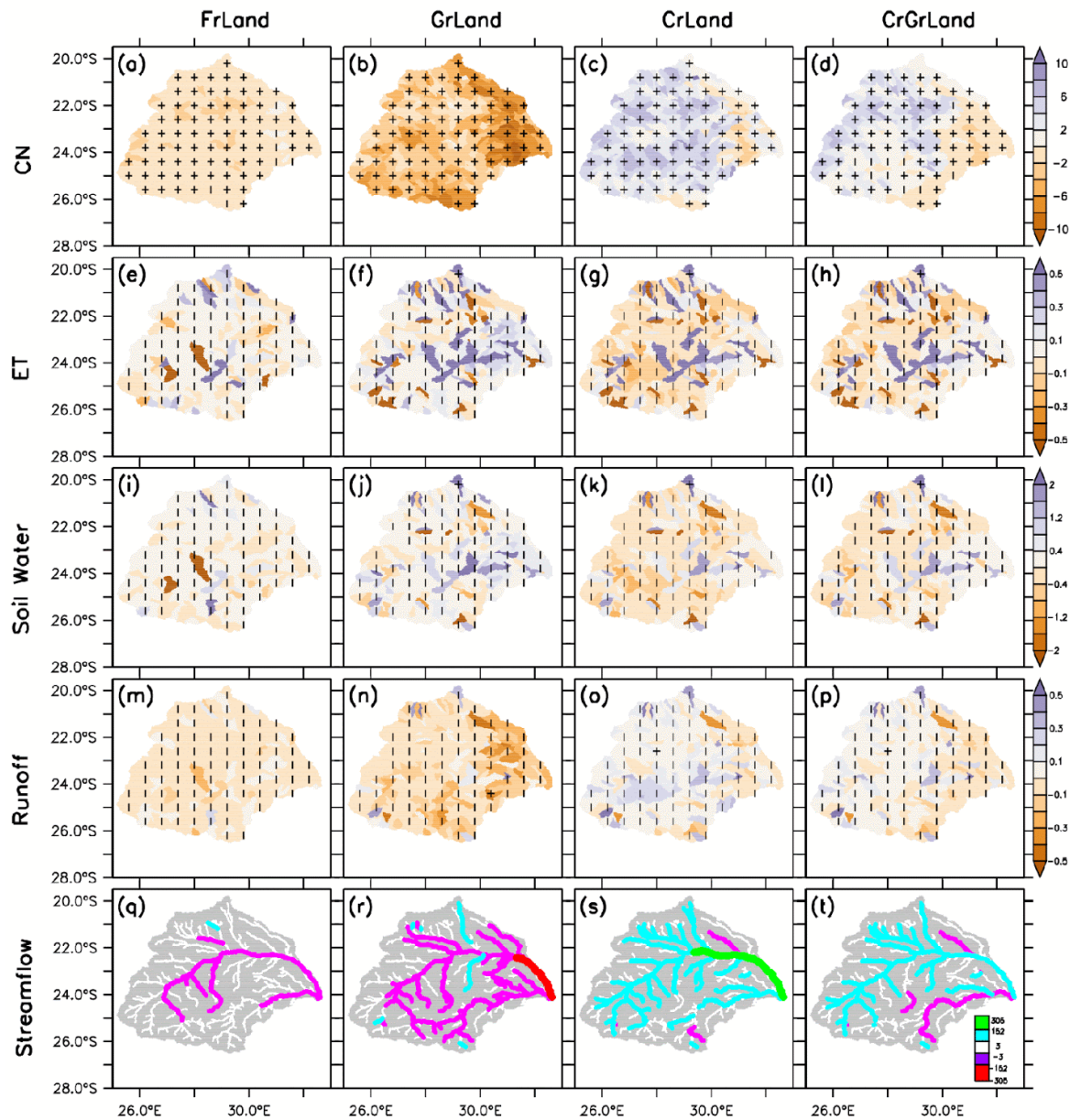


Figure 6.6: Impacts of LULC changes on hydrological variables over the Limpopo River basin: CN (unitless), soil water (mm month^{-1}), surface runoff (Runoff, $\text{m}^3 \text{s}^{-1}$) and streamflow ($\text{m}^3 \text{s}^{-1}$). The vertical strip (|) indicates where at least 80% of the simulations agree on the sign of the changes, while the horizontal strip (—) indicates where at least 80% of the simulations agree that the projected change is statistically significant (at 99% confidence level). The cross (+) shows where both conditions are satisfied, hence the change is robust.

6.5 A comparison of impacts of climate and LULC changes

In general, the level of uncertainty (simulation spread) is higher for climate change impacts than for LULC change impacts. This makes the comparison a bit difficult. However, for a fair comparison, we use the median of the ensemble spread. For all the hydroclimatic variables, the

impacts of LULC changes are lower than those of climate change at any GWL. The most comparable impacts occur on runoff for GrLand and CrLand. While the impacts of GrLand enhance the climate change impacts on runoff (by up to half the climate change impacts at GWL2.5), the impacts of CrLand reduce the climate change impacts (by up to half the climate change impacts at GWL2.5). However, regardless of the magnitude, both FrLand and GrLand reduce the climate change impacts on soil water and percolation, but enhance the impacts on runoff, water yield and streamflow. In contrast, both CrLand and CrGrLand enhance the climate change impacts on soil moisture, but reduce the impacts on runoff, water yield and streamflow.

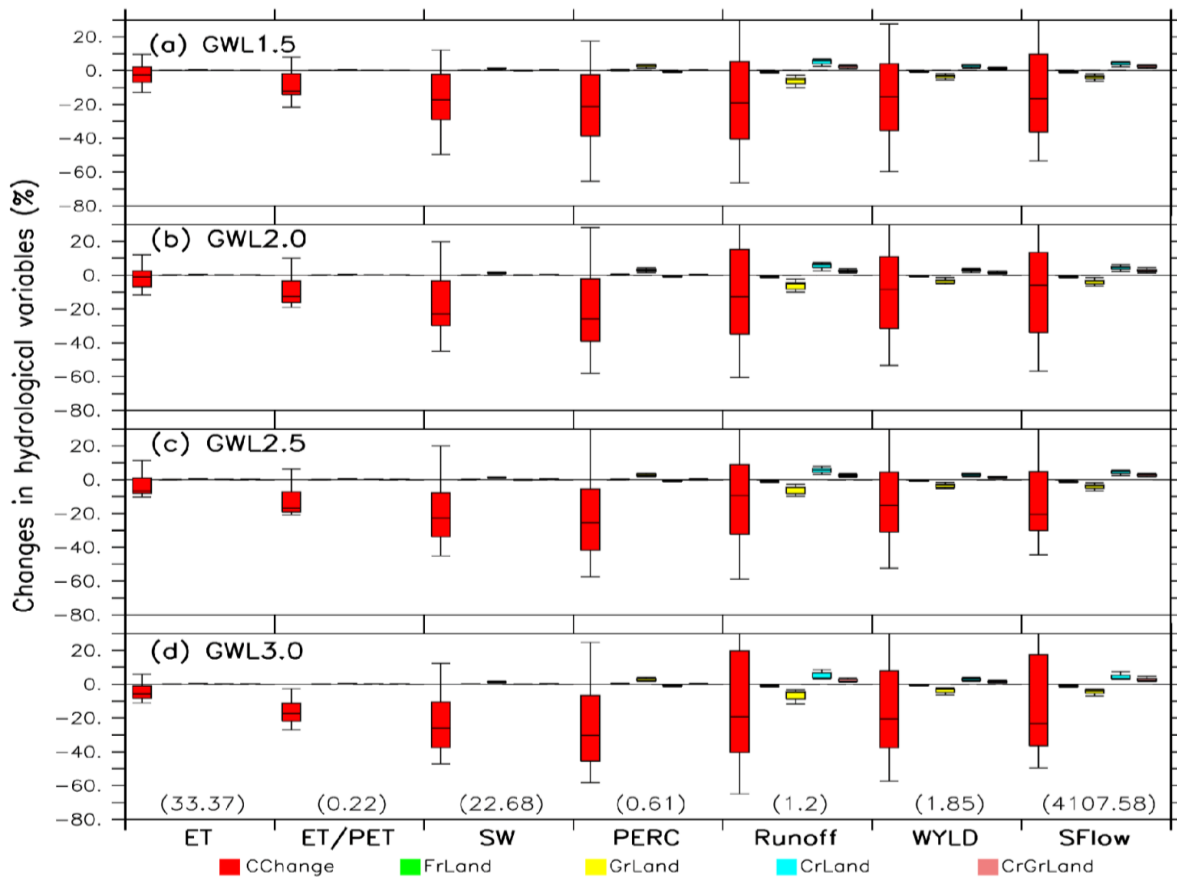


Figure 6.7: A comparison of the impacts of climate change (CChange) and LULC change (FrLand, GrLand, CrLand, and CrGrLand) on hydrological variables: ET, ET/PET, soil water (SW), percolation (PERC), Runoff, water yield (WYLD), and streamflow over the Limpopo River basin at different global warming levels. The present-day climatological value for each variable is indicated in brackets.

The impacts of climate change and LULC change scenarios on the hydrological droughts are compared in Figure 6.8. With climate change, the projected increase in the frequency of the hydrological droughts (i.e. SWI, PERCI, RFI, WYLDI and SFI) falls within that of the meteorological droughts (SPEI and SPI). This because the projected increase in the ET (due to climate change) makes the increase in the hydrological drought frequency higher than that of the SPI; but, because the increased ET is lower than the increased PET, the increase in the

hydrological drought frequency is much lower than that of the SPEI. Among the hydrological droughts, the climate change impacts are the most pronounced in respect of the soil drought frequency (SWI). The impacts of all the LULC changes scenarios are very small and negligible for SWI and PERCI. However, the impact of GrLand on RFI is in the same direction as (and comparable to) that of climate change. This is consistent with the decrease in runoff due to the decreased CN from the restoration of the grassland.

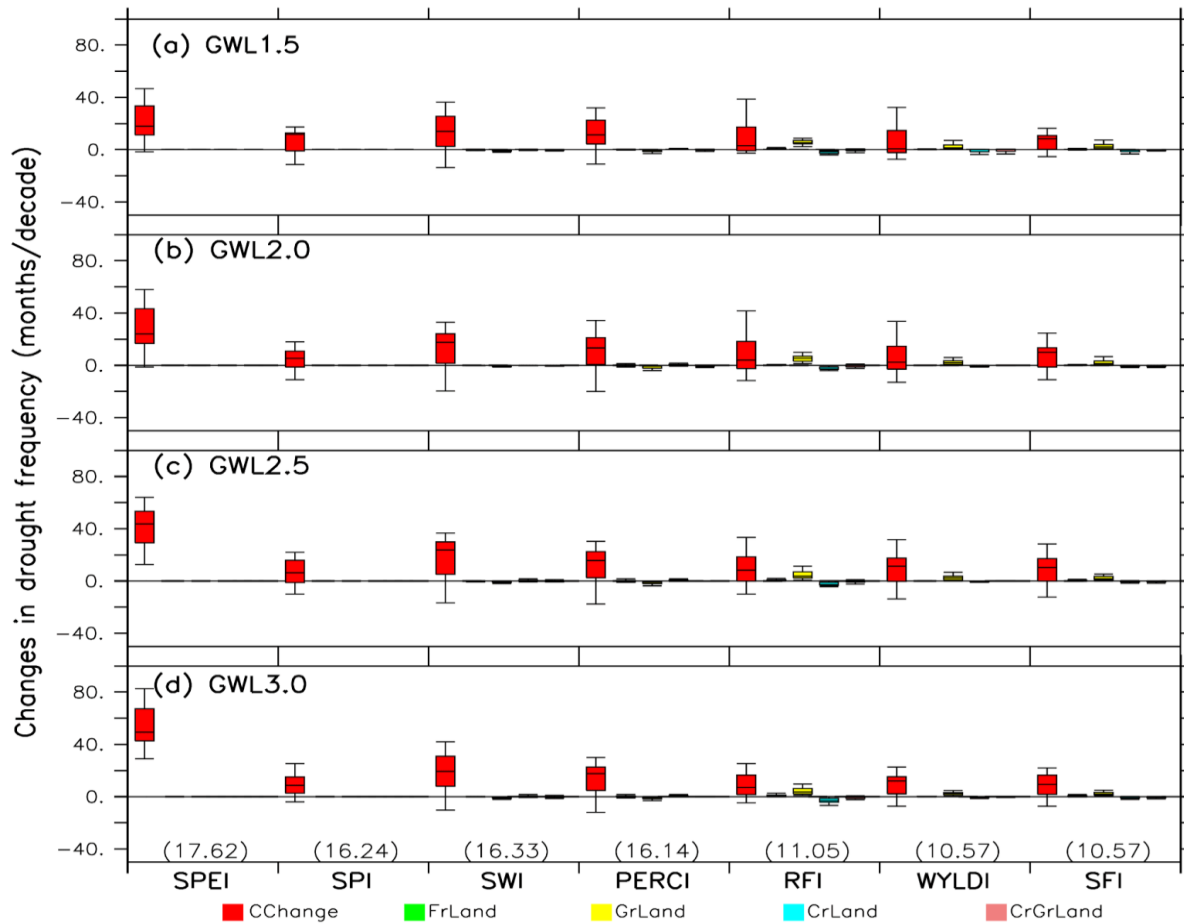


Figure 6.8: A comparison of the impacts of climate change (CChange) and LULC change (FrLand, GrLand, CrLand, and CrGrLand) on the frequency of droughts (SPEI, SPI, SWI, PERCI, RFI, WYLDI and SFI) over the Limpopo River basin at different global warming levels (GWL1.5, GWL2.0, GWL2.5 and GWL3.0). The present-day climatological value for each variable is indicated in brackets.

6.6 Summary

This chapter has quantified and compared the future impacts of climate change and LULC changes over the LRB with the aim of investigating the possibility of using the LULC to reduce or offset the climate change impacts. For the study, the bias-corrected CORDEX dataset was used to force the SWAT+ model in projecting the future hydrology in the Limpopo River at various GWL under the RCP8.5 future climate scenario. The sensitivity of the projection to the extreme but realistic LULC change scenarios over the basin was investigated. These LULC

change scenarios include the expansion of forests, grassland cropland, and cropland/grassland mosaic. The results of the projection indicate that the LRB is warming faster than the global warming rate. Although there is no discernible trend in the precipitation time series, the spatial distribution of the rainfall projection shows an increase in precipitation and hydrological variables over the southern part, but a decrease in these variables over the eastern part of the basin. This results in increased hydrological drought frequency over the basin. The replacement of savanna and the expansion of grassland scenarios mitigate the impacts of climate change on the frequency of soil moisture droughts because they increase soil moisture. However, they aggravate the impacts of climate change on the frequency runoff and streamflow droughts, as they further decrease runoff and streamflow over the flow. Conversely, the expansion of cropland and grassland/cropland reduces the impacts of climate change on the frequency of runoff and streamflow droughts but enhances the climate change impacts on soil moisture.

Chapter 7: Using land-use change to mitigate future impacts of climate change on hydrological droughts in the Western Cape River basins

7.1 Introduction

The Western Cape Province had one of its worst multi-year droughts in 2015-2017, when a meteorological drought cascaded to agricultural, hydrological, and socio-economic impacts. During this extended drought, the water storage levels of the Western Cape's major dams deteriorated to about 23%, and in addition, the last 12% of the dam water was unusable (Botai et al., 2017). The province was declared a disaster region, and the crisis triggered the local government to impose severe water restrictions on agricultural, urban, and industrial consumers, while exploring strategies to avert a situation where the taps ran completely dry. The drought had a significant impact on agriculture, livelihoods, and communities. For instance, the agricultural sector suffered economic losses estimated at ZAR 5.9 billion, and at least 30 000 jobs were lost (Green Cape, 2019). However, the Western Cape is likely to become drier and to experience moderate to strong warming in the future. The need to minimise future drought impacts on water availability in the province has necessitated studies on mitigating the impacts of climate change on hydrological droughts. While several studies have documented hydrological responses to land-use changes in South African catchments, no study has investigated how these responses can mitigate climate change impacts on hydrological droughts in the WRB. This chapter thus reports on our study in this direction.

7.2 Land-use change experiments

SWAT+ was applied to perform five experiments (Table 7.1). The first experiment (CtrLand) represents the control scenario, i.e. using the SWAT+ default land-use pattern. The SWAT+ land-use file was then modified to perform four additional experiments. The second experiment (FrLand) represents a future land-use scenario with an increase in invasive alien vegetation. Hence, mixed forest “invades” river basin areas outside their current distributional range. The area of land-use change for this scenario was delineated after consideration of the Working for Water programme that mapped the distribution of alien invasive tree species and identified invaded riparian and non-riparian areas across South Africa's quaternary catchments (Kotzé et al., 2010). The third scenario (GrLand) describes an expansion of grassland expansion (i.e. grass invasion, where GRAS replaces CRDY, CRGR and CRWO). The fourth (CrLand) describes an extensive cropping scenario (where CRDY replaces CRWO, GRAS, and CRGR), while the fifth experiment of land-use change (SrLand) describes a restoration of shrubland in areas currently covered by bare ground/sparse vegetation (BSVG). These experiments were not designed to simulate accurate scenarios of vegetation change, but rather to assess the magnitude and type of regional hydrological impact that might occur from a hypothetical, albeit potential, change in vegetation. All the simulations were run for 148 years (1951-2099), but the simulation of the first five years was discarded as the spin-up period, and only the simulations

of the remaining 143 years were analysed. The CTRL simulation was analysed to evaluate the performance of the hydrological model in simulating the Western Cape’s climate, and to ascertain the projected future hydrological impacts that could be due to climate change and resulting changes in vegetation. All future projections of land cover change are provided as an anomaly (i.e. those of FrLand, GrLand, CrLand, and SrLand are relative to that of CtrLand).

Table 7.1: Summary of LULC change experiments in the Western Cape River basins.

Experiments	Description	LULC pattern
CtrLand	<ul style="list-style-type: none"> ● Control LULC, which is SWAT+ default land use. 	Figure 7.1(a)
FrLand	<ul style="list-style-type: none"> ● Increase in mixed forest (e.g. eucalyptus, pine, and black wattle trees in river basin areas). ● FOMI occupies 14.45% of the basin 	Figure 7.1(b)
SrLand	<ul style="list-style-type: none"> ● Shrubland restoration. ● SHRB replaces BSVG. ● SHRB covers 32.74% of the basin. 	Figure 7.1(c)
CrLand	<ul style="list-style-type: none"> ● Extensive cropping. ● CRDY replaces GRAS, CRGR and CRWO. ● CRDY covers 63.98% of the basin. 	Figure 7.1(d)
GrLand	<ul style="list-style-type: none"> ● Expansion of grassland expansion (i.e. grass invasion). ● GRAS replaces CRDY, CRGR and CRWO. ● GRAS occupies 63.98% of the basin. 	Figure 7.1(e)

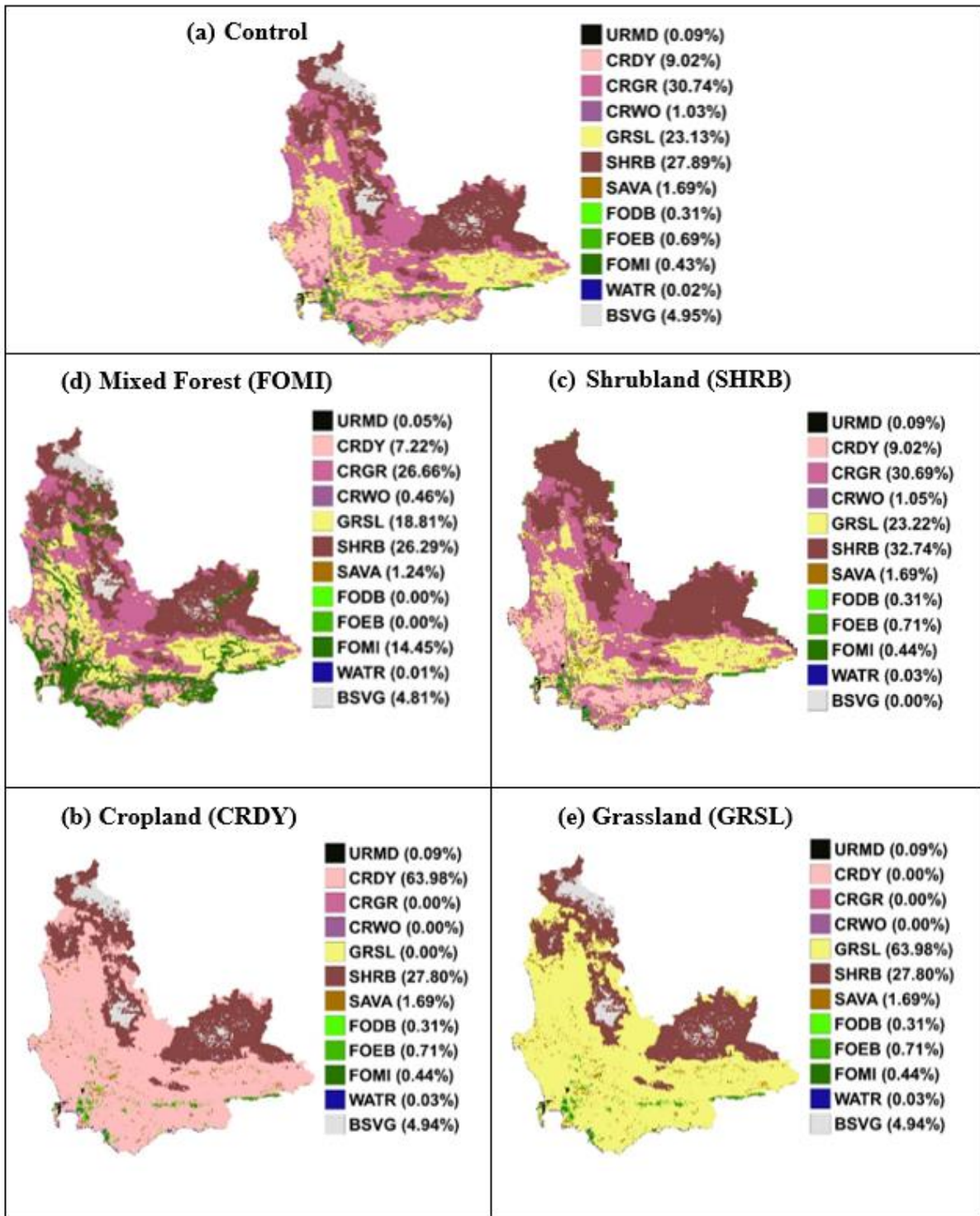


Figure 7.1: The LULC patterns used in the LULC change experiments for Western Cape River basins: (a) CtrLand (b) FrLand, (c) SrLand (d) CrLand (e) GrLand. The land-use types are urban residential medium density (URMD), cropland/dryland and pasture (CRDY), cropland/grassland mosaic (CRGR), cropland/woodland mosaic (CRWO), grassland (GRAS), shrubland (SHRB), savanna (SAVA), forest – deciduous broadleaf (FODB), forest – evergreen broadleaf (FOEB), forest – mixed (FOMI), water (WATR), bare ground/sparse vegetation (BSVG). The percentage of each LULC type is indicated in brackets.

7.3 Impacts of climate change

Figure 7.2 shows the time series of projected climate changes across the Western Cape for the period 1980-2100. These projections show a gradual increase in mean temperature, from about 1°C in 2030, and reaching about +4°C by the end of the century. The spatial distribution of the warming is generally uniform across the region, but the magnitude of the warming increases with the GWLs (Figure 7.3). For example, the temperature increase may be between 1.5 and 2.5°C, under GWL1.5 and GWL2.0, or as high as 3.0-4.5°C, under GWL2.5 and GWL3.0 across the catchments. These climate projections for temperature are in line with those of the previous study, which suggests increased temperatures (up to 4°C) could occur in this region before the end of the century (Field, 2014; Haensler et al., 2011; Naik and Abiodun, 2016). Note that, for higher GWLs, increased warming tends to occur further inland, over the north-eastern regions. For example, under GWL3.0, the increase is about 4.5°C over the north-eastern parts of the Olifants River catchment, but about 2.5°C along southern parts of the Berg and Breede rivers. This is in line with previous projections and may be due to the moderating effects of the ocean on temperature along the coastline (e.g. Mbokodo et al., 2020; Naik and Abiodun, 2016). This projected increase in temperature leads to an increase in potential evaporation (PET), which also shows a gradual increase by the end of the century (from about +10 mm month⁻¹ in 2030 to about +20 mm month⁻¹ by 2100 (Figure 7.2). The areas where the largest changes in PET occur compare well spatially to areas where the largest changes in temperature occur (Figure 7.3), and the magnitude of the PET change increases with higher GWLs (2.0, 2.5 and 3.0). The largest increase occurs over the north-eastern parts of the Olifants River and northern Gouritz River catchments, where PET may increase by between about +10 mm month⁻¹ (GWL1.5) to more than +20 mm month⁻¹ (GWL3.0), respectively. Several studies confirm that PET rates may increase with higher temperatures in the future. This is because global warming (and associated higher temperatures) lead to an increase in the vapour pressure deficit of air and increased atmospheric evaporative demand (Dai et al., 2018; Yuan and Bai, 2018).

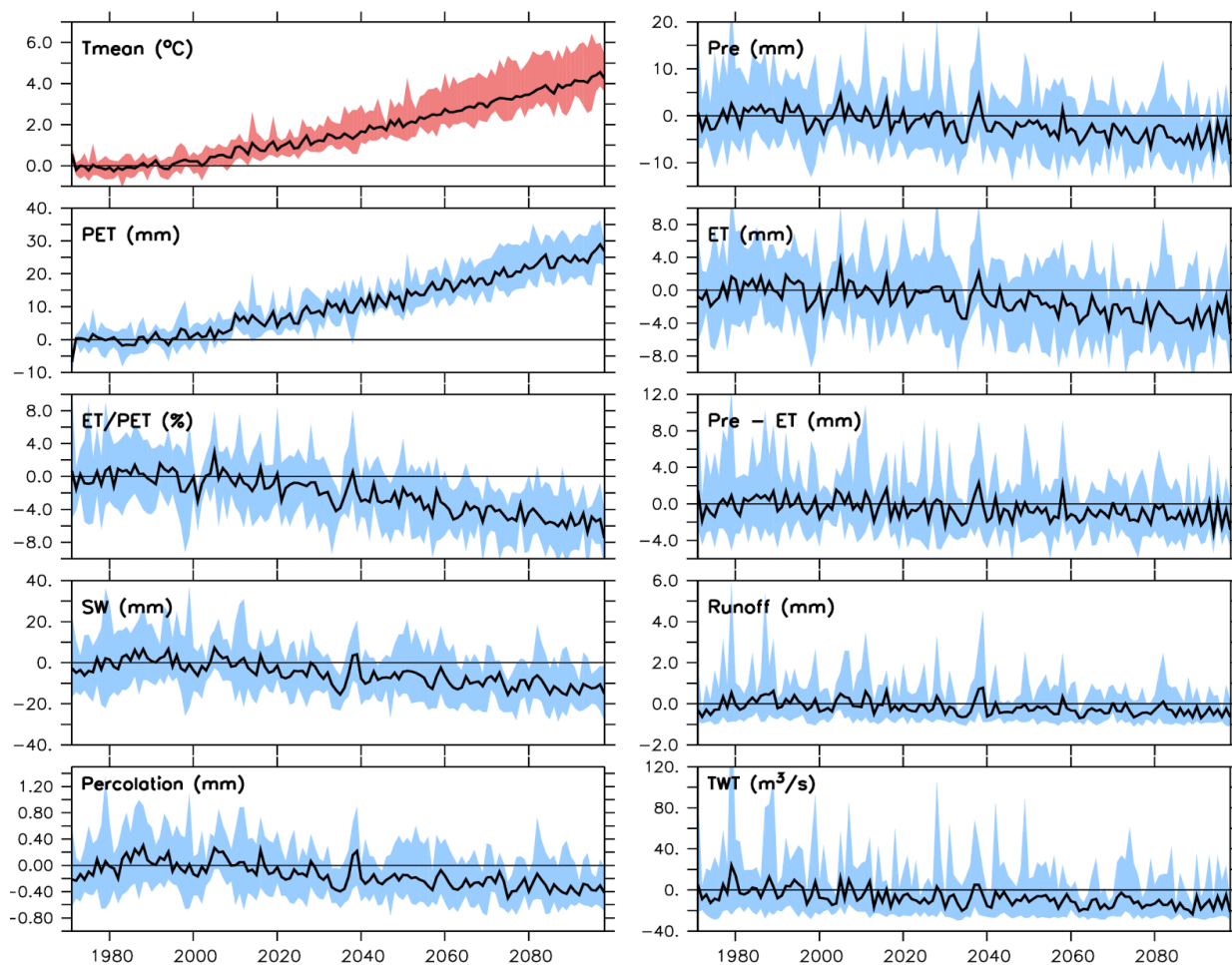


Figure 7.2: Temporal variation of the changes in hydroclimatic variables over the Western Cape River basins in the period 1971-2099 under the RCP8.5 climate scenario. The changes are calculated with reference to the present-day climate (1971-2000). The solid lines represent the multi-model ensemble mean of selected climate models, and the spreads represent the range of selected climate models.

The projected changes in precipitation are more complex than those of temperature. Precipitation projections show no discernible change in the trend before 2040, but a decreasing trend afterwards until the end of the century. However, changes in the spatial distribution do occur (Figure 7.3). The pattern of the precipitation change differs spatially across the Western Cape catchments. While there is a general decrease in precipitation across the entire region, the projections under GWL 1.5 suggest more drying (about -2 mm month^{-1}) may occur over some areas, like parts of the southern Gouritz and the south-eastern Breede, while only modest change occurs over other areas like the central Olifants. Generally, this pattern is similar across the GWLs, only that the magnitude of the change increases under higher GWLs and that the spatial extent of the drying increases. For instance, the area of maximum drying includes the southern margin of the Gouritz and Berg ($-1.5 \text{ mm month}^{-1}$) for GLW2.0, and it extends across the entire Gouritz, Breede, and parts of the Berg and Olifants, where it exceeds $-2.5 \text{ mm month}^{-1}$ for GWL 3.0. Only few areas show wetter conditions over the Western Cape in the

future. The exception to the general drying over the region occurs over a limited area of the central Berg (near a large dam), where increased PRE (+2 mm month⁻¹) occurs, and over central-southern parts of the Olifants (+1 mm month⁻¹). However, this only occurs for GWL1.5, but not under higher GWLs, when the drying signal dominates. The large-scale forcing mechanisms potentially responsible for the decreased rainfall across the Western Cape region may include an increase in the intensity and frequency of upper-level highs, and the migration of subtropical anticyclones towards the mid-latitudes across the Southern African subcontinent (Sousa et al., 2018). The poleward shift of the Southern Hemisphere moisture corridor and the displacement of the South Atlantic storm-track may create significantly drier conditions under conditions of future climate change. The projected ET can be linked to the changes in precipitation. While there is no discernible trend in future ET time series projections over the Western Cape (Figure 7.2), there are changes spatially. The spatial pattern of the ET change is not uniform across the Western Cape for GWL1.5. ET may decrease over some catchments, such as the Gouritz (-2 mm month⁻¹), but increase over others, such as the south-central Olifants (+1 mm month⁻¹) or the Berg (+1 mm month⁻¹). Generally, however, the areas where the largest changes in ET occur are comparable to the areas where the precipitation changes occur. The magnitude of the ET change also increases with higher GWLs (2.0, 2.5 and 3.0). For example, the projections show that, for higher GWLs, ET may decrease over much of the region (-1.5 mm month⁻¹), and particularly over the south-western Gouritz and central Olifants. This decrease may be up to -1.5 mm month⁻¹ under GWL1.5, -2 mm month⁻¹ under GWL2.0 and exceed -2.5 mm month⁻¹ under GWL3.0.

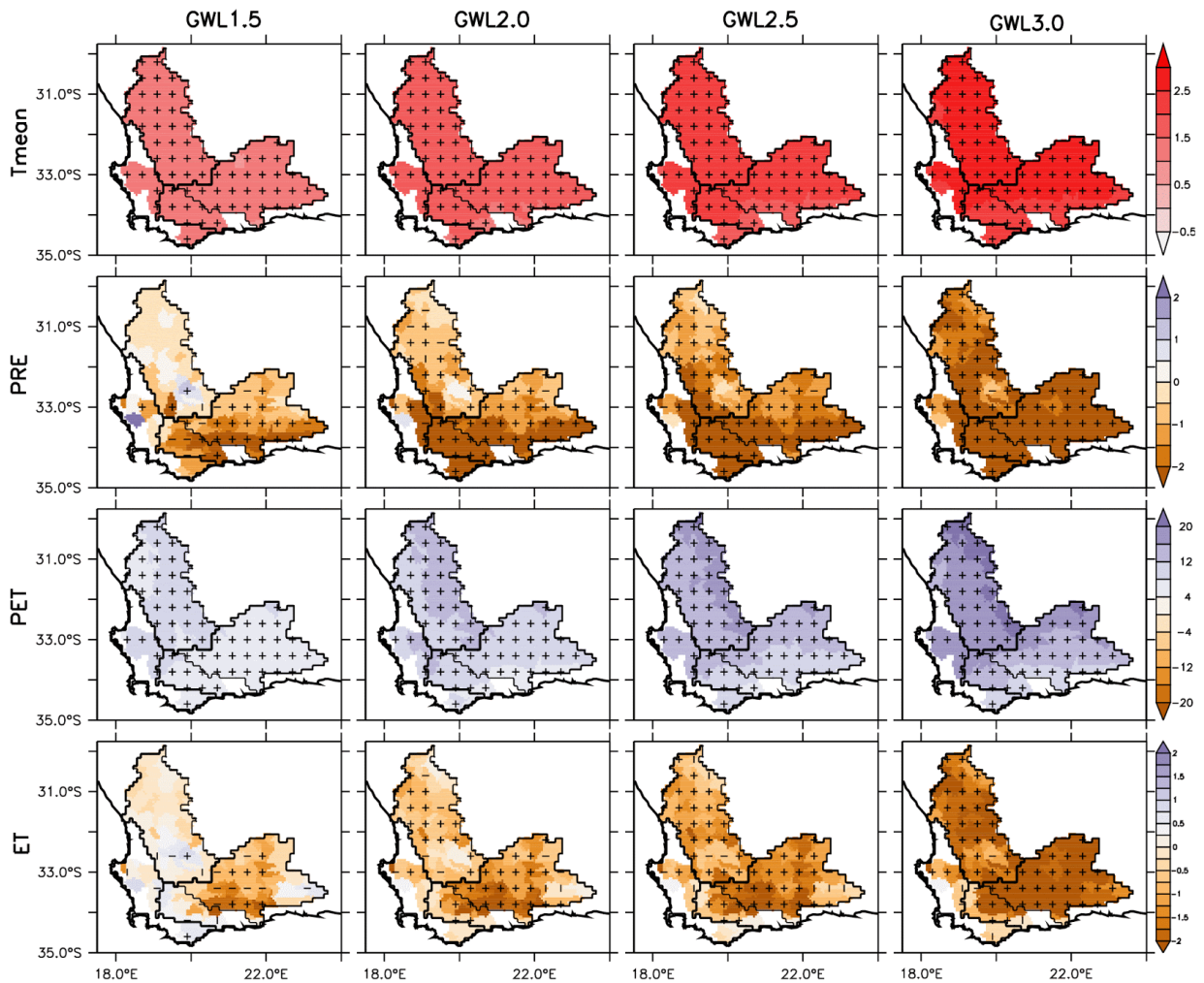


Figure 7.3: Spatial distribution of the projected changes in temperature ($^{\circ}\text{C}$), precipitation ($\text{mm}/\text{month}^{-1}$), potential evapotranspiration (PET, $\text{mm}/\text{month}^{-1}$) and evapotranspiration (ET, $\text{mm}/\text{month}^{-1}$) over the Western Cape River basins at different global warming levels (GWL1.5, GWL2.0, GWL2.5, and GWL3.0). The vertical strip (|) indicates where at least 80% of the simulations agree on the sign of the changes, while the horizontal strip (-) indicates where at least 80% of the simulations agree that the projected change is statistically significant (at 99% confidence level). The cross (+) shows where both conditions are satisfied, hence the change is robust.

The projected decrease in hydrological variables can be linked to the decrease in precipitation (Figures 7.3 and 7.4). The spatial distribution of these hydrological changes is consistent with that of precipitation. For example, the projections show a general decrease in soil water across the region ($-10 \text{ mm}/\text{month}^{-1}$), which is enhanced over the eastern Olifants ($-20 \text{ mm}/\text{month}^{-1}$) and the central Berg ($-20 \text{ mm}/\text{month}^{-1}$) under GWL3.0. The spatial distribution of the drying is comparable for higher GWLs, except that the magnitude of the drying increases with the GWLs. This is because the projected decrease in PRE negatively affects the overall soil water budget of the affected areas. Over time, this causes a gradual decrease in the volumetric water content of the soil over the region (soil water; about -10 mm) from 2050 to 2100 (Figure 7.3).

This negative change in storage (i.e. soil water content) occurs when outputs, such as percolation and surface runoff, exceed precipitation. As seen in Figure 7.4, the distribution of the future drying is spatially comparable for these variables. Since the soil does not reach saturation, reduced percolation occurs and there is also a consistent decrease in overland runoff. (Note that the differences in percolation and runoff are comparable to the spatial variation in soil types (Figure 2(e)) because loam and sandy loam textures differ in their respective water-holding capacities). This is consistent with our projected changes in hydrological variables over various channels (Figure 7.5). There is a decrease in channel precipitation over many areas of the Western Cape ($-10 \text{ mm month}^{-1}$), and this drying increases under higher GWLs. For instance, drying of $-8.4 \text{ mm month}^{-1}$ occurs along channels of the southern Gouritz and Breede, under GLW2.0, and it extends across the entire Western Cape, where it exceeds up to $16.9 \text{ mm month}^{-1}$ for GWL 3.0. The projected increase in PET leads to an increase in stream ET, which occurs for all GWLS, and over all the Western Cape catchments, but it is enhanced over the Olifants and Gouritz catchments ($+19 \text{ mm month}^{-1}$). Since more water is lost through evaporation, there is an associated decrease in streamflow over many of the region's channels ($+10 \text{ mm month}^{-1}$), but particularly over the Olifants and Gouritz catchment ($+19 \text{ mm month}^{-1}$). This is consistent with the decreasing trend in future projections of channel discharge entering the largest dam in the Western Cape at Theewaterskloof (TWT) (Figure 7.5) and reaching about $-2 \text{ m}^3 \text{ s}^{-1}$ by the end of the century. While there are few studies on the hydrological projections for the Western Cape, several studies recognise that this region has historically experienced increased surface aridity due to decreased precipitation. The hydrological projections here are in line with historical analysis, which found increased surface temperature, decreased precipitation, and increased occurrence of dry spells, which have depleted water resources in the Southwest Cape (Jury, 2018).

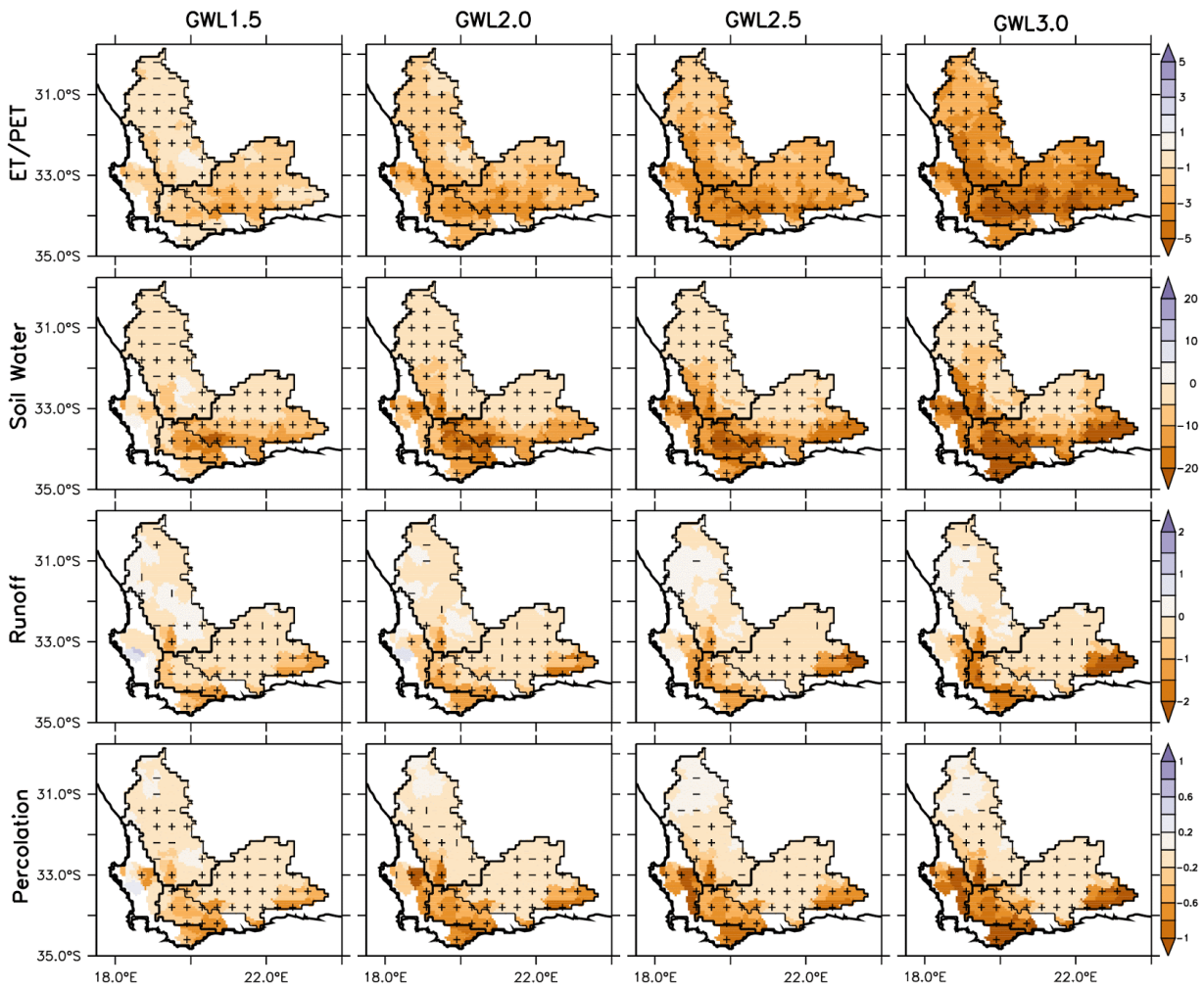


Figure 7.4: Same as Figure 7.3, except for ET/PET (%), soil water (mm month^{-1}), surface runoff (Runoff, $\text{m}^3 \text{s}^{-1}$) and percolation (mm month^{-1}).

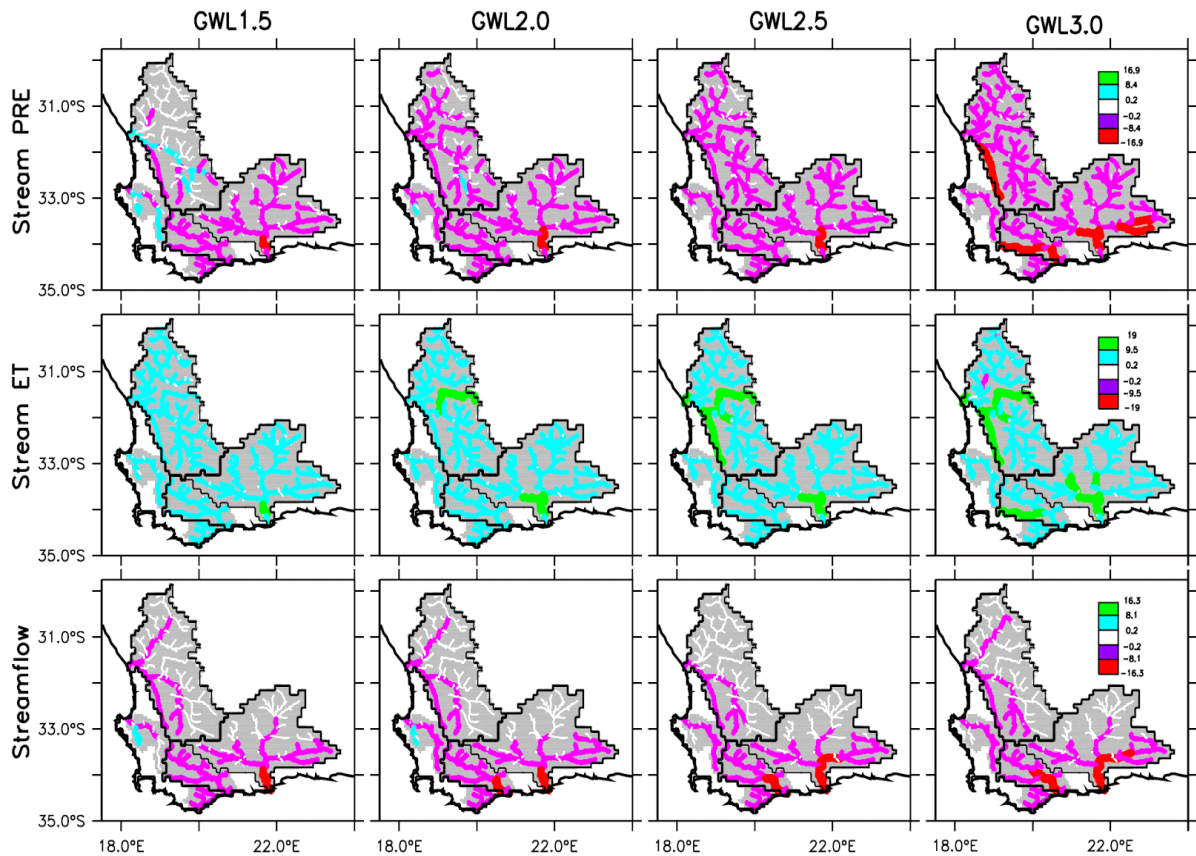


Figure 7.5: Same as Figure 7.3, but for channel variables: precipitation (mm month^{-1}), stream ET (mm month^{-1}), and streamflow ($\text{m}^3 \text{s}^{-1}$).

7.4 Impacts of LULC changes

The impacts of the LULC changes (i.e. FrLand, GrLand, CrLand, and CrGrLand) on the hydrological projections can be explained by the influence of the LULC changes on the curve number (CN; Figure 7.6). With FrLand, there is a decrease in CN, which is consistent with the area of mixed forest land-use change (CN of about -3 ; Figure 7.6). The lower runoff potential is linked to more permeable soil surface and hence, there is less runoff from rainfall. As such, FrLand increases the amount of soil water available over the catchment. For instance, soil water increases occur over parts of the southern Berg ($+2 \text{ mm month}^{-1}$) catchment, and the southwest Breede ($+2 \text{ mm month}^{-1}$) catchment. The increase in soil water may be due to the deeper rooting network of trees, which alters the physical properties of the upper soil layers, improving infiltration and percolation. As the amount of available soil water at the surface increases, more water is available for conversion through evapotranspiration (ET). Thus, for FrLand, ET also increases over these parts of the Berg and Breede ($+0.5 \text{ mm month}^{-1}$), and these increases are spatially comparable to those of soil water. However, although FrLand generally decreases runoff over the region ($-0.2 \text{ mm month}^{-1}$), particularly over parts of the central Berg and western Breede ($-0.5 \text{ mm month}^{-1}$), FrLand also increases the streamflow over most catchments. The largest increases in streamflow occur over parts of the western Olifants, the northern Berg and the south-eastern Gouritz (about $+61.9 \text{ m}^3 \text{ s}^{-1}$; Figure 7.6). Decreases in streamflow occur only

in some sub-basins of the western Breede and southern Berg (about $-61.9 \text{ m}^3 \text{ s}^{-1}$). These hydrological changes suggest that the increase in streamflow is unlikely due to surface runoff (from precipitation runoff over the landscape, i.e. overland flow) but rather due to percolation of water past the soil profile (subsurface) to become groundwater recharge, or via lateral movement in the profile (interflow), which eventually reaches streamflow (not shown). Several studies confirm that forests may have a positive impact on soil hydraulic properties, by functioning as water harvesters and contributing to infiltration, deeper drainage, and groundwater recharge (e.g. Bargués Tobella et al., 2014; Luo et al., 2020).

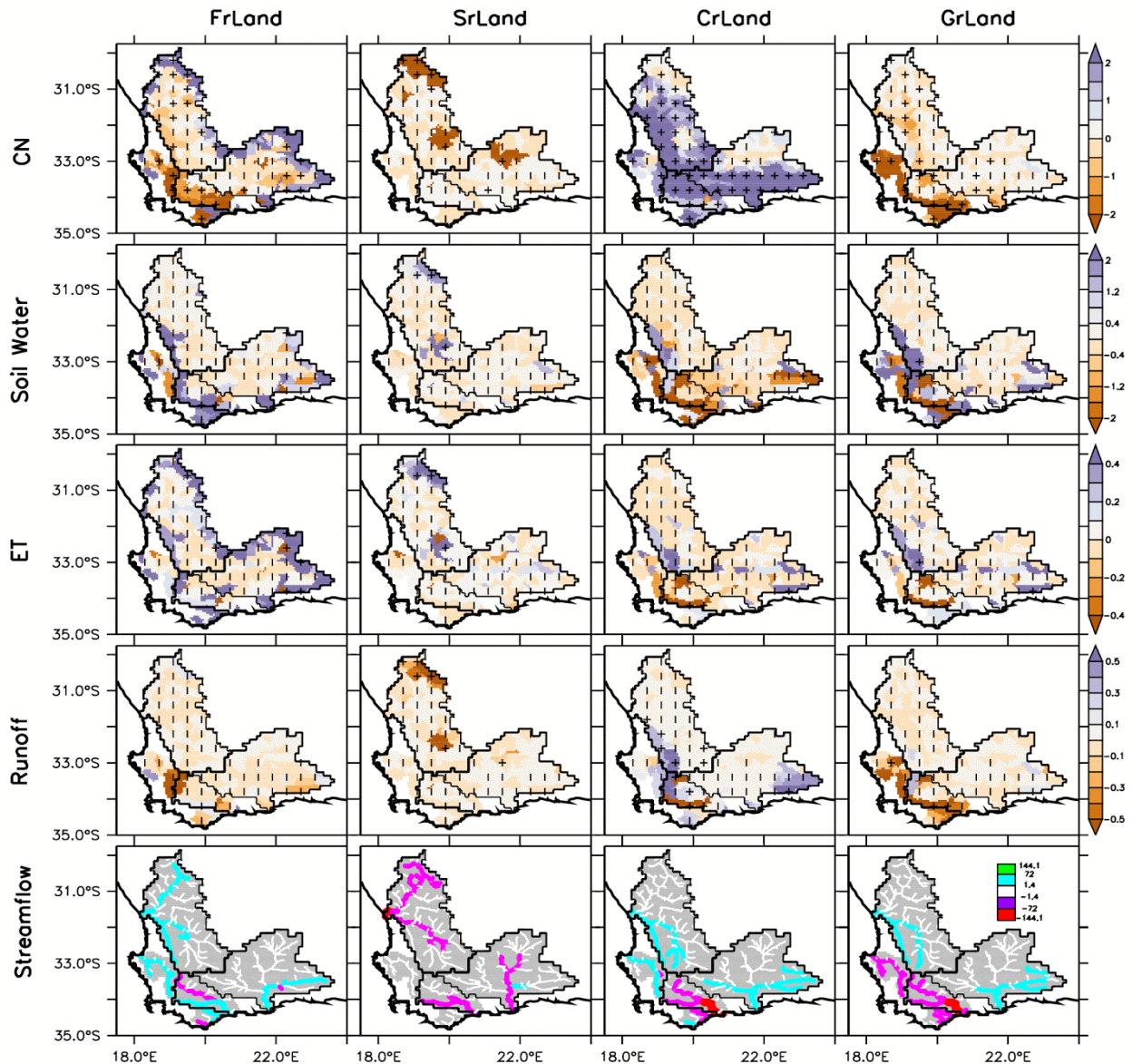


Figure 7.6: Impacts of LULC changes on hydrological variables over the Western Cape River basins: CN (unitless), soil water (mm month^{-1}), surface runoff (Runoff, $\text{m}^3 \text{ s}^{-1}$) and streamflow ($\text{m}^3 \text{ s}^{-1}$). The vertical strip (|) indicates where at least 80% of the simulations agree on the sign of the changes, while horizontal strip (-) indicates where at least 80% of the simulations agree that the projected change is statistically significant (at 99% confidence level). The cross (+) shows where both conditions are satisfied, hence the change is robust.

The hydrological impact of SrLand is similar to that of FrLand. With SrLand, there is a decrease in CN (of about 8) over the areas where shrubland restoration replaces bare ground (Figure 7.6). This occurs particularly over sub-basins of the northern and central Olifants and northern Gouritz. Over the central and northern Olifants sub-basins, SrLand increases soil water (+2.0 mm month⁻¹) and increases ET (+0.4 mm month⁻¹). But SrLand decreases runoff over the region (-0.2 mm month⁻¹), particularly over the central Olifants and northern Gouritz (-0.5 mm month⁻¹). However, unlike FrLand, SrLand decreases water yield over most Western Cape catchments. The streamflow decreases (about -61.9 m³ s⁻¹) occur over the Olifants, Gouritz and Breede. However, SrLand does not influence water yield over the Berg River, since no land-use change occurred in this catchment. Overall, these hydrological changes suggest that the restoration of shrubland may decrease streamflow and may have negative impacts on the water security of the region.

The response of CrLand is complex, as it includes both increases and decreases in hydrological conditions. CrLand (i.e. expansion of cropland/dryland area) increases the curve number (CN), such that the area of LULC is spatially consistent with the area of higher CN (about +5; Figs.7.6). While CrLand decreases soil water over some sub-basins, it increases it over other sub-basins. For instance, it decreases soil water over the eastern and southern Berg (-2 mm month⁻¹), the northern and southern Breede (-2 mm month⁻¹) and the eastern Gouritz (-1.6 mm month⁻¹), but it increases soil water over the southwestern Olifants (+0.8 mm month⁻¹). However, the hydrological response of CrLand differs from FrLand, in that, while the soil water changes are spatially consistent with ET in some catchments, they are not consistent in others. For instance, the decrease in ET (-2 mm month⁻¹) over the Breede is consistent with the decrease in soil water over the catchment, and the increase in ET (+0.4 mm month⁻¹) over the southwestern Olifants also agrees with the increase in soil water over this sub-basin. However, the increase in ET (+0.2 mm month⁻¹) over the southern Breede is not consistent with the decrease in soil water over the sub-basins. Moreover, CrLand increases runoff and streamflow over the southern Olifants and eastern Gouritz (+0.5 mm month⁻¹ and about +61.9 m³ s⁻¹) but decreases them over much of the Breede (-0.5 mm month⁻¹ and up to about -123.8 m³ s⁻¹, respectively). Unlike with FrLand, the increase in the streamflow obtained with CrLand is likely due to an increase in surface runoff over the landscape. It may be that the percolation rate is slower with CrLand than with FrLand. Nevertheless, the CrLand changes have complex impacts on the hydrology of the region, possibly due to the complex topography and local soil conditions.

The hydrological response to GrLand is also complex. GrLand (i.e. restoration of grassland) generally decreases the curve number (CN), with areas of lowest CN₂ spatially consistent with areas converted from CrLand to GrLand (CN about -4; Figure 7.6). GrLand is associated with a lower curve number (compared to CrLand) and hence, less runoff from rainfall. Compared to CrLand, GrLand increases soil water over many catchments. For example, soil water increases occur over the southwestern Olifants (+2 mm month⁻¹), the eastern Gouritz (+2 mm month⁻¹) and several sub-basins of the Berg. Although, like CrLand, for GrLand soil water decreases occur over the southern margins of the Breede (-2 mm month⁻¹). Even so, the changes in ET for the two land-uses (CrLand and GrLand) are spatially comparable. Nevertheless, unlike

CrLand, GrLand reduces runoff ($-0.5 \text{ mm month}^{-1}$) over many catchment areas. And, while changes in streamflow for the two land-uses are similar over the Olifants and Gouritz catchments (increases), and over the Breede (decreases), unlike CrLand, GrLand reduces streamflow over the Berg ($-61.9 \text{ m}^3 \text{ s}^{-1}$).

7.5 A comparison of the impacts of land-use change with climate change projections

The impacts of projected future climate change decrease all the hydrological variables over the catchments studied herein, but the percentage of the decrease varies among the variables and with the GWLs (Figure 7.7). Generally, the magnitude of the projection increases for higher GWLs, with the largest impacts of land-use change under GWL3.0. For instance, at GWL3.0, while the ET decreases by only 10%, the percolation decreases by more than 40%. The decrease in ET may be linked to the projected decreases in PRE, which makes less water available for evaporation over the catchments. The capability of the basin to meet atmospheric water demand (ET/PET) also decreases (by -20%), not only because the ET decreases, but because PET, the atmospheric water demand, is also projected to increase across the catchments (Figure 7.3). These changes drive the decrease in other hydrological variables, because they alter the overall soil water (SW) of the river basin areas, inducing a 30% decrease in soil water, a 40% decrease in PERC and a 30% decrease in runoff. Since less water percolates into deep soil layers, it also decreases the water yield (WYLD). Hence, there is also a decrease in water yield (-30%) and discharge (-35%) at the Theewaterskloof dam (TWT). This pattern is similar for successive GWLs (1.5, 2.0, and 2.5; Figures 7.7(a), (b), and (c), respectively), except that the magnitude of the decrease in hydrological variables is lower than that of GWL3.0.

The impacts of some land-use changes offset the climate change impacts on the mean hydrological variables (Figure 7.7). For example, CrLand may increase the runoff by 10% under GWL3.0. This may mitigate the impacts of climate change on runoff (to about 30%). While it does not occur across the entire Western Cape, CrLand may also offer potential climate change offset due to its impact on water yield at the TWT, where CrLand may increase discharge (+5%). For FrLand, SrLand, and GrLand land-use changes, the impact on the hydrological variables is almost negligible relative to the impact of future climate change.

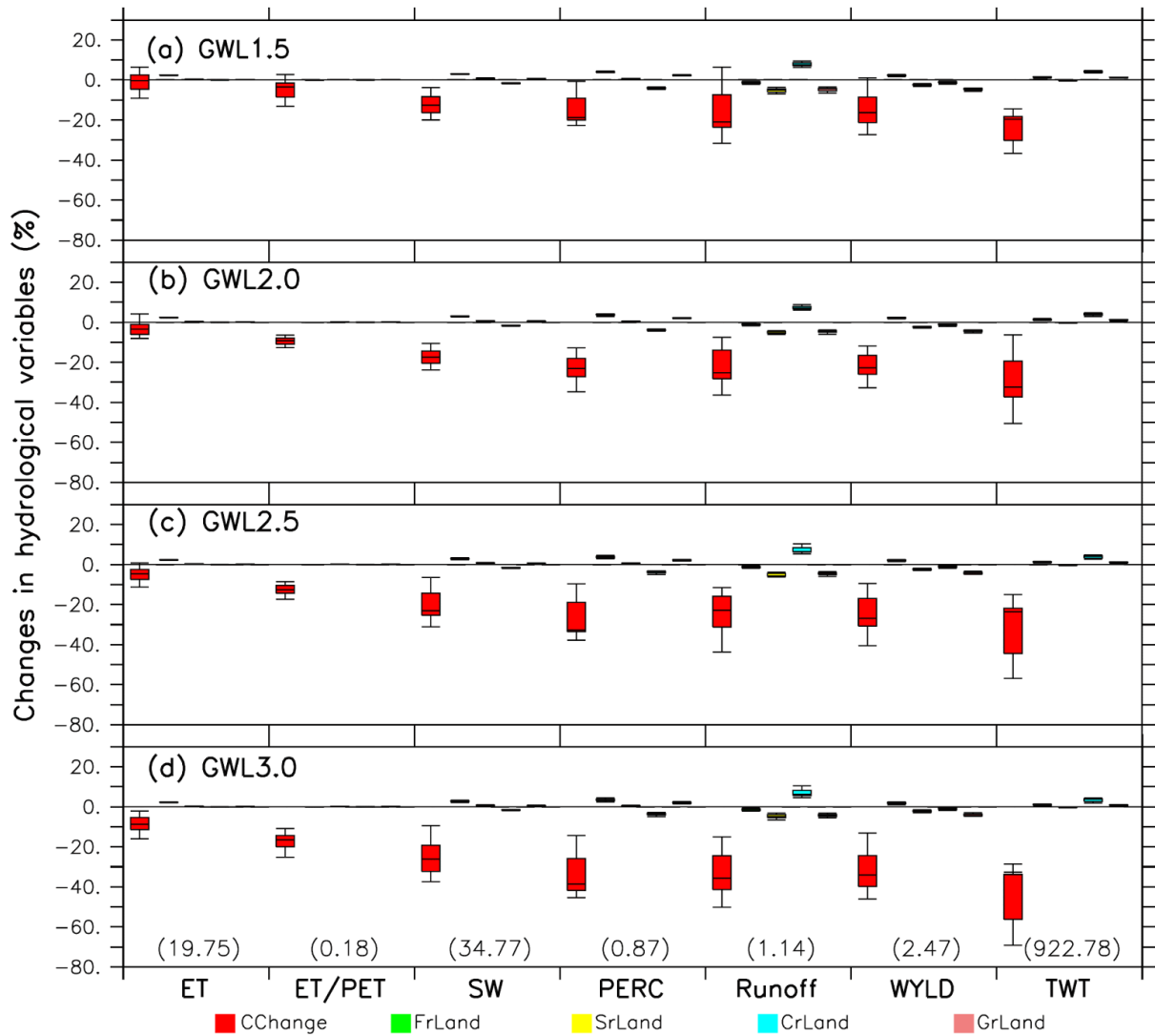


Figure 7.7: A comparison of the impacts of climate change and LULC change (FrLand, SrLand, CrLand, and GrLand) on hydrological variables: ET, ET/PET, soil water (SW), percolation (PERC), Runoff, water yield (WYLD), and streamflow over the Western Cape River basin at different global warming levels. The present-day climatological value for each variable is indicated in brackets.

The changes in the hydrological variables are also linked to changes in drought frequency (Figure 7.8). The projections indicate that impacts of climate change may increase drought frequency in the future. Climate change may increase the drought frequency in both the SPEI (about +75 months decade⁻¹) and the SPI (+20 months decade⁻¹) (Figure 7.8). Note that, while SPEI drought is more severe than SPI drought, for both indices, a moderate drought is defined as a condition in which the drought index (SPI or SPEI) is less than or equal to -1.0. These projections are in line with those of a previous study, which suggests that changes in the intensity and frequency of droughts are weaker when using the SPI than the SPEI, and that SPI projections may in fact underestimate the influence of global warming on drought because they do not account for the influence of PET (Naik and Abiodun, 2020). The changes in the SPEI/SPI drought provide the upper/lower range that is linked to changes in hydrological drought for other variables. For instance, climate change may increase the frequency of the soil water drought index (SWI) by +38 months decade⁻¹, the percolation drought index (PERCI) by +30 months decade⁻¹, the runoff drought index (RFI) by +10 months decade⁻¹, and the water yield drought index (WYLI) by +12 months decade⁻¹.

Some land-use changes may offset the climate change impacts on the hydrological drought variables (Figure 7.8). Most notably, changes occur under GWL3.0, where FrLand may decrease the SWI, PERCI and the WYLDLI, and it may thus mitigate the impacts of climate change on both types of droughts by about -3 to -5 months decade⁻¹. SrLand may increase the RFI by -3 months decade⁻¹. Similarly, CrLand may also decrease the RFI and may thus mitigate the impacts of climate change by about -5 months decade⁻¹. However, while GrLand may decrease the PERCI by about -3 months decade⁻¹, and it may increase the impacts of climate change on RFI by about +5 months decade⁻¹. This pattern is similar for successive GWLs (1.5, 2.0, and 2.5; Figures 7.8(a), (b), and (c), respectively). Generally, however, the impact of the drought in terms of the hydrologic variables is almost negligible relative to the frequency of future climate change drought.

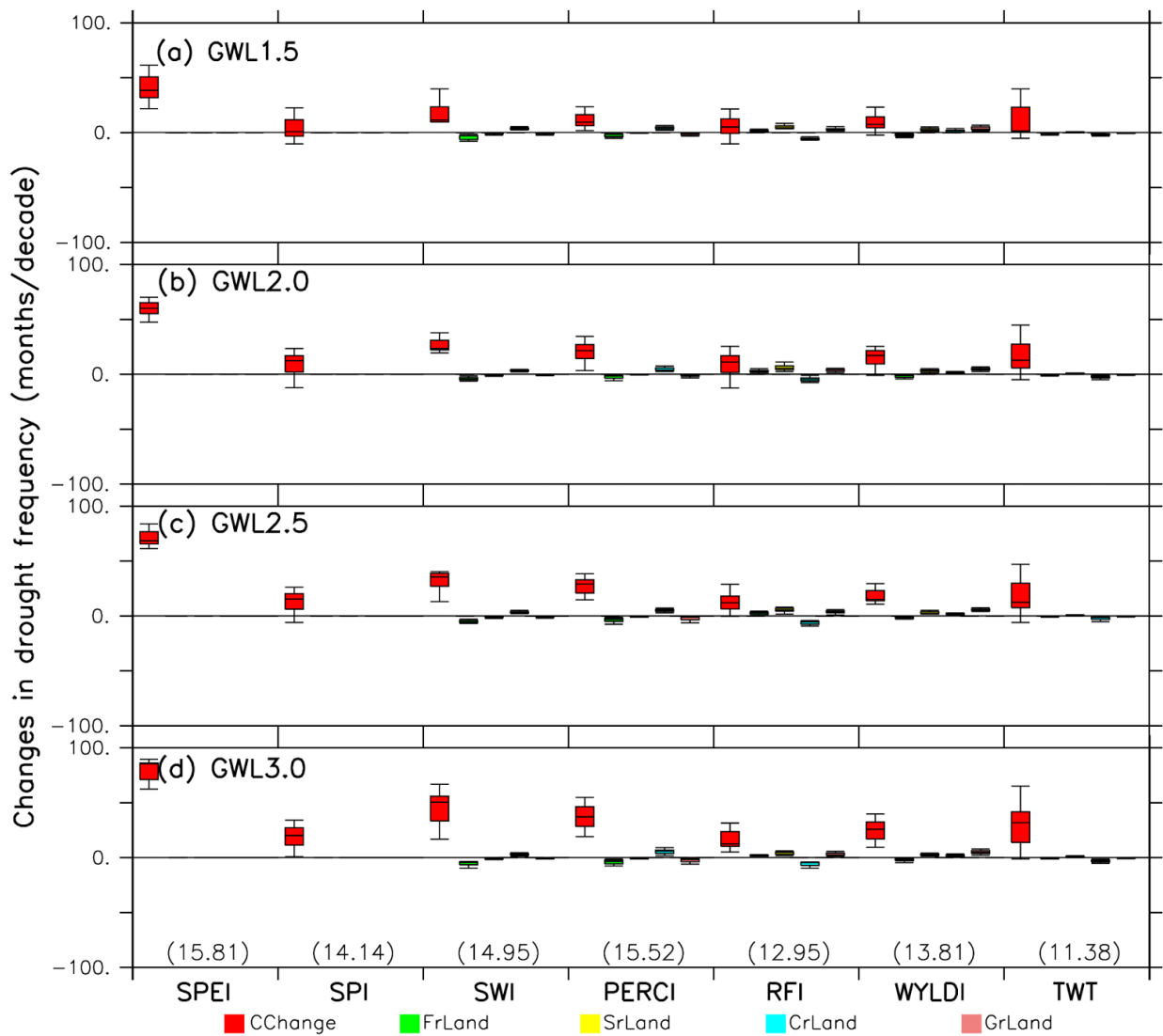


Figure 7.8: A comparison of the impacts of climate change (CChange) and LULC change (FrLand, GrLand, CrLand, and CrGrLand) on the frequency of droughts (SPEI, SPI, SWI, PERCI, RFI, WYLDI and SFI) over the Western Cape River basins at different global warming levels (GWL1.5, GWL2.0, GWL2.5 and GWL3.0). The present-day climatological value for each variable is indicated in brackets.

7.6 Summary

The chapter has examined the extent to which LULC changes can reduce the projected impacts of climate change on hydrological droughts in the WRB. We applied the calibrated SWAT+ model with the bias-corrected CORDEX dataset to simulate future hydrological conditions over the basin under different LULC changes and studied the sensitivity of the hydrological variables and drought indices to these LULC changes. The land-use scenarios considered are the spread of forest, the restoration of shrubland, the expansion of cropland, and the restoration of grassland. The climate change projection features an increase in temperature and potential evaporation, but a decrease in precipitation and all the hydrological variables. The drying occurs across the entire Western Cape, with the magnitude increasing with higher GWLs. The land-use changes alter these climate change impacts through changes in the hydrological water balance. The spread of forest increases streamflow and decreases runoff, while the restoration of shrubland decreases streamflow and runoff. The hydrological responses of CrLand and GrLand are more complex, as they include both increases and decreases in hydrological conditions. The impacts of FrLand, SrLand, CrLand and GrLand on the hydrological variables and drought frequency are negligible relative to the impact of future climate change. Hence, land-use changes in the Western Cape may not be the most efficient strategies for mitigating the impacts of climate change on hydrological droughts over the region. The results of this study have application in improving water security in the WRB catchments.

Chapter 8: Conclusion and recommendations

8.1 Conclusion

As part of efforts to reduce the impacts of drought over river basins in South Africa, this study has successfully calibrated, validated, and applied the SWAT+ model in order to investigate the extent to which LULC change can be used to mitigate the impact of climate change on hydrological droughts over selected river basins in South: the Vaal River basin (VRB), the Limpopo River basin (LRB), and the Western Cape River basins (WRB). The description of the basins and the SWAT+ model with the relevant input datasets was given in Chapter 2. We investigated the influence of bias correction of the climate dataset on the quality of the hydrological simulation before quantifying the impacts of climate change and LULC scenarios on characteristics of future hydrological droughts under the RCP8.5 scenario. The results of the study can be summarised as follows:

- SWAT+ reliably simulates the hydrology over all three basins studied herein. It captures the annual cycle of the observed streamflow at the hydrological stations in the VRB (i.e. C3H007, C5H016, C2H003, and C9H009), LRB (i.e. A2H059, A2H029, B3H017 and B7H015), and WRB (i.e. G1H013, H7H006, E2H003, and J1H019) during both calibration and validation periods. It also reproduces the timing and magnitude of most peak flows at these stations. The coefficient of correlation (R) between the simulated and observed streamflows is more than 0.6 over most of the stations. However, there are notable biases in the simulations.
- The SWAT+ simulation that used the bias-corrected CORDEX dataset captures the spatial distribution of hydroclimatic variables over the basin better than the simulation that used the original CORDEX datasets.
- The future projections over all the basins features an increase in temperature, and with no substantial trend in the time series of precipitation and hydrological variables. However, a decrease in precipitation and hydrological variables (soil water, runoff, and streamflow) is projected over all the basins, leading to an increase in hydrological droughts.
- Over the VRB, the expansion of grassland reduces the impact of climate change on soil water, percolation, and the associated drought frequency, but it enhances the impacts of climate change on runoff, water yield, streamflow, and the associated drought frequency. The expansion of cropland, cropland/grassland mosaic and barren land lowers the impacts of climate change on runoff, streamflow, and the associated drought frequency, but it reinforces the impact of climate change on soil water and the associated drought frequency.
- Over the LRB, the replacement of savanna and the expansion of grassland scenarios mitigate the impacts of climate change on the frequency of soil moisture droughts, because they increase soil moisture. However, they aggravate the impacts of climate change on the frequency runoff and streamflow droughts, as they further decrease runoff

and streamflow over the flow. The influence of expansion of cropland and grassland/cropland is in the opposite direction.

- Over the WRB, the spread of forest enhances the climate change impacts on runoff (by further decreasing runoff) and reduces the climate change impacts on the streamflow and streamflow droughts (by further decreasing the streamflow). The restoration of shrubland enhances the climate change impacts by runoff and streamflow and the associated droughts (by decreasing both variables). The expansion of cropland and the restoration of grassland produce more complex changes, featuring increases and decreases in hydrological variables in different parts of the basins.

The results of this study show that, while LULC change scenarios can reduce the impacts of climate change on some hydrological droughts in the selected river basins, they can also enhance the impacts on other hydrological droughts. Nevertheless, the impacts of the land-use change scenarios are small compared to the climate change impacts.

8.2 Recommendations

The results of the study suggest that, while these extreme LULC change scenarios could either mitigate or aggravate the climate change impacts on hydrological drought frequency over the selected three basins, the magnitudes of these impacts are in most cases less than 30% of the climate change impacts. This implies that LULC changes may not be sufficient to offset the climate impacts over the basins; hence, there is a need to explore other climate change mitigation options over these basins. In addition, as all the LULC changes reduce the climate change impacts on one hydrological drought and aggravate the impacts on another, there is a need to weigh the pros and cons of any LULC change before implementing it.

The approach used in this study only offers insight into the potential hydrological impacts of using LULC changes to mitigate droughts in the river basins. It is by no means intended to be prescriptive about land-use activities for a particular river basin, but it may assist stakeholders and decision makers in making better decisions for land management and water resource planning in a future impacted by drought due to climate change.

For simplicity and ease of interpretation, all the LULC change experiments in this study have assumed that the future climate projection would sustain the prescribed LULC patterns, so the vegetation did not respond to the climate variability and change. This may not always be the case. Hence, there is a need to extend the study to perform more sophisticated experiments that would enable vegetation to respond to future atmospheric conditions. The results of such experiments could alter the magnitude of the LULC changes obtained in the present study. However, the present study has provided the framework for model setup and result interpretation for such experiments.

Solar radiation management (SRM) has been proposed as a global and more effective option to mitigate climate change impacts. SRM aims to eliminate global warming by artificially reflecting a small amount of inbound sunlight out into space. However, although SRM is still

in its early stages of research, controversy exists because its full effect on different components of the earth system is unknown. There is a need to investigate the potential impacts of SRM on the hydrological drought over the basins and compare the results with those of LULC changes obtained in the present study. This will provide an opportunity for comparing global and local climate change mitigation strategies over the selected basins.

References

- Abbott, M.B., Bathurst, J.C., Cunge, J.A., O'Connell, P.E. and Rasmussen, J. (1986). An introduction to European hydrological system – Système hydrologique Européen (SHE) Part 2. Structure of a physically based distributed modelling system. *Journal of Hydrology*, 87(1-2), pp. 61-77.
- Abiodun, B.J., Makhanya, N., Petja, B., Abatan, A.A. and Oguntunde, P.G. (2019). Future projection of droughts over major river basins in Southern Africa at specific global warming levels. *Theoretical and Applied Climatology*, 137, pp. 1785-1799. <https://doi.org/10.1007/s00704-018-2693-0>.
- Abiodun, B.J., Mogebeisa, T.O., Petja, B., Abatan, A.A. and Roland, T.R. (2020). Potential impacts of specific global warming levels on extreme rainfall events over southern Africa in CORDEX and NEX-GDDP ensembles. *International Journal of Climatology*, 40(6), pp. 3118-3141
- Aich, V., Liersch, S., Vetter, T., Huang, S., Tecklenburg, J., Hoffmann, P., Koch, H., Fournet, S., Krysanova, V., Müller, E.N. and Hattermann, F.F. (2014). Comparing impacts of climate change on streamflow in four large African river basins. *Hydrology and Earth System Sciences*, 18(4), pp. 1305-1321.
- Akanbi, R.T., Ndarana, T., Davis, N. and Archer, E.R.M. (2021). Integrated assessment of the influence of climate change on current and future intra-annual water availability in the Vaal River catchment. *Journal of Water and Climate Change*, 12(2), pp. 533-551.
- Arnold, J.G., Engel, B.A. and Srinivasan, R., 1993. A continuous time, grid cell watershed model. *Application of advanced information technologies for management of natural resources*, pp.17-19.
- Arnold, J.G., Moriasi, D.N., Gassman, P.W., Abbaspour, K.C., White, M.J., Srinivasan, R., Santhi, C., Harmel, R.D., Van Griensven, A., Van Liew, M.W., Kannan, N. and Jha, M.K. (2012). SWAT: Model use, calibration, and validation. *Transactions of the American Society of Agricultural and Biological Engineers (ASABE)*, 55(4), pp. 1491-1508.
- Bargués Tobella, A., Reese, H., Almaw, A., Bayala, J., Malmer, A., Laudon, H. and Ilstedt, U. (2014). The effect of trees on preferential flow and soil infiltrability in an agroforestry parkland in semiarid Burkina Faso. *Water Resources Research*, 50(4), pp. 3342-3354.
- Beguiría, S., Vicente-Serrano, S.M., Reig, F. and Latorre, B. (2014). Standardized precipitation evapotranspiration index (SPEI) revisited: Parameter fitting, evapotranspiration models, tools, datasets and drought monitoring. *International Journal of Climatology*, 34(10), pp. 3001-3023.

- Bellprat, O., Lott, F.C., Gulizia, C., Parker, H.R., Pampuch, L.A., Pinto, I., Ciavarella, A. and Stott, P.A. (2015). Unusual past dry and wet rainy seasons over Southern Africa and South America from a climate perspective. *Weather and Climate Extremes*, 9, pp. 36-46.
- Benson, C. and Clay, E.J. (1998). The impact of drought on sub-Saharan African economies: A preliminary examination. *World Bank Technical Papers*, March (Vol. 401). World Bank Publications. <https://doi.org/10.1596/0-8213-4180-4>.
- Blamey, R., Mahlalela, P. and Reason, C. (2019). The Cape Town ‘Day Zero’ Drought: Mechanisms behind early winter rainfall variability in the southwestern Cape, South Africa. *Geophysical Research Abstracts*, 21 (January), p. EGU2019-15602.
- Botai, C.M., Botai, J.O., de Wit, J.P., Ncongwane, K.P. and Adeola, A.M. (2017). Drought characteristics over the Western Cape Province, South Africa. *Water*, 9(11), p. 876.
- Braune, E. and Rogers, K.H. (1987). The Vaal River catchment: Problems and research needs. *South African national scientific programme*. Report No. 143. ISBN 0 7988 4122 2.
- Cannon, A.J., Sobie, S.R. and Murdock, T.Q. (2015). Bias correction of simulated precipitation by quantile mapping: How well do methods preserve relative changes in quantiles and extremes? *Journal of Climate*, 28, pp. 6938-6959. doi:10.1175/JCLI-D-14-00754.1.
- Cannon, A.J. (2016). Multivariate bias correction of climate model output: Matching marginal distributions and intervariable dependence structure. *Journal of Climate*, 29(19), pp. 7045-7064. <https://doi.org/10.1175/JCLI-D-15-0679.1>.
- Cannon, A.J. (2018). Multivariate quantile mapping bias correction: An N-dimensional probability density function transform for climate model simulations of multiple variables. *Climate Dynamics*, 50(1), pp. 31-49.
- Chen, J., Brissette, F.P., Chaumont, D. and Braun, M. (2013). Finding appropriate bias correction methods in downscaling precipitation for hydrologic impact studies over North America. *Water Resources Research*, 49(7), pp. 4187-4205.
- Cook, B.I., Mankin, J.S., Marvel, K., Williams, A.P., Smerdon, J.E. and Anchukaitis, K.J. (2020). Twenty-first century drought projections in the CMIP6 forcing scenarios. *Earth's Future*, 8(6), p. e2019EF001461.
- Dai, A., Zhao, T. and Chen, J. (2018). Climate change and drought: A precipitation and evaporation perspective. *Current Climate Change Reports*, 4(3), pp. 301-312.
- Davis, C.L. and Vincent, K. (2017). *Climate risk and vulnerability: A handbook for Southern Africa*. <http://researchspace.csir.co.za/dspace/handle/10204/10066>

- Dennis, I. and Dennis, R. (2012). Climate change vulnerability index for South African aquifers. *Water SA*, 38(3), pp. 417-426.
- Department of Water Affairs and Forestry (DWAf). (2003). *Upper Vaal Water management area: Overview of water resources availability and utilization*. Report No. P WMA 08/000/00/0203.
- Déqué, M., Calmanti, S., Christensen, O.B., Aquila, A.D., Maule, C.F., Haensler, A., Nikulin, G. and Teichmann, C. (2017). A multi-model climate response over tropical Africa at +2°C. *Climate Services*, 7, pp. 87-95. <https://doi.org/10.1016/J.CLISER.2016.06.002>.
- Devia, G.K., Ganasri, B.P. and Dwarakish, G.S. (2015). A review on hydrological models. *Aquatic Procedia*, 4, pp. 1001-1007.
- Dosio, A., Jones, R.G., Jack, C., Lennard, C., Nikulin, G. and Hewitson, B., 2019. What can we know about future precipitation in Africa? Robustness, significance and added value of projections from a large ensemble of regional climate models. *Climate Dynamics*, 53(9), pp. 5833-5858.
- Edwards, D. C.; and T. B. McKee. 1997. "Characteristics of 20th century drought in the United States at multiple time scales." *Climatology Rep.* 97-2, Department of Atmospheric Science, Colorado State University, Fort Collins, Colorado
- Ehret, U., Zehe, E., Wulfmeyer, V., Warrach-Sagi, K. and Liebert, J. (2012). HESS Opinions 'Should we apply bias correction to global and regional climate model data?'. *Hydrology and Earth System Sciences*, 16(9), pp. 3391-3404.
- Engelbrecht, F., Adegoke, J., Bopape, M.J., Naidoo, M., Garland, R., Thatcher, M., McGregor, J., Katzfey, J., Werner, M., Ichoku, C. and Gatebe, C. (2015). Projections of rapidly rising surface temperatures over Africa under low mitigation. *Environmental Research Letters*, 10(8), p. 085004.
- Eskom, 2020, Matimba Power Station. Available online at: https://www.eskom.co.za/Whatweredoing/ElectricityGeneration/PowerStations/Pages/Matimba_Power_Station.aspx. Accessed on 7 July 2020.
- Falkenmark, M., Andersson, L., Castensson, R., Sundblad, K., Batchelor, C., Gardiner, J., Lyle, C., Peters, N., Pettersen, B., Quinn, P., Rockstrom, J. and Yapijakis, C. (1999). *Water: A reflection of land use*. Swedish Natural Science Research Council, Sweden.
- Field, C.B., Barros, V.R., Mastrandrea, M.D., Mach, K.J., Abdrabo, M.K., Adger, N., Anokhin, Y.A., Anisimov, O.A., Arent, D.J., Barnett, J. and Burkett, V.R. (2014). Summary for policymakers. In: *Climate Change 2014: Impacts, adaptation, and vulnerability*. Part A: Global and sectoral aspects. Contribution of Working Group II to the Fifth Assessment Report of the Intergovernmental Panel on Climate Change (pp. 1-32). Cambridge University Press.

- Food and Agriculture Organization (FAO). (2004). *Drought Impact Mitigation and Prevention in the Limpopo River Basin: A Situation Analysis*. Land and Water Discussion Paper. Food and Agriculture Organization (FAO): Rome, Italy.
- Funk, C., Davenport, F., Harrison, L., Magadzire, T., Galu, G., Artan, G.A., Shukla, S., Korecha, D., Indeje, M., Pomposi, C. and Macharia, D. (2018). Anthropogenic enhancement of moderate-to-strong El Niño events likely contributed to drought and poor harvests in Southern Africa during 2016. *Bulletin of the American Meteorological Society*, 99(1), pp. S91-S96. <https://doi.org/10.1175/BAMS-D-17-0112.1>.
- Giorgi, F., Jones, C. and Asrar, G.R. (2009) Addressing climate information needs at the regional level: The CORDEX framework. *World Meteorological Organization (WMO) Bulletin*, 58(3), pp. 175-183.
- Green Cape. (2019). *Sustainable Agriculture 2019 Market Intelligence Report*. Cape Town, South Africa. Available online at: <http://www.greencape.co.za>. Accessed on 01 May 2021
- Gudmundsson, L., Bremnes, J.B., Haugen, J.E. and Engen-Skaugen, T. (2012). Downscaling RCM precipitation to the station scale using statistical transformations – A comparison of methods. *Hydrology and Earth System Sciences*, 16(9), pp. 3383-3390.
- Gyamfi, C., Ndambuki, J.M. and Salim, R.W. (2016a). Hydrological responses to land use/cover changes in the Olifants Basin, South Africa. *Water*, 8(12), p. 588.
- Haensler, A., Hagemann, S. and Jacob, D. (2011). Dynamical downscaling of ERA40 reanalysis data over southern Africa: Added value in the simulation of the seasonal rainfall characteristics. *International Journal of Climatology*, 31(15), pp. 2338-2349. <https://doi.org/10.1002/joc.2242>.
- Hargreaves, G.H. and Samani, Z.A. (1985). Reference crop evapotranspiration from temperature. *Applied Engineering in Agriculture*, 1(2), pp. 96-99.
- Hughes, D.A., Andersson, L., Wilk, J. and Savenije, H.H.G. (2006). Regional calibration of the Pitman model for the Okavango River. *Journal of Hydrology*, 331(1-2), pp. 30-42.
- Hurry, L. and Van Heerden, J. (1982). *Southern Africa's weather patterns: A guide to the interpretation of synoptic maps*. Via Afrika, Goodwood.
- Intergovernmental Panel on Climate Change (IPCC) (2013) *Climate Change 2013: The Physical Science Basis*. Contribution of Working Group I to the Fifth Assessment Report of the Intergovernmental Panel on Climate Change [Stocker, T.F., D. Qin, G.-K. Plattner, M. Tignor, S.K. Allen, J. Boschung, A. Nauels, Y. Xia, V. Bex and P.M. Midgley (eds.)]. Cambridge University Press, Cambridge, United Kingdom and New York, NY, USA, 1535 pp.

- James, R. and Washington, R., 2013. Changes in African temperature and precipitation associated with degrees of global warming. *Climatic change*, 117(4), pp.859-872.
- Johnson, F. and Sharma, A. (2015). What are the impacts of bias correction on future drought projections? *Journal of Hydrology*, 525 (June), pp. 472-485.
- Jury, M.R. (2016). Climate influences on Vaal River flow. *Water SA*, 42(2), pp. 232-242.
- Jury, M.R. (2018). The climate of desiccation in the SW Cape. *Hydrology and Earth System Sciences Discussions*, pp. 1-19. <https://doi.org/10.5194/hess-2018-223>, 2018
- Jury, M. R.: The climate of desiccation in the SW Cape, *Hydrol. Earth Syst. Sci. Discuss.* <https://doi.org/10.5194/hess-2018-223>, 2018
- Kalognomou, E.A., Lennard, C., Shongwe, M., Pinto, I., Favre, A., Kent, M., Hewitson, B., Dosio, A., Nikulin, G., Panitz, H.J. and Büchner, M., 2013. A diagnostic evaluation of precipitation in CORDEX models over southern Africa. *Journal of climate*, 26(23), pp.9477-9506.
- Koneti, S., Sunkara, S.L. and Roy, P.S. (2018). Hydrological modeling with respect to impact of land-use and land-cover change on the runoff dynamics in Godavari River Basin using the HEC-HMS model. *ISPRS International Journal of Geo-Information*, 7(6), p. 206.
- Kotzé, I., Beukes, H., Van den Berg, E. and Newby, T., 2010. National invasive alien plant survey. Report number: gw/a/2010/21.
- Kruger, A.C. (2004). *Climate of South Africa – Climate Regions*. Pretoria: South African Weather Service.
- Li, K.Y., Coe, M.T., Ramankutty, N. and De Jong, R. (2007). Modeling the hydrological impact of land-use change in West Africa. *Journal of Hydrology*, 337(3-4), pp. 258-268.
- Li, C., Sinha, E., Horton, D.E., Diffenbaugh, N.S. and Michalak, A.M. (2014). Joint bias correction of temperature and precipitation in climate model simulations. *Journal of Geophysical Research: Atmospheres*, 119(23), pp. 13-153.
- Li, L., Diallo, I., Xu, C.Y. and Stordal, F., (2015) Hydrological projections under climate change in the near future by RegCM4 in Southern Africa using a large-scale hydrological model. *Journal of Hydrology*, 528, pp.1-16
- Li, S., Yang, H., Lacayo, M., Liu, J. and Lei, G. (2018). Impacts of land-use and land-cover changes on water yield: A case study in Jing-Jin-Ji, China. *Sustainability*, April 10(4), p. 960.

- Limpopo Business. (2017). *The guide to business and investment in The Limpopo Province*. Global Africa Network. Available online at: <https://webkiosk.globalafricanetwork.com/limpopo-business-2019-20-edition/62780110>. Accessed on 26 October 2020.
- Lumsden, T.G., Jewitt, G.P.W. and Schulze, R.E. (2003). *Modelling the Impacts of Land Cover and Land Management Practices on Runoff Responses*. WRC Report No. 1015/1/03. Pretoria, RSA.
- Luo, J., Zhou, X., Rubinato, M., Li, G., Tian, Y. and Zhou, J. (2020). Impact of multiple vegetation covers on surface runoff and sediment yield in the small basin of Nverzhai, Hunan Province, China. *Forests*, 11(3), p. 329.
- Maraun, D. (2016). Bias correcting climate change simulations – A critical review. *Current Climate Change Reports*, 2(4), pp. 211-220.
- Maúre, G., Pinto, I., Ndebele-Murisa, M., Muthige, M., Lennard, C., Nikulin, G., Dosio, A. and Meque, A. (2018). The Southern African climate under 1.5°C and 2°C of global warming as simulated by CORDEX regional climate models. *Environmental Research Letters*, 13(6), p. 065002.
- Mbaye, M.L., Diatta, S. and Gaye, A.T. (2018). Climate change signals over the Senegal river basin using regional climate models of the CORDEX Africa simulations. In: *International Conference on Innovations and Interdisciplinary Solutions for Underserved Areas* (March, pp. 123-132). Springer, Cham.
- Mbokodo, I., Bopape, M.-J., Chikoore, H., Engelbrecht, F. and Nethengwe, N. (2020). Heatwaves in the future warmer climate of South Africa. *Atmosphere (Basel)*, 11(7), p. 712.
- McCluskey, A. and Strzepek, K. (2007). *The impacts of climate change on regional water resources and agriculture in Africa*. The World Bank.
- McKee, T.B., Doesken, N.J. and Kleist, J. (1993). The relationship of drought frequency and duration to time scales. In: *Proceedings of the 8th Conference on Applied Climatology* (pp. 179-183). American Meteorological Society Boston, MA.
- Meque, A. and Abiodun, B. (2014). Simulating the link between ENSO and summer drought in Southern Africa using regional climate models. *Climate Dynamics*, 44, pp. 1881-1990.
- Merz, L., Yang, D. and Hull, V. (2020). A Metacoupling Framework for Exploring Transboundary Watershed Management. *Sustainability*, 12(5), p. 1879.

- Monteith, J.L. (1965). Evaporation and the environment in the state and movement of water in living organisms. *Proceedings of the Society of Experimental Biology*, Symposium No. 19, Cambridge University Press: Cambridge, pp. 205-234.
- Mosase, E., Ahiablame, L., Park, S. and Bailey, R. (2019). Modelling potential groundwater recharge in the Limpopo River Basin with SWAT-MODFLOW. *Groundwater for Sustainable Development*, 9, p. 100260.
- Naik, M. and Abiodun, B.J. (2016). Potential impacts of forestation on future climate change in Southern Africa. *International Journal of Climatology*, 36(14), pp. 4560-4576. <https://doi.org/10.1002/joc.4652>.
- Naik, M. and Abiodun, B.J. (2020). Projected changes in drought characteristics over the Western Cape, South Africa. *Meteorological Applications*, 27(1), p. e1802.
- Neitsch, S.L., Arnold, J.G. and Srinivasan, R. (2002). *Pesticides fate and transport predicted by the soil and water assessment tool (SWAT): Atrazine, Metolachlor and Trifluralin in the Sugar Creek Watershed*. BRC Publications Report, 3.
- Neitsch, S.L., Arnold, J.G., Kiniry, J.R., Williams, J.R. and King, K.W. (2005). *SWAT theoretical documentation version 2005*. Soil and Water Research Laboratory, ARS, Temple Texas, USA.
- Odoulami, R.C., Wolski, P. and New, M. (2021). A SOM-based analysis of the drivers of the 2015-2017 Western Cape drought in South Africa. *International Journal of Climatology*, 41, pp. E1518-E1530.
- Omar, S.A. and Abiodun, B.J. (2020). Characteristics of cut-off lows during the 2015-2017 drought in the Western Cape, South Africa. *Atmospheric Research*, 235, p. 104772.
- Otieno, F., Oching, G., Haji, H. and Dzwairo, B. (2009). Integrated water management of the Vaal River catchment. *Civil Engineering*, 17(5), 37-40.
- Otter, A. (n.d.). South Africa's Water Challenge. Available online at: <https://mediahack.co.za/work/water/>. Accessed on 5 November 2020.
- Otto, F.E., Wolski, P., Lehner, F., Tebaldi, C., Van Oldenborgh, G.J., Hogesteeger, S., Singh, R., Holden, P., Fučkar, N.S., Odoulami, R.C. and New, M. (2018). Anthropogenic influence on the drivers of the Western Cape drought 2015-2017. *Environmental Research Letters*, 13(12), p. 124010.
- Padrón, R.S., Gudmundsson, L., Ducharme, A., Lawrence, D.M., Mao, J., Peano, D., Decharme, B., Krinner, G., Kim, H. and Seneviratne, S.I. (2020). Dry season water availability changes attributed to human-induced climate change. In: 22nd EGU General Assembly Conference Abstracts, 4-8 May, p. 12658.

- Pascale, S., Kapnick, S.B., Delworth, T.L. and Cooke, W.F. (2020). Increasing risk of another Cape Town ‘Day Zero’ drought in the 21st century. In: *Proceedings of the National Academy of Sciences*, 117(47), pp. 29495-29503.
- Querner, E.P. and Zanen, M. (2013). Modelling water quantity and quality using SWAT: A case study in the Limpopo River basin, South Africa. Alterra-report No. 2405, Wageningen, Alterra. Available online at: <https://edepot.wur.nl/250348>. Accessed on 01 May 2021
- Randall, D.A., Wood, R.A., Bony, S., Colman, R., Fichet, T., Fyfe, J., Kattsov, V., Pitman, A., Shukla, J., Srinivasan, J. and Stouffer, R.J. (2007). Climate models and their evaluation. In: *Climate Change 2007: The physical science basis*. Contribution of Working Group I to the Fourth Assessment Report of the IPCC (FAR) (pp. 589-662). Cambridge University Press.
- Reason, C.J. and Smart, S., 2015. Tropical southeast Atlantic warm events and associated rainfall anomalies over southern Africa. *Frontiers in Environmental Science*, 3, p.24.
- Real Economy Bulletin (REB). (2016.) *The Real Economy Bulletin. Provincial Review 2016. Limpopo*. Available online at: https://www.tips.org.za/images/The_REB_Provincial_Review_2016_Limpopo.pdf. Accessed on 01 May 2021
- Refsgaard, J.C. (1997). Parameterisation, calibration and validation of distributed hydrological models. *Journal of Hydrology*, 198(1-4), pp. 69-97.
- Scheiter, S., Gaillard, C., Martens, C., Erasmus, B.F.N. and Pfeiffer, M., 2018. How vulnerable are ecosystems in the Limpopo province to climate change? *South African Journal of Botany*, 116, pp.86-95.
- Schulze, R.E. (1995). *Hydrology and agrohydrology: A text to accompany the ACRU 3.00 agrohydrological modelling system*. Water Research Commission.
- Seibert, M., Merz, B. and Apel, H. (2017). Seasonal forecasting of hydrological drought in the Limpopo Basin: A comparison of statistical methods. *Hydrology and Earth System Sciences*, 21(3), pp. 1611-1629.
- Setyorini, A., Khare, D. and Pingale, S.M. (2017). Simulating the impact of land use/land cover change and climate variability on watershed hydrology in the Upper Brantas basin, Indonesia. *Applied Geomatics*, 9(3), pp. 191-204.
- Sheffield, J., Goteti, G. and Wood, E.F. (2006). Development of a 50-year high-resolution global dataset of meteorological forcings for land surface modeling. *Journal of Climate*, 19(13), pp. 3088-3111.

- Singh, R., Van Werkhoven, K. and Wagener, T. (2014). Hydrological impacts of climate change in gauged and ungauged watersheds of the Olifants basin: A trading-space-for-time approach. *Hydrological Sciences Journal*, 59(1), pp. 29-55.
- Sorooshian, S., Hsu, K.L., Coppola, E., Tomassetti, B., Verdecchia, M. and Visconti, G. (Eds.). (2008). *Hydrological modelling and the water cycle: Coupling the atmospheric and hydrological models* (Vol. 63). Springer Science and Business Media.
- Sousa, P.M., Blamey, R.C., Reason, C.J., Ramos, A.M. and Trigo, R.M. (2018). The ‘Day Zero’ Cape Town drought and the poleward migration of moisture corridors. *Environmental Research Letters*, 13(12), p. 124025.
- Spinoni, J., Barbosa, P., De Jager, A., McCormick, N., Naumann, G., Vogt, J.V., Magni, D., Masante, D. and Mazzeschi, M. (2019). A new global database of meteorological drought events from 1951 to 2016. *Journal of Hydrology: Regional Studies*, 22, p. 100593.
- Statistics South Africa. (2010). *Water Management Areas in South Africa, National Accounts: Environmental Economic Accounts*. Pretoria 0001.
- Taylor, K.E., Stouffer, R.J. and Meehl, G.A. (2012). An overview of CMIP5 and the experiment design. *Bulletin of the American Meteorological Society*, 93(4), pp. 485-498.
- Teutschbein, C. and Seibert, J. (2012). Is bias correction of Regional Climate Model (RCM) simulations possible for non-stationary conditions? *Hydrology and Earth System Sciences Discussions*, 9(11), pp. 12765-12795.
- Teutschbein C, Wetterhall F, Seibert J (2011) Evaluation of Different Downscaling Techniques for Hydrological Climate-Change Impact Studies at the Catchment Scale. *Climate Dynamics*, vol. 37(9-10), pages 2087-2105, doi:10.1007/s00382-010-0979-8.
- Trambauer, P., Werner, M., Winsemius, H.C., Maskey, S., Dutra, E. and Uhlenbrook, S. (2015). Hydrological drought forecasting and skill assessment for the Limpopo River basin, Southern Africa. *Hydrology and Earth System Sciences*, 19(4), pp. 1695-1711.
- Tyson, P.D. (1986). *Climatic change and variability in Southern Africa*. Oxford University Press.
- Uhe, P., Philip, S., Kew, S., Shah, K., Kimutai, J., Mwangi, E., van Oldenborgh, G.J., Singh, R., Arrighi, J., Jjemba, E. and Cullen, H. (2018). Attributing drivers of the 2016 Kenyan drought. *International Journal of Climatology*, 38(51), pp. e554-e568.
- Ujeneza, E. and Abiodun, B. (2014). Drought regimes in Southern Africa and how well GCMs simulate them. *Climate Dynamics*, 44(5-6), pp. 1595-1609.
- Van Vuuren, L. 2008. Start saving or start paying, river studies warn. *The Water Wheel*, 7(3), pp. 14-18.

- Vicente-Serrano, S.M., Beguería, S. and López-Moreno, J.I. (2010). A multiscalar drought index sensitive to global warming: The standardized precipitation evapotranspiration index. *Journal of Climate*, 23(7), pp. 1696-1718.
- Wilcke, R.A.I., Mendlik, T. and Gobiet, A. (2013). Multi-variable error correction of regional climate models. *Climatic change*, 120(4), pp. 871-887.
- Wolski, P. (2018). How severe is Cape Town's 'Day Zero' drought? *Significance*, 15(2), pp. 24-27.
- Yen, H., Park, S., Arnold, J.G., Srinivasan, R., Chawanda, C.J., Wang, R., Feng, Q., Wu, J., Miao, C., Bieger, K. and Daggupati, P. (2019). IPEAT+: A Built-in optimization and automatic calibration tool of SWAT+. *Water*, 11(8), p. 1681.
- Yuan, X. and Bai, J. (2018). Future projected changes in local evapotranspiration coupled with temperature and precipitation variation. *Sustainability*, 10(9), p. 3281.
- Zhu, T. and Ringler, C. (2012). Climate change impacts on water availability and use in the Limpopo River Basin. *Water*, 4(1), pp. 63-84.

Websites:

Shuttle Radar Topography Mission (SRTM): <https://srtm.csi.cgiar.org>

Waterbase: <http://www.waterbase.org>

Department of Water and Sanitation (DWS):
<https://www.dws.gov.za/Hydrology/>

QDM R-package: <https://rdrr.io/cran/MBC/man/QDM.html>

Appendix

Table A1: CN values of different soil types and land use types under medium soil moisture.

SWAT+ cover classification	land	Corresponding SCS Land use	CN for different HSG				Hydrological condition
			(A)	(B)	(C)	(D)	
URMD		Urban	98	98	98	98	Poor
CRDY		Straight row crops	72	81	88	91	Poor
CRGR		Straight row crops	67	78	85	89	Good
CRWO		Woods-grass combination	43	65	76	82	Fair
GRAS		Pasture-grassland	39	61	74	80	Good
SHRB		Brush-brush-weed- grass_mixture_with_brush_the_ major_element	30	48	65	73	Good
SAVA		Woods-grass combination	32	58	72	79	Good
FODB		Deciduous evergreen forest	33	58	72	77	–
FOEB		Evergreen broadleaf forest	30	55	70	77	–
FOMI		Mixed forest	32	57	71	77	–
WATR		Water	100	100	100	100	–
BSVG		Fallow	77	86	91	94	–